TWO STUDIES ON SELF-ASSEMBLY OF AMPHIPHILIC MOLECULES: (1) 3-DIMENSIONAL ASSEMBLY OF HYDROPHOBICALLY MODIFIED WATER SOLUBLE POLYMER (HMWSP); (2) 2-DIMENSIONAL ASSEMBLY OF SURFACTANTS AT THE SOLID/WATER AND AIR/WATER INTERFACES.

by

VIKRAM KUMAR

A dissertation submitted to the Graduate Faculty in Engineering in partial fulfillment of the requirements for the degree of Dcctor of Philosophy, The City University of New York

1997

This manuscript has been read and accepted for the Graduate Faculty in Engineering in satisfaction of the dissertation requirement for the degree of Doctor of Philosophy.

9/18/97
Date

Prof. Carol A. Steiner
Chair of Examining Committee

9/23/97
Date

Dean Gerard Lowen
Executive Officer

Prof. Charles Maldarelli

Prof. Alexander Couzis

Prof. Leslie Isaacs

Prof. Milton J. Rosen

Supervisory Committee

THE CITY UNIVERSITY OF NEW YORK

ABSTRACT

TWO STUDIES ON SELF-ASSEMBLY OF AMPHIPHILIC MOLECULES:
(1) 3-DIMENSIONAL ASSEMBLY OF HYDROPHOBICALLY MODIFIED WATER SOLUBLE POLYMER (HMWSP);
(2) 2-DIMENSIONAL ASSEMBLY OF SURFACTANTS AT THE SOLID/WATER AND AIR/WATER INTERFACES.

by

Vikram Kumar

Adviser: Professor Carol A. Steiner

In the first study I investigated structure/property relationships in hydrophobically modified hydroxyethyl cellulose (HMHEC)/surfactant hydrogels. This study encompasses the effects of polymer degree of polymerization, side chain content, side chain length and structure, and surfactant structure on the gel forming ability and gel quality. Strong gels were characterized further in terms of rheology and hydrophobicity. Gel formation is favored when the side chain level on the polymer is below a critical number

of side chains/backbone. This critical number lies between 210 and 390. In general, gel quality improves with increasing degree of polymerization, increasing solubility of the polymer side chains in water and decreasing critical micelle concentration (cmc) of surfactants.

In the second study I investigated the role of surfactants in enhancement of spreading of aqueous solutions over hydrophobic surfaces. Based on the differentiated form of Young's equation, spreading can be enhanced by using surfactants which pack very densely at the hydrophobic surface/water interface. To identify the structural parameters of surfactants, viz. size of hydrophilic and hydrophobic groups, which exhibit dense packing, packing densities of 2 members of a homologous series of surfactants were studied. My results show that for hydrocarbon based ethoxylated surfactants (CH_3-$(CH_2)_{m-1}$-$(OCH_2CH_2)_n$-OH) (designated C_mE_n), packing density increases with a decrease in n (n considered was 1 and 6). Furthermore I provide, for the first time, visual and quantitative evidence of dense packing (~20 A^2/molecule) for $C_{14}E_1$. Visual evidence is provided by using the technique of fluorescence microscopy while quantitative evidence is provided by using attenuated total reflection - Fourier transform infrared (ATR-FTIR) spectroscopy.

ACKNOWLEDGMENTS

I would like to take this opportunity to express my sincere thanks to my parents, who have always encouraged me to attain the highest goals, and have sacrificed and cared for me.

I would like to express my deepest gratitude to my adviser, Professor Carol A. Steiner, for her patient guidance, rigorous training, numerous invaluable suggestions and discussions during the course of this research. It was her support, inspiration and friendship that made this work possible. I greatly appreciate Professors Charles Maldarelli and Alexander Couzis for their deep involvement, invaluable contributions and bright insights in the second half of my thesis work. I am also grateful to Professor Milton J. Rosen and Professor Leslie Isaacs for their helpful suggestions and advice on the content of this thesis.

Particular thanks to Dr. Maria Pollard for her pioneering research in the field of surfactant adsorption which was the foundation of a part of this work and Mr. Srinivasan Krishnan for his invaluable contributions towards the Langmuir trough and Fourier transform infrared (FTIR) experiments. In addition, I wish to express my sincere thanks to Professor Herbert Weinstein for his continuous encouragement during the course of this work.

I would like to thank my fellow graduate students and Dr. Andrew Edwards and Ms Lillian Barruos for their support,

encouragement and assistance. Thanks also to the department technicians, Mr. Zhengrong Shu and Mr.Andi Eng, for their constant help in many occasions.

This work is dedicated in memory of my dear friend and colleague, Dr. Apostolos E. Kostazos, who passed away on December 5, 1996 after a brief illness at age 26.

TABLE OF CONTENTS

LIST OF TABLES

LIST OF FIGURES

PART 1

Chapter 1
Introduction

Amphiphilic hydrogels are a new class of polymeric hydrogels. They are characterized by a water-swollen polymer network with dispersed hydrophobic microdomains. The microdomains serve as linkage points in the network, and may also act as reservoirs or sinks for organic solutes permeating the gel. These materials show promise as media for controlled release of drugs, wastewater treatment, separations on the basis of solute hydrophobicity, and other important applications. Their efficacy in these applications will depend on the affinity of the microdomains for the particular solutes of interest, the maximum loading capacity of the gels for the solutes, the structure of the interface between the dispersed and continuous phases, and the mechanical strength and integrity of the gels themselves. These material properties will depend in turn on the structure and concentration of the microdomains within the gel.

Amphiphilic hydrogels form via the self-assembly of hydrophobically modified water-soluble polymers (HMWSPs) in aqueous systems. The hydrophobic side chains on the polymer aggregate so as to exclude water, resulting in the formation of micelle-like microdomains. Studies on these systems to date have suggested that the number and length of the hydrophobic side chains on the polymer will govern the overall concentration of microdomains in the hydrogel and their

aggregation number. In addition, it is reasonable to expect that the structure of the side chains will influence the properties of the bulk/microdomain interface. Hence it should be possible to control these important gel properties a priori by manipulating structural parameters of the polymer. This investigation is designed to uncover important structure/property relationships at work in these systems.

To date six types of polymers have been used to make amphiphilic hydrogels. They are hydrophobically modified hydroxyethyl cellulose (HMHEC), ethyl hydroxyethyl cellulose (EHEC), Hyaluronan (made of alternating units of glucuronic acid and N-acetylglucosamine)(Hy), polyacrylate (PA), hydrolyzed terpolymer of acrylamide, sodium acrylate and alkylacrylamide (HRAM , where R connotes to the presence of hydrophobic side chains), a tetra-polymer (HRAM-AA) of acrylamide, alkylacrylamide, acrylic acid and sodium acrylate. HMHEC and EHEC are nonionic while Hy, PA, HRAM and HRAM-AA are negatively charged polymers.

The work presented here is divided into chapters as follows. Chapter 2 is a literature review covering solution and gel properties of water soluble polymers (WSPs) and HMWSPs. Chapter 3 covers the materials, methods and experimental techniques that were used in this study. Chapter 4 contains the results and discussion of this study and Chapter 5 provides the summary, conclusions and recommendations for future work.

Chapter 2

Literature review

In this chapter the literature review on solution and gel properties of water-soluble polymers and hydrophobically modified water-soluble polymers in the presence of surfactants is presented.

2.1 Solution properties of water-soluble homopolymers and HMWSPs in the presence of surfactants

Interactions of water-soluble homopolymers with surfactants has been studied extensively. A comprehensive review on this topic has been published by Goddard [1]. The nature of homopolymer/surfactant interactions in aqueous solutions depends on the particular polymer and surfactant pair. For example, neither hydroxyethyl cellulose (HEC) [2] nor poly(acrylamide) (PAM) [3] interacts with sodium dodecyl sulfate (SDS). Other homopolymers, such as poly(oxyethylene) [4,5], poly(vinylpyrrolidone) [6] ,and poly(vinyl acetate) [7], nucleate the formation of surfactant aggregates in aqueous solutions in a complex manner depending on surfactant concentration [8]. In aqueous solutions of these polymers with surfactant, the surfactant forms aggregates which are bound to the polymer backbone. This binding occurs at concentrations, known as the critical aggregation concentration C1, below the critical micelle concentration (cmc) of the surfactant in pure water. C1 is independent of polymer concentration. A second critical

surfactant concentration, C2, is observed where polymer becomes saturated with surfactant; further increase in surfactant concentration leads to the formation of free surfactant micelles. The value of C2 increases linearly with polymer concentration. C1 and C2 are always located, respectively, below and above the cmc of the surfactant in pure water. In these systems, there are no well-defined nucleation sites for surfactant binding to the polymer.

Interactions of hydrophobically modified water-soluble polymers (HMWSPs) with surfactant differ from those of water soluble homopolymers in that the side chains serve as nucleation sites for surfactant binding. This is evident from the fact that SDS does not bind to HEC [2] or PAM [3] but exhibits a strong affinity for HMHEC [9-13] and hydrophobically modified PAM [14]. This is due to the formation of hydrophobic aggregates consisting of surfactant molecules and polymer side chains. At appropriate ratios of surfactant to polymer, these aggregates may act as physical cross-links among the polymer chains. A schematic of these aggregates is shown in Figure 2.1.

The properties of HMWSP/surfactant solutions depend on the solution composition. For example, the viscosity of these solutions exhibits a peak with surfactant concentration, typically occurring at or near the surfactant critical micelle concentration (cmc) [12, 16, 17, 18]. This has been interpreted as follows. If surfactant concentration is below

the cmc, geometric packing constraints on surfactant aggregates dictate that stable aggregates must contain multiple polymer side chains. This results in the formation of intermolecular 'bridges' between various polymer chains and a highly viscous solution results. A schematic of how the composition of the polymer/surfactant aggregates changes with addition of surfactant is shown in Figure 2.2. The effect of polymer concentration on HMWSP/surfactant solutions has also been studied. It has been shown that for HMHEC/surfactant systems [17], for a given surfactant concentration, there is critical polymer concentration above which viscosification of solutions occur. This is reasonable since the polymer chains have to be close to each other in order to interact. In addition, the higher the polymer concentration the higher is the surfactant concentration required to solubilize the polymer side chains. Thus the surfactant concentration at which the viscosity of solution shows a peak increases with polymer concentration [18].

The structure of both the HMWSP and the surfactant influences the solution properties. Some of the structural parameters of the polymers which have been studied are degree of polymerization (DP) [20], side chain length [20] and degree of side chain substitution (DS) [19].

The effect of surfactant structure on the solution properties of HMHEC has been studied by Tanaka et al. [12]. In particular they investigated the influence of surfactant

head group charge and tail group length on the viscosity of HMHEC/surfactant solutions at constant polymer concentration. Charged surfactants such as SDS and sodium hexanoate give rise to a much more viscous solution as compared to the nonionic alkylpoly(oxyethylene) ether-type surfactants $C_{11}E_8$ and $C_{13}E_8$. This was attributed to the fact that in the case of charged surfactants the bound surfactant produces more extended polymer chains, leading to a highly viscous solution. Among the charged surfactants, the nature of the headgroup (carboxylated vs sulfated) does not have much effect on the network strength. The viscosity of the solution goes up with the length of the surfactant tail group. This was attributed to the relatively high energy with which the long-chain alkyl groups are bound within the aggregates. The surfactant concentration at which the maximum viscosity occurs decreases with the length of the surfactant tail group. This was attributed to the fact that with an increase in the tail length the tendency of surfactants to self-assemble increases.

In the case of charged HMWSPs, apart from considering the polymer degree of polymerization (DP), side chain length and degree of substitution of side chains (DS) it is also necessary to consider the charge on the polymer [21-23]. The charge, among other factors, dictates the polymer dimensions in solution and thus is important in forming aggregates. When the charge is high, even though the chains are extended the intermolecular electrostatic repulsion may inhibit aggregation

[21,23,24].

2.2 Hydrogels made from HMWSPs

Hydrogels made from HMWSPs are a new class of polymeric hydrogels characterized by a water-swollen polymer network with dispersed hydrophobic microdomains. The microdomains serve as linkage points in the network. The hydrogels exhibit highly viscoelastic behavior, with a high plateau value of the dynamic storage modulus, G'.

To date six types of polymers have been used to make amphiphilic hydrogels. They are HMHEC [9-13, 18, 25], EHEC [28, 29], Hy [39], PA [39], HRAM [21] and HRAM-AA [27]. HMHEC and EHEC are nonionic while Hy, PA, HRAM and HRAM-AA are negatively charged polymers. The gels made from HMHEC, Hy and PA precipitate out of the solution and form a separate phase, while the EHEC, HRAM and HRAM-AA gels, in general, do not precipitate out and are macroscopically homogeneous. Note however that irrespective of how these gels are formed, viz. by precipitation out of the solution or not, all the gels are highly viscoelastic and this is attributed to the presence of hydrophobic aggregates.

The properties of gels made from HMHEC have been investigated as a function of solvent type and composition [10,11,25], temperature [13] and shear history [13]. To date HMHEC gels have been prepared using two different solvents, sodium dodecyl sulfate (SDS) in water [10,11] and ethanol and

water [25,26]. In the case of SDS/water solvent the aggregates are composed of polymer side chains and SDS molecules (Figure 2.1). On the other hand in the case of ethanol/water the hydrophobic aggregates are composed of polymer side chains alone. For both solvents the strength of the polymer network increases with polymer concentration. This increase in gel strength may arise due to an increase in the number of linkage points, an increase in the number of polymer side chains from different polymer chains incorporated in each microdomain, or both. The effect of solvent composition on the gel properties for each of the two solvents is as follows. With an increase in [SDS] the strength of the polymer network decreases. This has been attributed to the fact [11] that the number of polymer side chains per aggregate decreases while the number of SDS molecules per aggregate increases as a function of SDS concentration. Thus the decrease in gel strength is expected due to the overall decrease in the physical cross-linking of the polymer chains. For the ethanol/water solvent there is a peak in the strength of the gels with volume fraction ethanol [25]. The composition of solvent where the peak occurs corresponds to that where the polymer solubility is maximized. Since high polymer solubility suggests highly extended polymer chains this result suggests that side chains are more likely to aggregate when the polymer backbone is extended and the side chains are free in solution. The gel strength shows a peak

with temperature [13]. With an increase in temperature polymer backbone tends to collapse while the polymer side chains become more soluble. The former hinders network formation while the latter aids it. Thus the peak is attributed to the competition between the polymer backbone and the polymer side chains to control the gel properties.

In summary, the strength of gels made from HMHEC is proportional to dimension of the polymer backbone and the solubility of side chains in the solvent. Thus far these two parameters have been manipulated by changing the solution composition and temperature. To date, no study on how these two parameters in specific and gel properties in general, depend on HMHEC and surfactant structure, such as polymer DP, side chain content, side chain structure and surfactant tail length and head group structure, has been reported.

Gels made by EHEC and two different surfactants, SDS and cetyl trimethylammonium bromide (CTAB), have been studied [28,29]. These gels form only above a certain temperature called the gelling temperature. With an increase in temperature the side chains of the polymer (ethoxy groups) become dehydrated due to breaking of the hydrogen bonds. The dehydrated ethoxy groups promote the formation of hydrophobic aggregates between themselves and the surfactant molecules. These aggregates interlink the polymer chains which leads to gel formation.

Gels made by Hy and PA and CTAB (the number of carbon

atoms in the alkyl chain varying from 10 to 14) surfactant have been studied [39]. The polymers are negatively charged while the surfactant is positively charged. For both the polymers gel formation is governed by electrostatics. This was demonstrated by the fact that gel formation was inhibited in the presence of salt. Preliminary studies show that the strength of the gels increase with the degree of polymerization of the polymer.

To date the properties of gels made from HRAM [21] and HRAM-AA [27] have been investigated as a function of solvent type, solution composition and polymer structure. The solvents are water, brine and SDS/water. In the case of water and brine the aggregates comprise polymer side chains alone while in case of SDS/water the aggregates are formed of the polymer side chains and SDS molecules.

The effect of solution composition and polymer structure (in terms of hydrophobe length and charge on the polymer) on HRAM gel properties has been studied [21]. The gel point, defined as the lowest polymer concentration at which an aqueous polymer system exhibits a rubbery plateau in the dynamic rheological spectra, decreases with side chain length and increases with backbone charge. The authors explain that the dependence of gel point on various aspects of polymer architecture is complex. For example, longer chains side will be relatively insoluble in water but will be more tightly bound to the aggregates (thus having a higher binding energy).

A higher charge on the polymer backbone will increase the number of polymer side chains solubilized in the solvent. On the other hand, a higher charge will make the polymer resistant to aggregation due to intermolecular electrostatic repulsion. It was found that strong viscoelastic hydrogels formed from C_{10}-substituted HRAMs even at high backbone charge levels where C_8-substituted HRAMs did not gel.

The elastic storage modulus of gels made from HRAM increases with an increase in polymer concentration. This is due to the concomitant increase in the total hydrophobe content of the system and a decrease in the degree of dissociation of the charges on the polymer. Thus the probability of formation of aggregates is increased. The strength of the network increases with hydrophobe length, for a constant polymer concentration and charge. This was attributed to the higher interaction energy for longer side chains. When using SDS/water as the solvent for HRAM a very interesting feature was observed. The gel point of the polymer having C_{10} as the side chain (the highest side chain length considered in this study) was lower than when water alone was used as the solvent. This demonstrates that SDS binds to the polymer and aids in the network formation, in spite of the fact that both the polymer and SDS are anionic in charge and thus we expect repulsion between the two. Thus the driving force for the formation of aggregates between the polymer side chains and SDS is sufficient to overcome the

intermolecular electrostatic repulsion (Figure 2.2).

Gels formed from a series of hydrophobically modified RAM-AA have been studied by Wu et al. [27]. They found that there is a critical side chain content for gel formation. Above this critical number the polymer is insoluble while below the number good gels are formed. Their results point to the importance of having a highly extended polymer chain in obtaining good gels.

HMHEC and EHEC are made from a naturally occurring polymer (viz. cellulose). On the other hand HRAM and HRAM-AA are synthetic polymers. Thus HMHEC gels may be more appropriate for the proposed applications of gels, particularly drug delivery. While the effect of polymer structure on gel properties has been studied for HRAM and HRAM-AA system, no such study is available for the HMHEC and EHEC gels.

2.3 This Work

The present study is the first investigation on the effects of polymer and surfactant structure on the gel forming ability, gel strength and degree of hydrophobicity of HMHEC based systems. HMHECs with 2 DPs, 3 hydrophobe contents, 3 hydrophobe types were used along with 3 surfactants. The results of this study will help in the design of gels with desired properties.

Figure 2.1: Schematic of Hydrogel Network

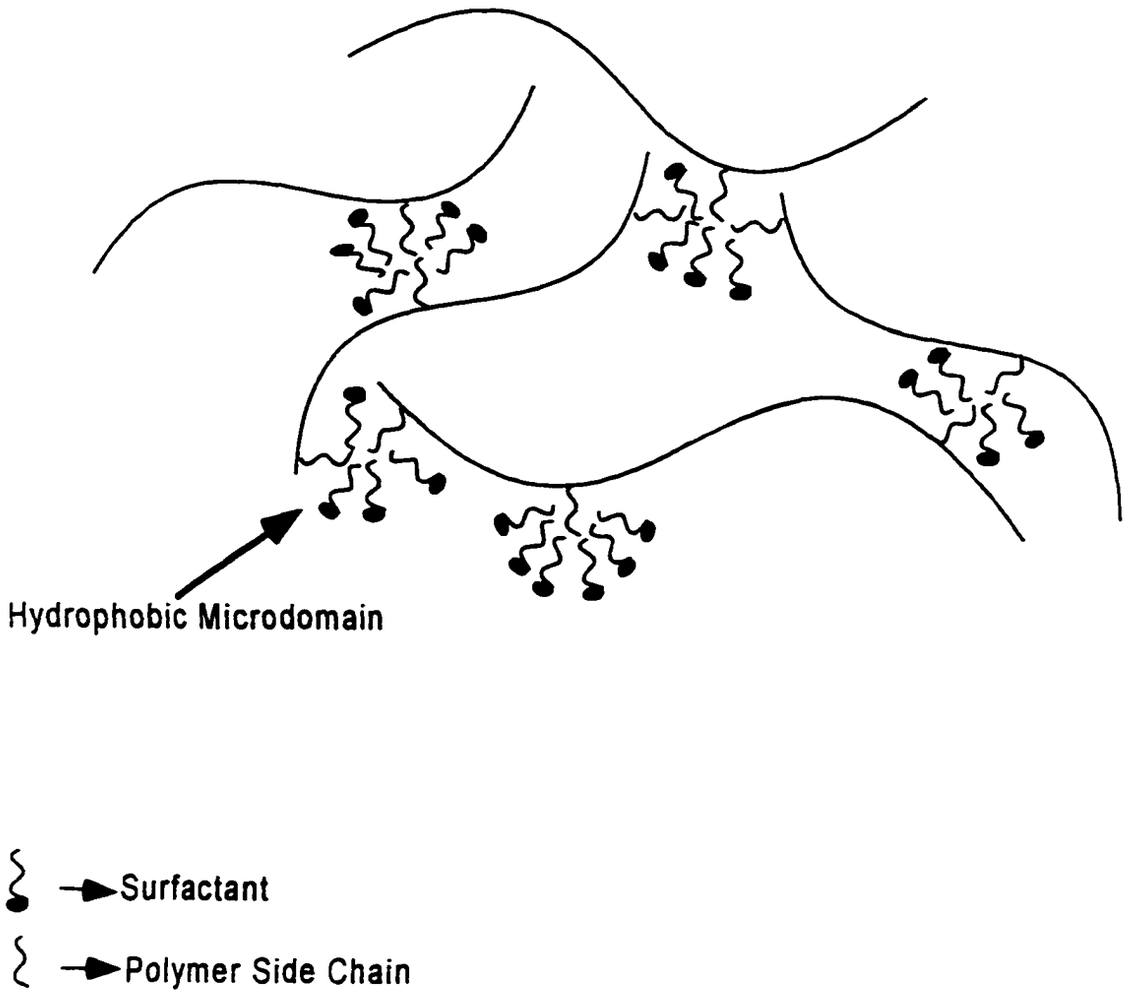

Figure 2.2: Effect of surfactant concentration on the structure of polymer/surfactant aggregates

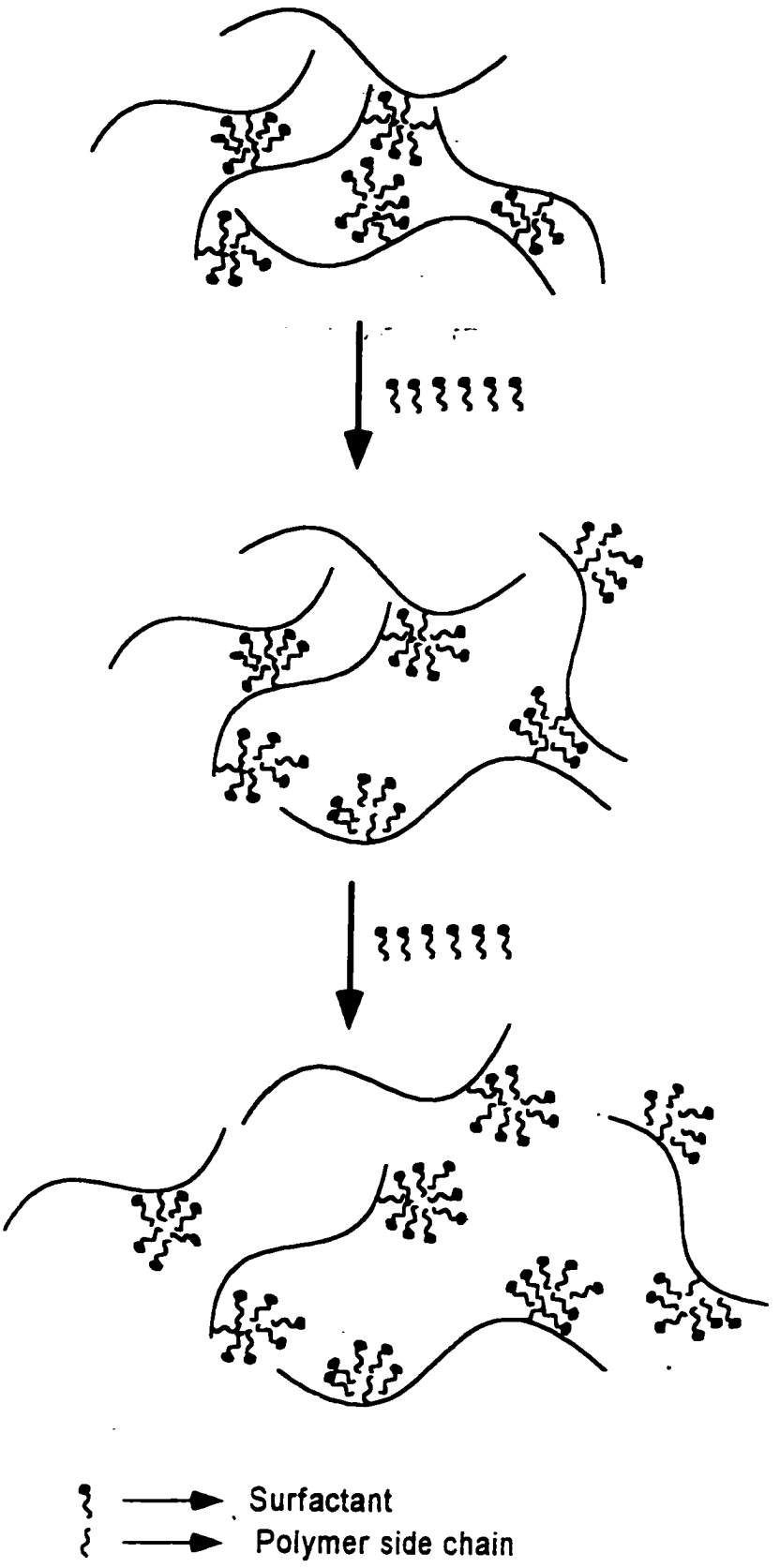

CHAPTER 3

EXPERIMENTAL SECTION

3.1 Materials

Hydrophobically modified hydroxyethyl cellulose (HMHEC) was a gift from Hercules Inc. (Wilmington, Delaware). The polymer chain (see Figure 3.1) consists of two components - a water soluble backbone (hydroxyethyl cellulose (HEC)) and water insoluble hydrocarbon side chains (R). The side chains are grafted onto HEC by reacting epoxide (terminal group of the side chains) with the hydroxyl groups present on HEC. The characteristics of all the polymers (HECs and HMHECs) used are given in table 3.1. The hydroxyethyl molar substitution (HEMS) of the HMHECs used in this study were in the range 2.5 - 4.0 per anhydroglucose unit. The degree of polymerization (DP) of the polymers was designated as "low" (1100 -1300) or "high" (3000). Three different kinds of hydrophobes were studied. Their structures and the corresponding designations used in this study are - linear $C_{12}H_{25}$ (C_{12}), branched C_9H_{19} chain attached to a phenyl group (C_9-ϕ) (the phenyl group being bound to the polymer backbone) and linear C_8H_{17} (C_8). Note that the source of the C_9-ϕ hydrophobe is commercial nonyl phenol, which is described as primarily "para" and branched [35]. To obtain some structural information we examined the NMR spectrum (supplied by Aldrich) of nonyl phenol (90 %) (Figure 3.2), the reactant used to make C_9-ϕ. However, no single structure could be identified, due two

factors - first the type and composition of the impurities present in nonyl phenol are not known, and second the nonyl phenol itself is heterogeneous. The degree of substitution of the hydrophobes (DS) used in this study ranged from 1.3 to 8.0 wt. %. Also shown in table 3.1 is the range of system compositions studied for each polymer, expressed in terms of the parameter N, where N is defined as the ratio of the total number of surfactant molecules to the total number of side chains in the system. Note that N is undefined for HEC (DS=0). The parameter N_{crit} given on this table will be defined in the next chapter.

Sodium dodecyl sulfate (SDS) (Fluka, > 99 %), sodium octyl 1 sulfate (SOS)(Pfaltz & Bauer) and sodium octyl 1 sulfonate (SS) (Sigma, 98 %) were used as received. The critical micelle concentrations (cmc) of these surfactants [36] are 8, 133 and 153 mM respectively. The fluorescence probe pyrene (Aldrich, 99 %) was used as received.

HMHEC/surfactant systems were prepared by stirring a carefully weighed amount of polymer in 50 mL of either an aqueous or pyrene saturated ($3*10^{-7}$ M) aqueous solution of surfactant. The mixtures were stirred overnight (12-16 hours) and then left standing for 2 days. The polymer concentrations used were 0.3, 0.8 and 1.2 g/dL and the surfactant concentrations used were 0.44, 0.65 and 0.86 * cmc. The polymer and surfactant concentrations refer to the overall system concentrations, unless otherwise noted. For two phase

systems, viz. a gel and a supernatant, polymer and surfactant concentrations refer to the system concentrations before phase separation.

3.2 Methods

Viscosity and dynamic rheology measurements were conducted using a Haake Rotovisco RV20 oscillatory shear rheometer with the temperature maintained at 25 C. The sensors used for the two measurements were double gap couette device (DA-45) and parallel plate (PQ-30), with 0.5 mm gap between the plates, respectively. In dynamic rheology measurements frequency sweeps were used to obtain the dynamic storage and loss moduli (G' and G", respectively) as a function of applied frequency, ω. The strain rate used was 3 %, which was found to be within the G' vs strain rate plateau in test strain sweeps for our gels (Figure 3.3). A plateau in the G' vs strain rate sweep indicates linear viscoelastic behavior, viz. the dynamic moduli are a function of ω alone, and not of the strain. The gel chosen for the strain test sweep, for a given polymer/surfactant system, was one made of the highest surfactant and lowest polymer concentration. Such a gel is the weakest among all gels for that polymer surfactant system, from previous studies [11]. It is reasonable to expect that in the range of strain rate for which the weakest gel exhibits linear viscoelastic behavior, other gels will exhibit linear viscoelastic behavior as well.

Fluorescence spectra of pyrene in the gels were obtained

on a Spex Model 112A Fluorolog-2 Fluorescence Spectrophotometer (Spex industries, Inc., Edison, NJ). The excitation wavelength was set at 310 nm, and the emission spectrum was scanned from 350 nm to 500 nm. Spectra were collected in the right angle (RA) mode. For collecting spectra of solutions all slit widths were set at 0.5 mm. In case of hydrogels, all slit widths were set at 1.25 mm. The experiments were conducted at room temperature (~ 24-25 C).

3.3 Experimental techniques

3.3.1 Rheology

When a viscoelastic material is subjected to an oscillatory shear, its response is characterized by a complex modulus (G*). When the material is made to oscillate sinusoidally, the stress developed leads the strain by an angle. The response can be described by G*, which is the vector sum of the storage modulus G' and loss modulus G",

$$G^* = G' + iG" \qquad \text{.....} \quad 3.1$$

where $i = (-1)^{1/2}$.

G' and G" are related to the molecular structure of the sample. In the case of permanently cross-linked materials the theory of rubber elasticity is used to find the molecular weight between crosslinks (M_e) [32]. This is done by relating M_e to G'_o, the plateau value of G'.

This enables one to evaluate M_e,

$$M_e = \frac{\rho \phi RT}{G'_o}$$

$$\phi^{2.3} \quad \text{.....} \quad 3.2$$

Where,

T = Temperature, K

R = Universal gas constant = $8.314*10^7$ dynes-cm/mol K

G'_o= Plateau of elastic modulus of the gel, dynes/cm^2

ρ = Dry density of polymer, gm/cm^3

ϕ = Volume fraction of polymer in the gel

3.3.2 Fluorescence spectroscopy

Fluorescence spectroscopy has played a very important role in the study of micelle structure [30]. In this methodology, one adds a small amount of a fluorescent dye (probe) to a micellar system and measures various features of the dye fluorescence. The fluorescence spectrum of the dye provides information about the microenvironment around the dye. Since the dye, which is usually an organic substance, resides preferentially in hydrophobic moieties, the spectrum provides information about these moieties.

Pyrene is a commonly used polarity-sensitive fluorescence probe to determine the hydrophobicity of microdomains. The pyrene monomer emission spectrum has five principal vibronic bands in the range 350 - 450 nm. The relative intensity of the third peak (at λ = 382 nm) with respect to the first (at λ = 371 nm) is inversely related to the polarity of the environment in which pyrene is solubilized [31]. Pyrene is a strongly hydrophobic probe with low solubility in water ($3 * 10^{-7}$ M). In a system containing hydrophobic microdomains, most

of the molecules of pyrene are incorporated in the microdomains, with the remaining residing in the aqueous phase. Thus, the fluorescence spectrum of such a solution gives a measure of the average hydrophobicity of the system, weighted by the partition coefficient of pyrene in the two phases.

Table 3.1. Properties of HMHEC and HMHEC/surfactant systems studied.

Polymer designation	DP category	DP	HEMS	Hydrophobe (C_n)	DS (wt. %)	C_n per backbone	Water soluble	Range of N studied (Surfactant*)	Ncrit
High DP HEC	high	3000	2.5	-	-	-	yes	-	
Low DP HEC	low	1100	2.5	-	-	-	yes	-	
A	high	3000	3.7	C_{12}	1.3	150	yes	3.8 - 94	> 94
B	"	"	3.3	"	4.2	470	no	1.5 - 9.3	< 1.5
C	"	"	3.3	"	8.0	900	no	0.6 - 4.8	< 0.6
D	low	1100	3.5	"	1.9	80	yes	2.6 - 20	> 20
E	"	1200	4.0	"	4.3	210	no	1.2 - 9.1	4.0
F	"	"	4.0	"	8.0	390	no	0.6 - 4.8	< 0.6
G	"	1300	4.0	C_9-ϕ	4.5	200	no	1.3 - 10.4	> 10.4
H	"	1100	3.6	C_8	2.1	130	yes	1.6 - 12.4	> 12.4
								26 - 200 (SOS)	150 -200
								30 - 230 (SS)	> 230

* Surfactant used is SDS unless otherwise noted.

Figure 3.1: Structure of Hydrophobically Modified Hydroxyethyl Cellulose (HMHEC).[22] Made HEC having a HEMS of 2.5.

R - Hydrophobic side chain

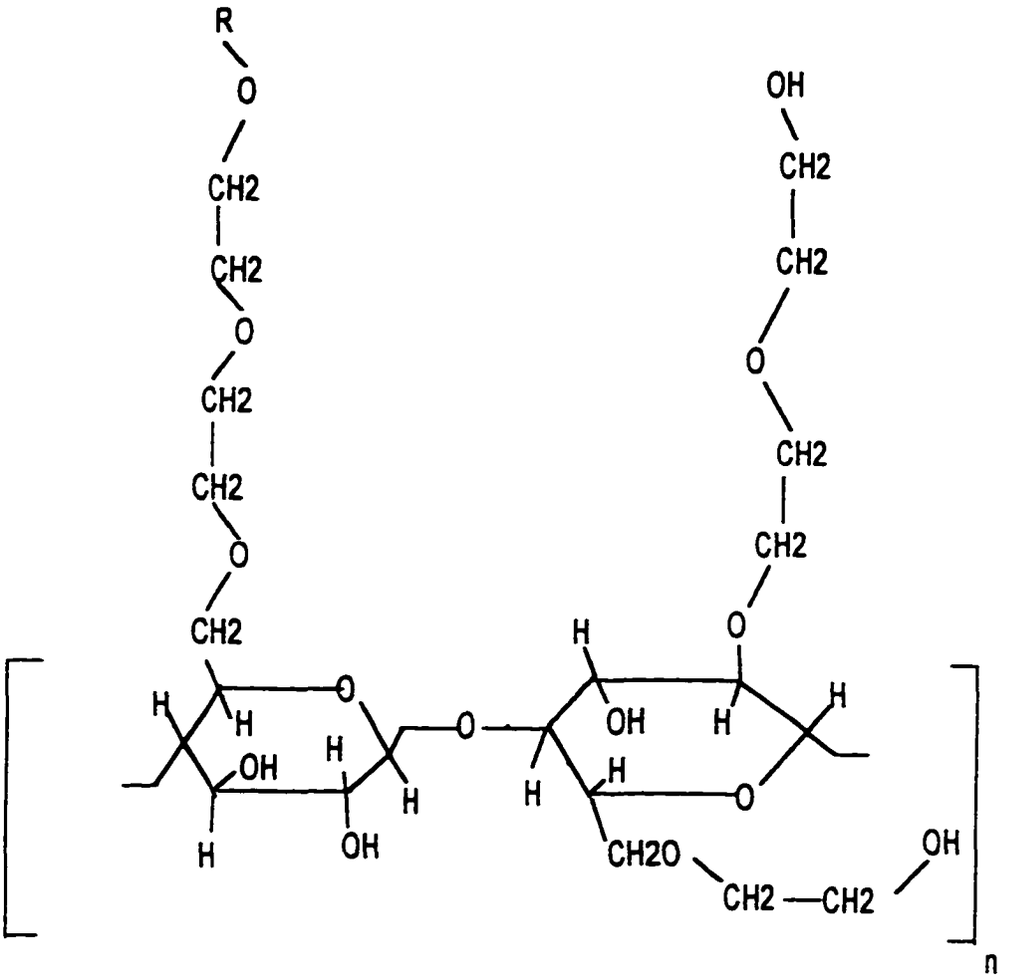

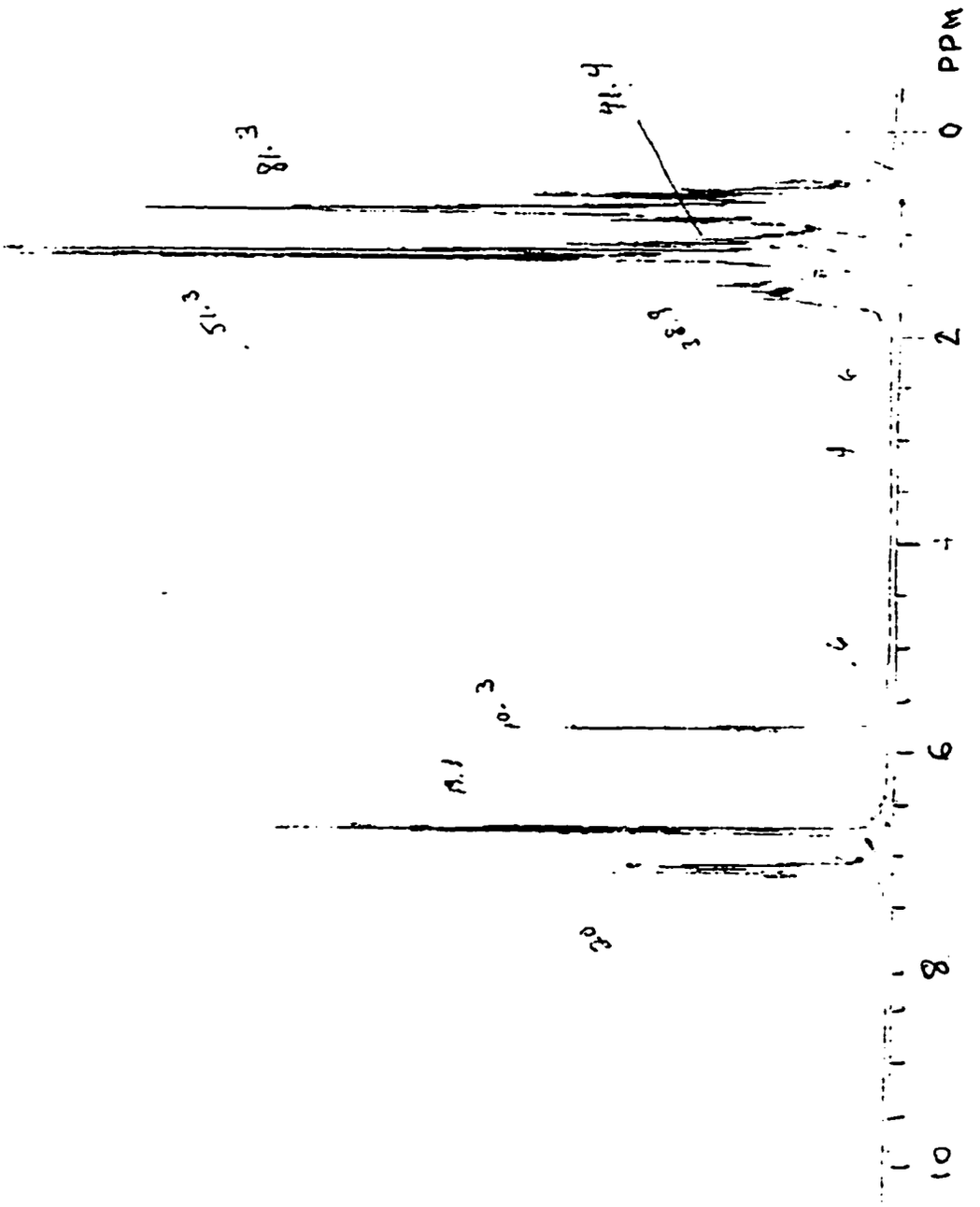

Figure 3.2 : ^1H NMR spectrum of nonyl-phenol (90% pure). (spectrum provided by Aldrich).

Figure 3.3 : Effect of strain rate (%) on G' (frequency = 6.3 radians/sec) of hydrogels made of (0.3 %HMHEC/(6.9 mM SDS) systems.

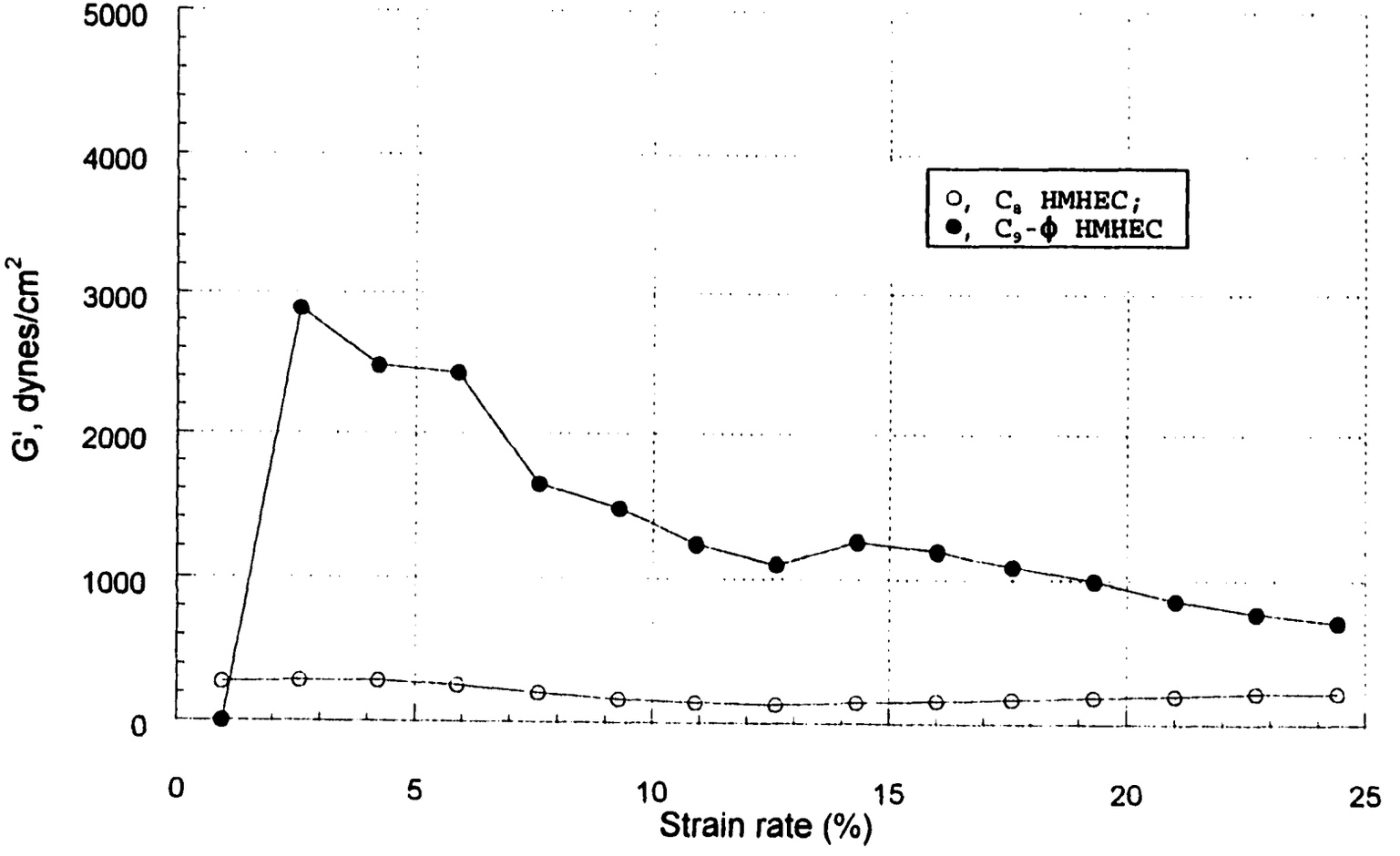

Chapter 4

Results and Discussion

Gel forming ability of HMHEC/surfactant systems was determined over a range of polymer and surfactant concentrations. Some systems form a single phase watery solution, while others form a watery supernatant with a viscoelastic hydrogel precipitate. We rated the characteristics of our HMHEC/surfactant systems on a scale of 1 to 5. For the purposes of these ratings, viscosity was assessed simply by eye (ratings 2 and 3). The precipitate phases in the two phase systems ranged from insoluble water-swollen polymer globules (rating 1) to a stiff viscoelastic hydrogel plug (rating 5). The quality of the hydrogel phase, which marks the difference between a rating of 4 (weak gel) and 5 (strong gel), was assessed by probing the precipitate with a spatula. A 4 means that the gel broke apart easily with gentle probing, while gels given a rating of 5 were strong enough to be lifted out of the container intact. Thus a rating of 1 means that the chain is collapsed and characterized by poor polymer/solvent interactions; systems rated 2 or 3 are homogeneous polymer solutions with (3) or without (2) some degree of intermolecular hydrophobic association; and gelled systems (4 and 5) are characterized by stable intermolecular mixed micelle-like aggregates composed of side chains plus

surfactant. The strength of the gel increases with both the number of intermolecular "bridging" aggregates, as for any viscoelastic material, and the number of side chains per aggregate [11], due to the severe restrictions such a configuration imposes on the number of states a polymer chain may occupy [33]. Thus for a strong (type 5) gel to form the polymer chains must be relatively expanded in the solvent initially with the hydrophobes free to associate. This requires that the side chains be highly compatible with the surfactant solution. Weak (type 4) gels form when the tendency for the side chains to interact in the bulk is finite but limited, either by a small total number of side chains, low polymer concentration, by the predominance of intramolecular interactions (driven by the polymer's incompatibility with the surfactant), or by an excess of surfactant which distributes itself among all the side chains, leading to a relatively low average number of side chains per microdomain.

We prepared phase diagrams (Figures 4.1 - 4.3 and Figure 4.48) on which the characteristics of various HMHEC/surfactant systems are given as a function of the system composition. These phase maps are modelled after those of Goddard [34]. Also shown on the Figures is the behavior of control systems containing HEC of the same molecular weight as the modified polymer in each case. On these diagrams each polymer is represented by a symbol, and the numeral under each symbol is

the rating, per Table 4.1. Each cluster of symbols represents systems with the same composition, which is given by the intersection of the grid lines passing nearest the cluster.

4.1 Effect of degree of hydrophobe substitution on phase behavior of C_{12} HMHEC in SDS and water.

The effect of hydrophobe level on the phase behavior of high DP C_{12}-substituted HMHEC solutions in SDS and water is shown in Figure 4.1. The control HEC forms one-phase watery solutions in SDS, and relatively viscous solutions in water. Thus pure water is apparently a better solvent for the HEC backbone than SDS solutions. The two relatively highly substituted HMHECs are insoluble in both water and SDS over the entire composition range studied, indicating that these high levels of side chain drive the polymer into a collapsed conformation. On the other hand, the 1.3% DS C_{12} HMHEC, containing 150 side chains/backbone, forms solutions in water and strong hydrogels in SDS. Thus as expected there is an optimum range of degree of substitution at which gel formation is favored in a given surfactant.

The analogous phase diagram for low DP C_{12}-substituted HMHEC solutions in SDS and water is shown in Figure 4.2. In common with the high DP material, the control polymer exhibits a higher viscosity in water than in SDS, again indicating that the backbone is relatively incompatible with the surfactant. The critical overlap concentration, c^*, of the backbone in

water is higher than that of the high DP HEC, as expected. As before, a high level (8.0% DS, 390 side chains/backbone) of side chains drives the HMHEC out of solution over the entire composition range studied. The least substituted polymer shown here (1.9% DS C_{12}, 80 side chains/backbone) is soluble in water, behaving in a manner analogous to that of HEC, but forms two phases with a weak gel over the entire composition range in SDS.

The low DP 4.3% DS C_{12} (210 side chains/backbone) HMHEC exhibits more complex behavior with system composition. This polymer is insoluble in water and also at low polymer and high SDS concentrations, conditions represented by the upper left quadrant of the phase diagram and characterized by values of $N>4$ (recall that N is defined as the ratio of the total number of surfactant molecules to the total number of side chains in the system). Elsewhere on the phase diagram $N<4$ and the system forms two phases with a weak gel. Hence $N=4$ can be regarded as the critical ratio below which gel formation occurs (N_{crit}).

The surfactant acts on the backbones and side chains in opposite ways. SDS drives the HEC moiety to collapse, but enhances the bulk solubility of the hydrocarbon side chains, driving the radius of gyration (r_g) up. Which of these two effects dominates will depend on both the polymer structure and the overall composition. With the HMHECs compared on Figure 4.2 it appears that the former effect dominates at high

DS, where the side chains tend to form intramolecular aggregates. This leaves the backbone exposed to the bulk solution, where its incompatibility with the surfactant contributes still further to its collapsed conformation. The latter effect dominates at low DS, where the polymer side chains are compatible with the surfactant. The intermediate (4.3%) DS polymer exhibits both realms of behavior, depending on the system composition. This polymer is relatively collapsed at high levels of SDS, indicating that under this condition intramolecular aggregates are favored, with relatively few side chains solubilized in the bulk phase. However when the ratio of surfactant to side chains in the bulk phase is appropriate it appears that r_g of this polymer in SDS is still sufficiently high that bridging aggregates can and do form.

By analogy to the behavior of this polymer, we expect to observe a critical value of N for other HMHECs as well. Although we did not observe a transition from insolubility to gel formation with any of our other polymers in the composition ranges studied, N_{crit} was estimated from the observed phase behavior, and is shown in Table 3.1 for all of the systems reported here. N_{crit} decreases with DS, for both the low and high DP polymers. Thus over the DS range used here the polymer concentration required for gelation increases with DS at constant SDS concentration as the polymer chains are driven to collapse. This is reasonable since in these

systems r_g of the polymer chains decreases with DS, inhibiting network formation. In view of the competing effects of side chain and backbone on r_g of HMHEC in surfactant solution, and given that for HEC (DS=0) the polymer concentration required for gelation is essentially infinite (because there can be no intermolecular hydrophobic association), it is likely that there exists an optimum DS at which this critical polymer concentration is minimized. The results in Table 3.1 also indicate that in general low DS polymers can form gels over a wider range of SDS concentration at a constant polymer concentration than high DS polymers, which prefer a relatively collapsed conformation.

Another important conclusion we derive from the results in Table 3.1 is that regardless of DP and hydrophobe structure, a side chain content >/=390 side chains/backbone renders HMHEC incompatible with both water and SDS over the composition range in this study; all polymers with </=210 side chains/backbone formed gels over at least part of our composition range. Within that range, the DP of the polymer is more important than DS in determining gel quality, and even at constant DP gel quality does not scale with DS. A similarly weak effect of DS on interactions with surfactant has been seen in other studies on a nonionic HMWSP (hydrophobically modified poly(N-isopropylacrylamide) [20].

4.2 Effect of side chain structure on phase behavior and rheological properties of HMHEC/SDS systems.

The effect of side chain structure on the phase behavior of HMHEC/SDS systems is shown in Figure 4.3. On this figure we compare three polymers, viz. 4.3% DS C_{12}, 4.5% DS C_9-ϕ, and 2.1% DS C_8, (designations E, G, and H) containing, respectively, 210, 200, and 130 side chains/backbone. The C_{12} polymer results are the same as those plotted on Figure 4.2. Several interesting features can be seen here. First, the C_{12} polymer forms the weakest gels, and is the only one that is incompatible with surfactant within the composition range studied. Thus this polymer assumes the most collapsed conformation of the three. Clearly this cannot be attributed to its side chain content. Rather, the linear C_{12}- group is the least water-soluble of the three hydrophobes compared here. A qualitative comparison of the solubilities of the three hydrophobes was obtained from the effect of hydrophobe structure on the cmcs of surfactants. The cmcs of sodium dodecyl sulfonate, sodium nonyl benzene sulfonate having branched hydrocarbon chain (note that the hydrocarbon chain of C_9-ϕ is branched [35]) and sodium octyl sulfonate are 9.8, 15.7 and 153 mM [36] respectively, at 25 C. This suggests that the dodecyl hydrocarbon chain is the least soluble of the three hydrophobes since typically, for a given headgroup, we expect the cmc to scale with the solubility of the hydrophobic part of the surfactant.

The hydrogels obtained from the C_8 and C_9-ϕ HMHECs were characterized in more detail with respect to gel volume, total

polymer concentration in the gel, dynamic rheological properties and hydrophobicity measurements.

4.2.1 Gel Volume

Gel volume increases with an increase in polymer concentration. Gel volume results for the C_8 and C_9-ϕ HMHEC hydrogels (for 3.5 and 6.9 mM SDS) are shown in Figures 4.4 and 4.5. The error bars represent the standard deviation obtained by 4 independent samples. It is difficult to interpret the volume results since we expect the gel volume to depend on the composition parameter (N, as defined earlier), polymer configuration, bridging aggregate concentration and composition in a non-linear way. Nevertheless, we plotted the volume of the gels in terms of the only one of the above parameters available to us, viz. N. The plot is shown in Figure 4.6. Clearly, gel volume does not exhibit a systematic trend with N.

4.2.2 Concentration of polymer in the gel

Both polymer and surfactant are expected to partition between the gel and supernatant phases in our systems. The partition coefficient was estimated from the viscosity of the supernatant solutions and comparison of these values to the calibration curves giving the viscosity of each polymer in water (Figure 4.7-4.9). This calibration, however, is imperfect in that the supernatant contains some surfactant. However, at low levels of polymer the effect of surfactants is to promote intermolecular interactions [9-12], thereby

increasing the solution viscosity relative to the case in pure water. Therefore, the estimates we obtained for the polymer concentration in the supernatant represent the upper bound for the polymer concentration in that phase. Knowing the upper bound allowed us, by conducting a mass balance over the gel and supernatant system, to evaluate the lower bound of polymer in the gel phase. Our results indicate that the maximum error in determining the polymer concentration in the gel, by assuming that all the polymer in the system resides in the gel phase is 0 % for the C_9-ϕ systems and 12 % for the C_8 systems.

Polymer concentration in the gel as a function of bulk polymer concentration for the C_8 and C_9-ϕ hydrogels (at 3.5 and 6.9 mM SDS) is shown in Figure 4.10 and 4.11 respectively. The error bars in Figure 4.10 represent the range of polymer concentrations possible for the C_8 hydrogels and all the data points in Figure 4.11 represent the total polymer concentration in the C_9-ϕ hydrogels. Polymer concentration in the gel increases with an increase in bulk polymer concentration, except for the case of HMHEC/3.5 mM SDS system in which case the polymer concentration in the gel exhibit a peak. We also plotted the data as a function of N (Figure 4.12). No systematic trend is seen for either the C_8 HMHEC/SDS or the C_9-ϕ HMHEC/SDS systems. One parameter which might be responsible for dictating the polymer concentration in the gel is ratio of number of SDS molecules in the gel to the number of polymer side chains in the gel. Suggestions on

how to estimate this parameter are given in chapter 5.

4.2.3 Rheology of C_s/SDS and C_s-ϕ/SDS gels

Rheological spectra of hydrogels of C_s/SDS systems are shown in Figures 4.13 - 4.20, showing frequency (ω, radians/sec) sweeps of the dynamic storage (G', dynes/cm^2) and loss (G", dynes/cm^2) moduli, clearly demonstrating the viscoelastic behavior of our gels. The error bars give average G' and G" of duplicate gels, and demonstrate the excellent reproducibility of our materials. The effect of C_s polymer concentration on G'_0, defined as the average G' (in the G' vs ω spectrum) in the region where G' is invariant with ω (typically occurring in the range ω = 29-61 radians/sec), is shown in Figure 4.21. The different behavior seen at the two surfactant concentrations could not be attributed to polymer concentration within the gel phase (Figure 4.22, the x axis error bars represent the range of polymer concentrations possible in the gels) or to N (Figure 4.23). Thus the rheological properties of the gels cannot be predicted from either the bulk or gel phase concentration of polymer. This has been observed in other studies as well [13]. Rather, the ultimate conformation of the polymer in the gel is a consequence of the diverse effects of polymer/surfactant interactions in the bulk solution prior to gel formation, and the resulting conformation of the polymer. For example, at 0.3 g/dL polymer in 6.9 mM SDS, where the ratio of surfactant molecules to side chains, N, is =12.4,

there are relatively few side chains available, and they are swamped with surfactant. Thus only a loose network forms, with G'_0=278±26 dynes/cm^2. At 1.2 g/dL polymer in 6.9 mM SDS, the parameter N=3.1. In this case each aggregate must contain more total side chains on average, and the network is stronger (G_0=4662±270 dynes/cm^2). At lower surfactant concentration (3.5mM), where N in our systems ranged from 1.6-6.3, the "swamping" effect is not seen in the polymer concentration range studied. However, G_0 does not climb as high and indeed drops off at high polymer concentration, perhaps due to insufficient surfactant at this high concentration of side chains.

Rheological properties of the C_9-ϕ hydrogels are shown in Figures 4.25 - 4.32. In common with the C_8/SDS gels, the C_9-ϕ are viscoelastic. A plot of G'_o (determined as for the C_8 gels) vs bulk polymer concentration for 3.5 and 6.9 mM SDS is shown in Figure 4.33. G'_o exhibits a peak with polymer concentration, occurring at 0.55 g/dL for 6.9 mM SDS. No such peak was observed for 3.5 mM SDS. In general for a given concentration of surfactant the C_9-ϕ gels are stronger than the C_8 gels, by a factor ranging from ~3-9. This probably reflects the higher degree of substitution of the C_9-ϕ polymer. The ratio N in these systems ranged from 1.3-5.3 in 3.5 mM SDS and 2.6-10.4 in 6.9 mM SDS. Here again, we found no consistent correlation of G'_o with bulk composition, polymer concentration in the gel (Figure 4.34), or N (Figure

4.23). The entire gamut of possible interactions may be seen in the high SDS concentration C_9-ϕ gels. At low polymer concentration the relatively few side chains are swamped with surfactant and the resulting gel is weak. At high polymer concentration it may be that the high level of surfactant drives the polymer chains out of solution, i.e. into a collapsed conformation which does not favor formation of a strong gel.

Recently Piculell, et. al. [37] analyzed data on HMHEC/surfactant systems previously published by Tanaka, et. al. [12] and determined that the value of the parameter β_{max}, defined as the surfactant to side chain ratio in the microdomains where G' is maximized, has a uniform value of 3 for a range of anionic and nonionic surfactants. This applied for systems with C_{12}-C_{18} substituted HMHECs with a DS of 1% and present at a constant concentration of 2% w/w with varying surfactant concentrations, and the systems formed homogeneous gels rather than precipitated gel plugs. Nevertheless it does provide us with a starting figure for comparison. With our C_8 polymer N=3 at ~0.7 % HMHEC in 3.5 mM SDS and ~1.3% HMHEC in 6.9 mM SDS. Inspection of Figure 4.21 reveals that these concentrations may in fact represent the optima with respect to G'_0. The agreement is not as good with the C_9-ϕ results, where N=3 at ~.5% polymer in 3.5 mM SDS and at ~1.1% polymer in 6.9 mM SDS. From Figure 4.33, these values are not as good predictors of the location of the maximum in G'_0. Note that

our ratio N was calculated based on the overall system composition rather than the gel phase composition, so it does not correspond exactly to the parameter ß. Nevertheless, the values are in the same ball park and suggest that all HMHEC/surfactant gels have both bulk and microstructural features in common. We also plotted our data as a function of Ngel or ß (Figure 4.24). N_{gel} was obtained by assuming that $[SDS]_{gel} = [SDS]_{bulk}$. As seen the values of N_{gel} for which the gel strength peaks are 1.3 and 1.8 for the C_8 and C_9-ϕ HMHEC/SDS systems. These values do not correlate well with the number obtained by Piculell et. al., viz. 3. The discrepancy might be due to our assumption of $[SDS]_{gel} = [SDS]_{bulk}$, or the other considerations mentioned above while comparing our results with Piculell et. al..

4.2.4 Hydrophobicity of gels

We characterized our gels in terms of the degree of hydrophobicity using pyrene as a polarity sensitive probe. The fluorescence spectra of pyrene solubilized in our systems are shown in Figures 4.35 to 4.41. The I3/I1 results for the control polymer (HEC)/SDS system as a function of polymer concentration at 0, 3.5 and 6.9 mM SDS are shown in Figure 4.42. Note that I3/I1 of pyrene is 0.61 in pure water and is 0.91 in an aqueous solution of SDS micelles. Thus all the HEC/SDS solutions are more hydrophobic than water and all except the solution containing 1.2g/dl HEC and 3.5 mM SDS are

less hydrophobic than a solution of SDS micelles. Note that this does not imply that there are HEC/SDS interactions, but rather that SDS influences the conformation and environment of HEC. At high SDS concentration (6.9 mM SDS), the hydrophobicity of the HEC/SDS solutions is invariant with polymer concentration. In the case of low SDS concentration (0 and 3.5 mM SDS), more data points are needed to ascertain the trend. From the few polymer concentrations at which I conducted experiments it is not clear whether I3/I1 of pyrene in the HEC/SDS solutions increases monotonically with an increase in polymer concentration or whether the hydrophobicity increases sharply at a certain polymer concentration (0.3 - 0.8 %). Experimental data between 0.3 - 0.8 % is required to ascertain which of the two trends is true. Nevertheless the fact that pyrene senses a more hydrophobic environment in HEC/(water or SDS) solutions than water can be explained as follows. In HEC/(water or SDS) solutions, apart from being solubilized in water, pyrene is also solubilized in the disordered water environment [38] at the HEC chain/water interface. The data also suggest that pyrene experiences a more hydrophobic environment at low SDS as compared to a high SDS concentration. This trend may be because at high SDS concentration HEC is more collapsed and thus fewer solubilization sites are available for pyrene at the polymer/water interface.

The I3/I1 results for the C_8 and C_9-ϕ HMHECs are shown in

Figures 4.43 and 4.44 respectively. The error bars represent the range of I3/I1 obtained for two identical gels. The hydrophobicity of the gels lies between that of water and SDS micelles. Note that the pyrene signal observed is a weighted average of the signal from all the sites where pyrene is solubilized. The possible sites in the gels where pyrene can be solubilized are free water, disordered water at the polymer backbone/water interface [38], surfactant "bridging" intermolecular aggregates, intramolecular aggregates, and surfactant micelles if present. It is not possible to decouple the effect from the different sites. The data suggest that our gels contain hydrophobic sites. However, no structural information can be inferred from the data. We plotted the data as a function of polymer concentration in the gel (Figure 4.45 and 4.46) and N (Figure 4.47). These plots do not provide any further insight. In conclusion, we found the pyrene data difficult to interpret. Also, we were not able to correlate the hydrophobicity data with the rheology data. This is because of the above mentioned solubilization sites for pyrene, only the surfactant "bridging" intermolecular aggregates are involved in giving rise to rheological properties. Thus the hydrophobicity and the rheological properties stem from different sites within the gel and hence the two properties cannot be correlated.

4.3 Effect of surfactant structure on the phase behavior of C_8 HMHEC

The effect of surfactant structure on the phase behavior of the C_8 substituted polymer (polymer H) is shown in Figure 4.48. The three surfactants studied were sodium dodecyl sulfate (SDS), sodium octyl-1-sulfate (SOS), and sodium octyl-1-sulfonate (SS), with critical micelle concentrations (cmc) of 8, 133 and 153 mM respectively. Polymer H was selected for this study because its side chains are identical to the tail groups of the two octyl surfactants studied and because the polymer forms good gels in SDS. Note that the vertical axis in Figure 4.48 gives the surfactant concentration normalized by the cmc. HEC forms watery (type 2) solutions in all three surfactants.

The effect of surfactant tail group length on the gel forming ability and gel quality of polymer H/surfactant systems can be seen by comparing the results with SDS and SOS. In SDS strong gels (type 5) form at all compositions studied. However, in SOS strong gels form far from the cmc, but the gel strength goes down as the cmc is approached. The better gel forming ability and gel strength of SDS as compared to SOS may be attributed to the fact that SDS is more surface active than SOS, as seen by comparing the cmcs of the two surfactants, viz. 8 mM for SDS vs 133 mM for SOS (note that surface activity of a homologous series of surfactants is inversely related to cmc). Recall that a similar finding was reported by Tanaka et. al. [12] when they were discussing the effect of surfactant tail length on the rheological properties of HMHEC

solutions, viz. with an increase in the tail length the tendency of surfactants to self-assemble increases.

The effect of surfactant head group structure on the gel forming ability and gel quality of polymer H/surfactant systems can be seen by comparing the results with SOS and SS. In SS weak gels (type 4) form throughout the composition range studied. The better gel forming ability and gel strength of SOS as compared to SS may be attributed to the electrochemical properties of the two head groups. The sulfate group is more electronegative, and thus more polar, as compared to the sulfonate group. Hence for a given hydrocarbon chain length, sulfate surfactant is more amphiphilic than a sulfonate one, due to the larger differential between the hydrophobic and hydrophilic characters in case of sulfate than sulfonate. Thus SOS is more likely to bind to polymer side chains than SS, resulting in better gel quality.

The above arguments can be reinforced by realizing that the Y-axis in Figure 4.48 gives the surfactant concentration normalized by the cmc. Thus by comparing different C_8/surfactant systems at the same point on the Y axis one is comparing systems containing different surfactant concentrations. Specifically, at any point on the Y-axis, [SS]=1.1*[SOS]=19*[SDS]. Due to the concentration differences the "surfactant-bridged" intermolecular aggregates (which are charged due to the presence of ionic surfactants) present in the case of SDS systems experience a much lower shielding

effect than the SOS or SS systems. This is because the surfactant concentration and hence the counterion concentration is much lower in case of SDS as compared to SS or SOS, as explained above. Due to the low shielding experienced by the intermolecular aggregates in case of SDS system, the polymer chains are more extended in SDS systems than in case of SOS or SS systems. Thus more polymer side chains are available for aggregation in case of SDS systems and thus the hydrogels formed are the strongest among the three systems compared.

Figure 4.1 Phase behavior of high DP C_{12} substituted HMHEC in SDS and water, showing the effect of hydrophobe level: ×, high DP HEC (0 C_{12}); ○, polymer A (1.3 % C_{12}); □, polymer B (4.2 % C_{12}); ▽, polymer C (8.0 % C_{12}).

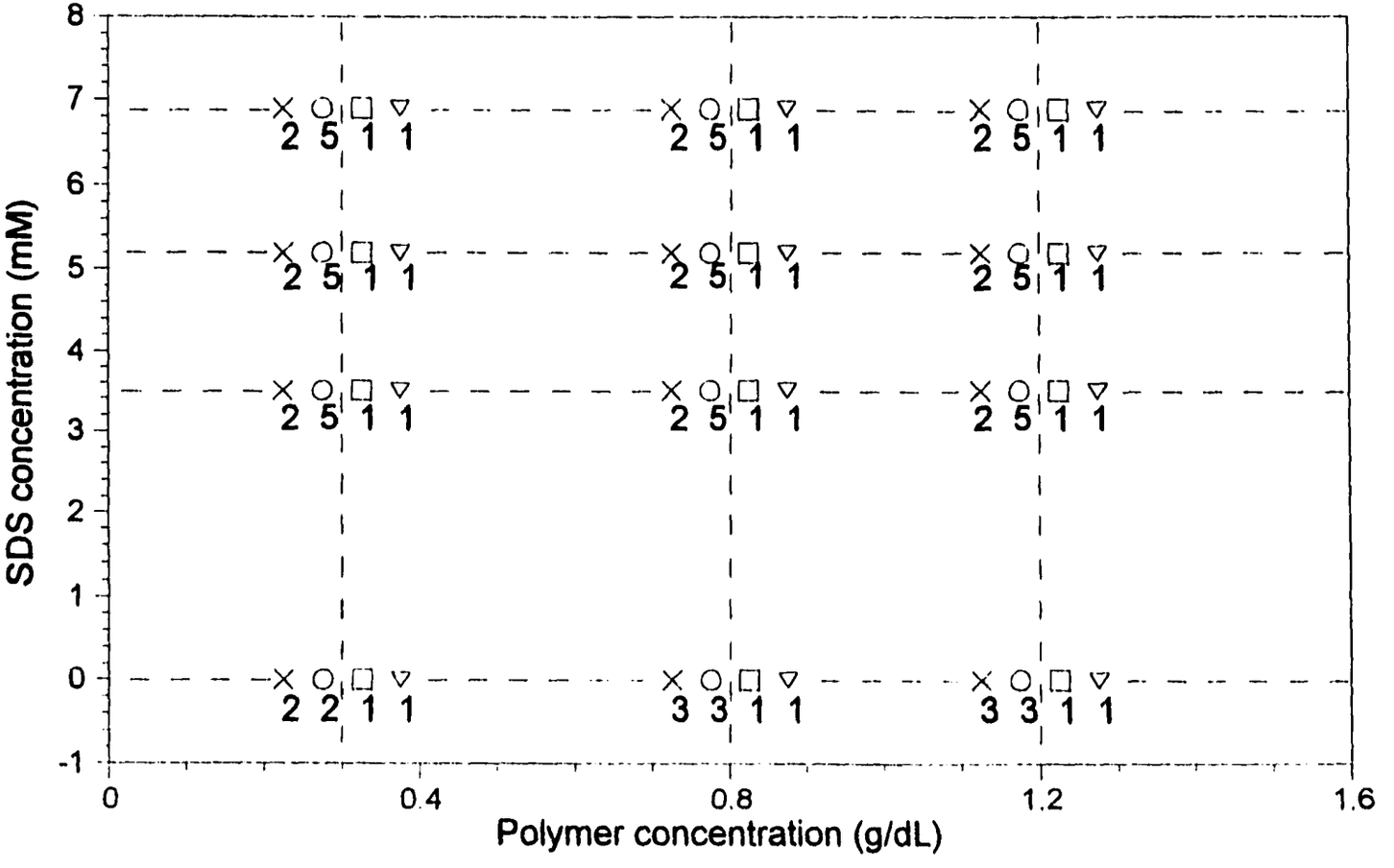

Figure 4.2 Phase behavior of low DP C_{12} substituted HMHEC in SDS and water, showing the effect of hydrophobe level: ×, low DP HEC (0 C_{12}); ○, polymer D (1.9 % C_{12}); □, polymer E (4.3 % C_{12}); ▽, polymer F (8.0 % C_{12}).

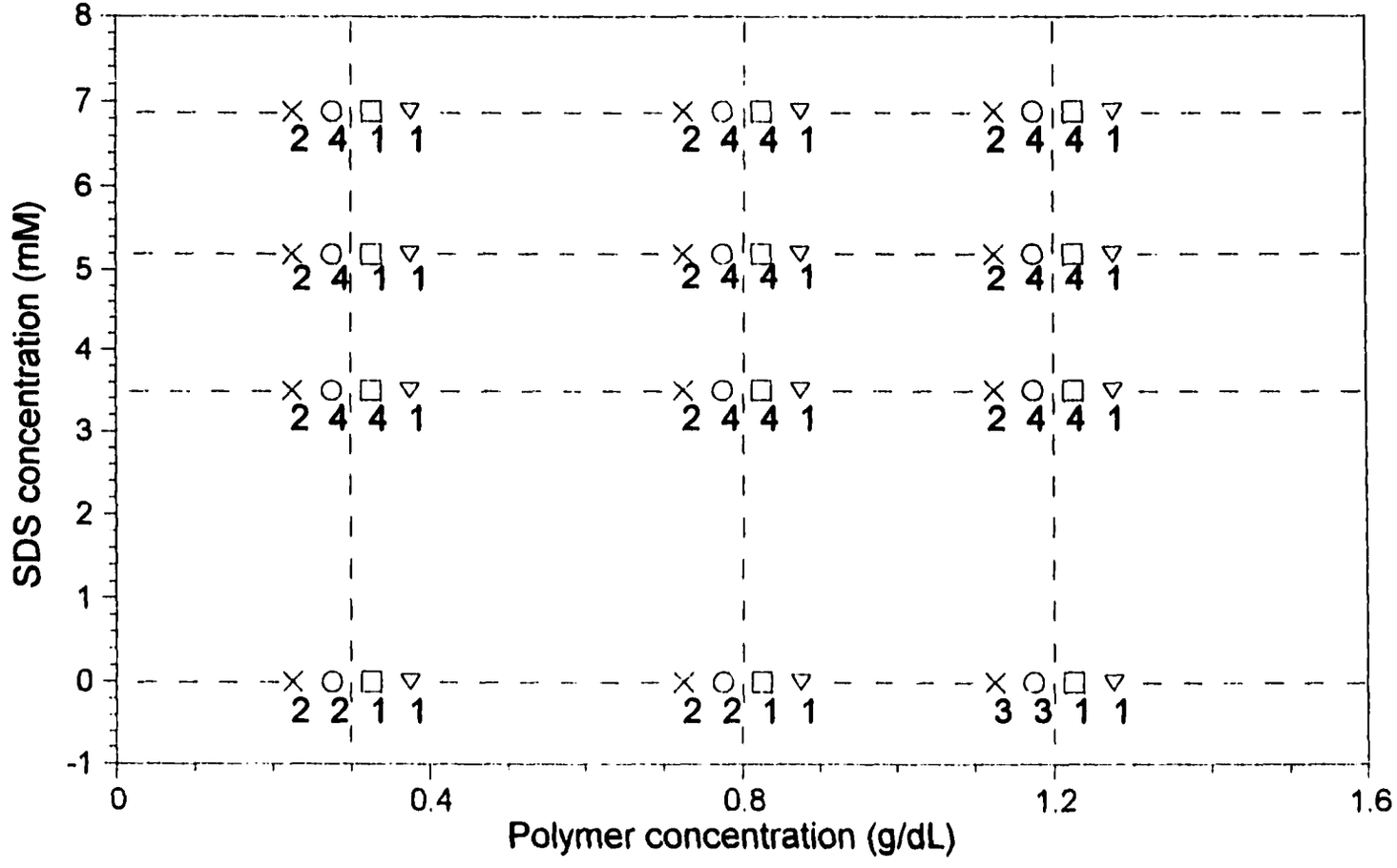

Figure 4.3 Phase behavior of low DP HMHECs in SDS and water as a function of hydrophobe structure: ○, polymer E (4.3 % C_{12}); □, polymer G (4.5 % C_9-ϕ); ▽, polymer H (2.1 % C_8).

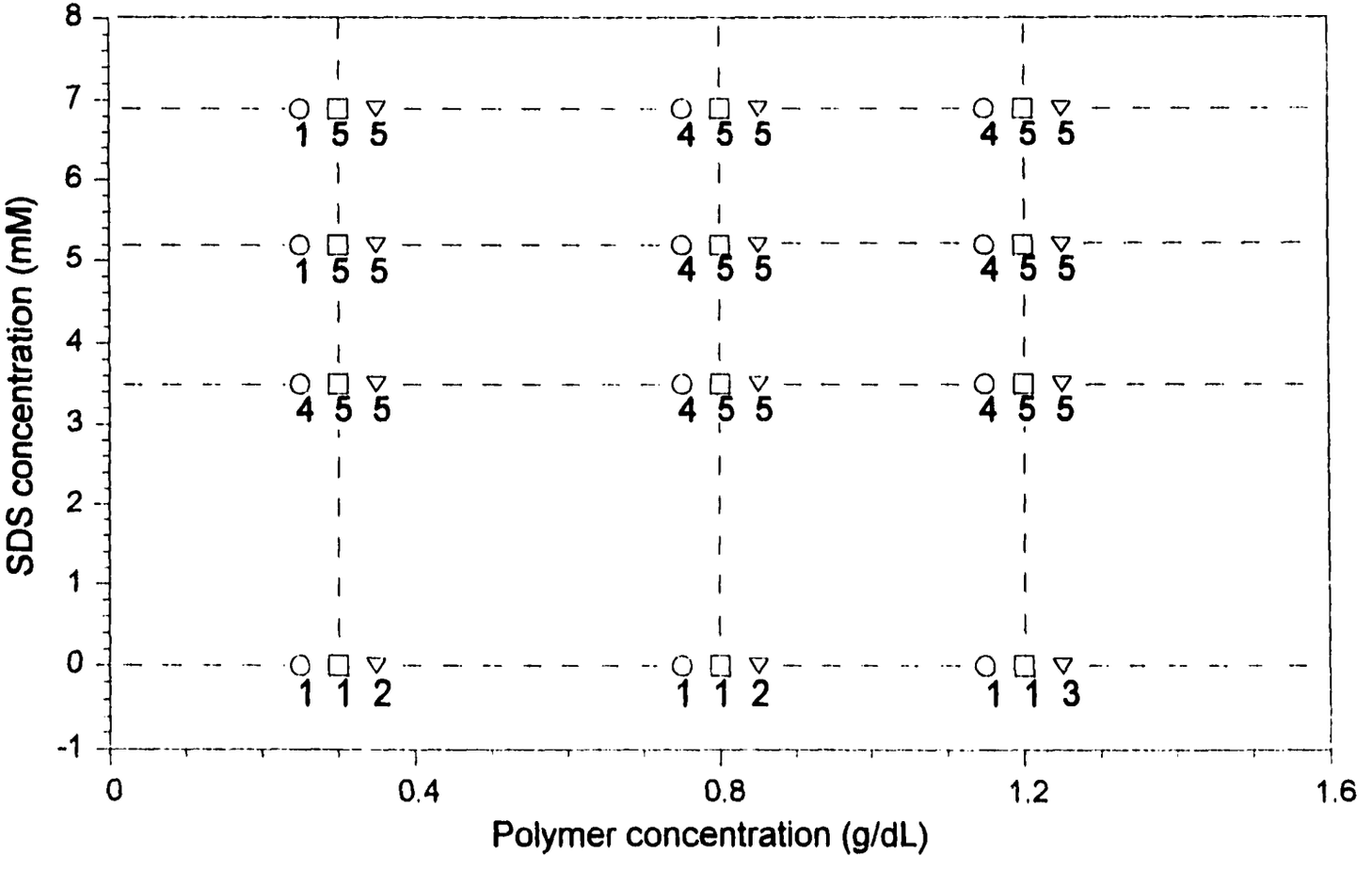

Figure 4.4 : Viscosity calibration curves for C_8 HMHEC/water solutions and viscosities of supernatant solutions of C_8 HMHEC/(3.5 mM SDS) systems.

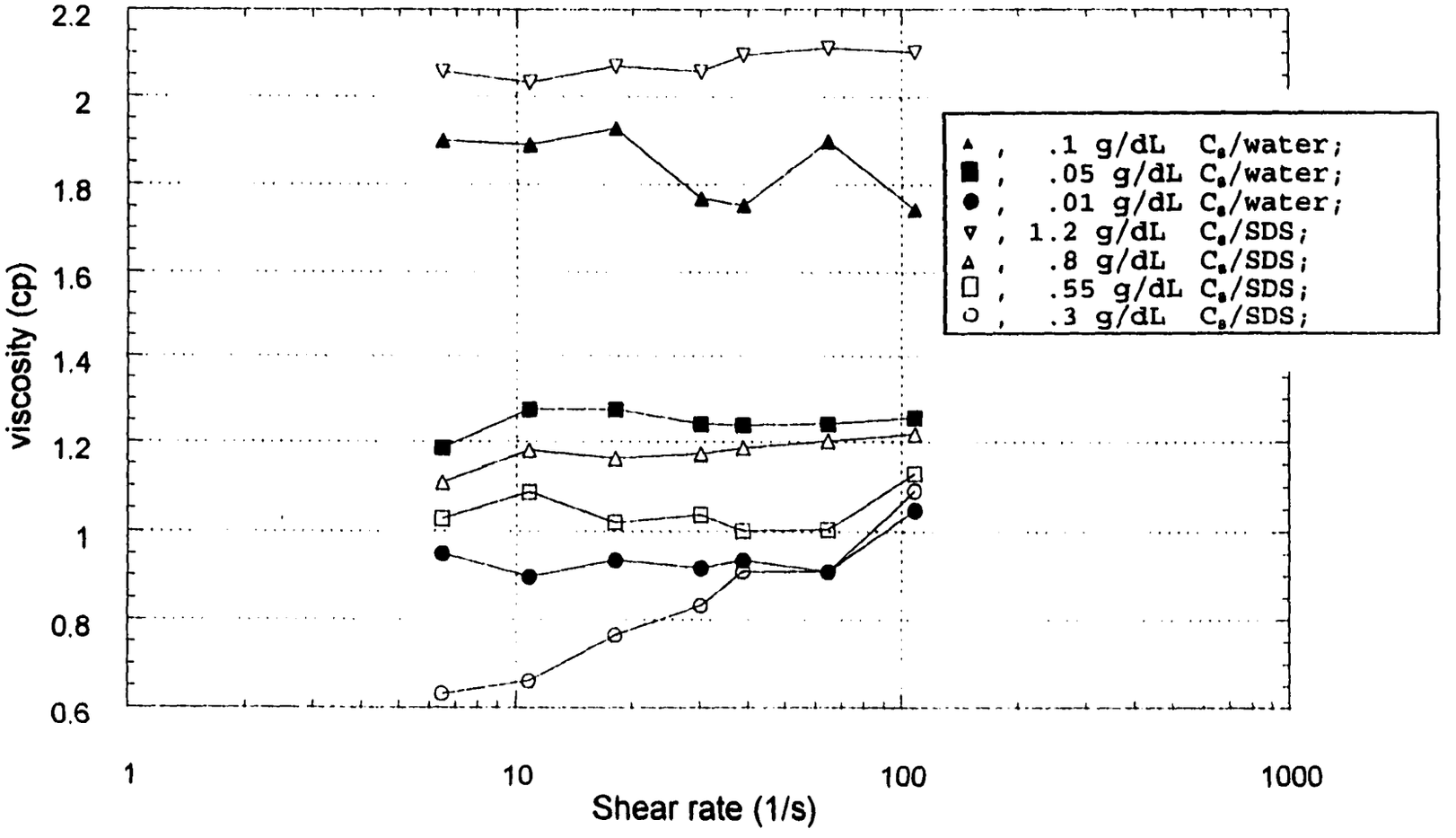

Figure 4.5 : Comparision of viscosities of supernatant solutions of C_s HMHEC/(6.9 mM SDS) systems and C_s HMHEC/water solutions.

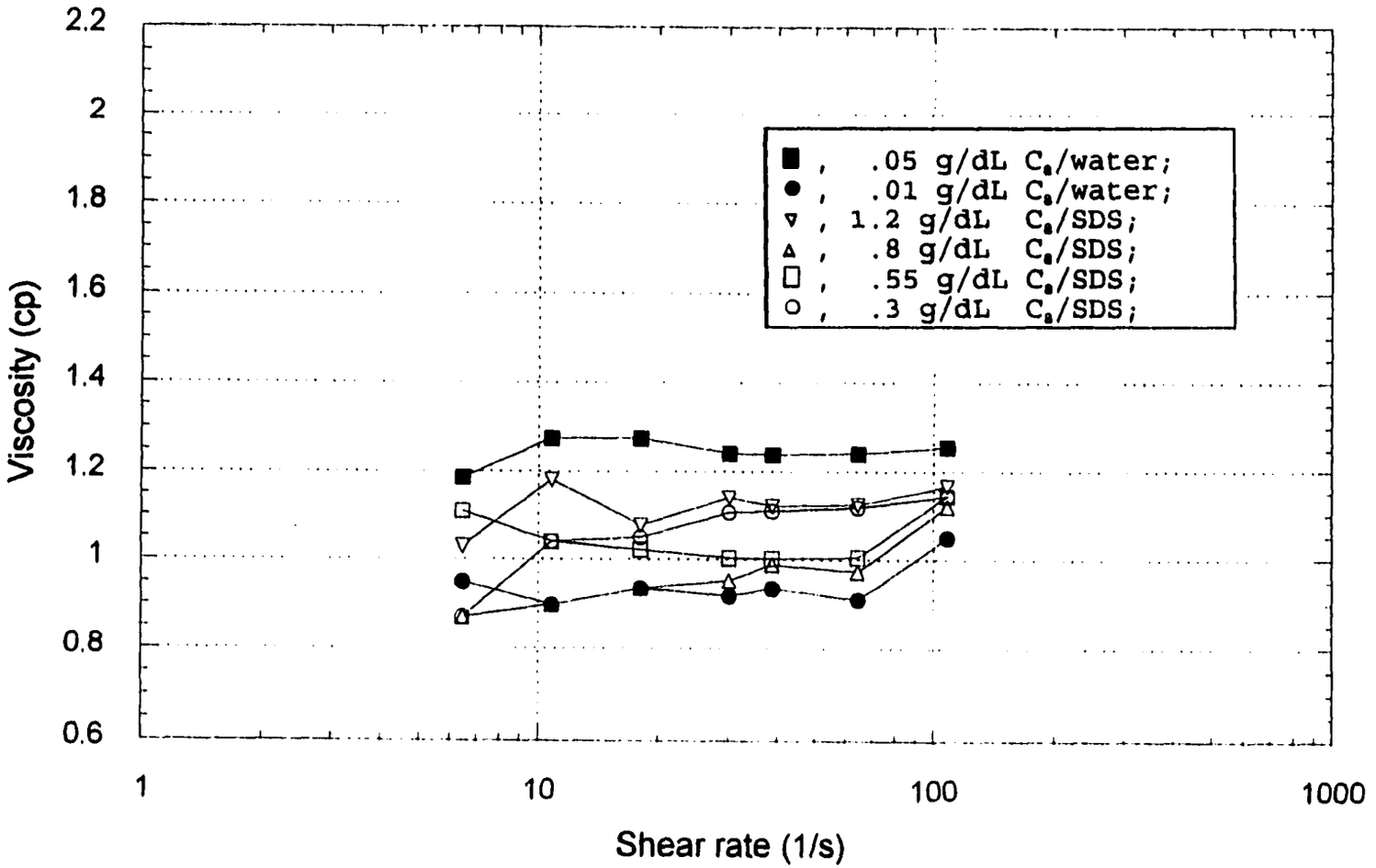

Figure 4.6 : Viscosities of supernatant solutions of C_9-ϕ HMHEC/SDS systems.

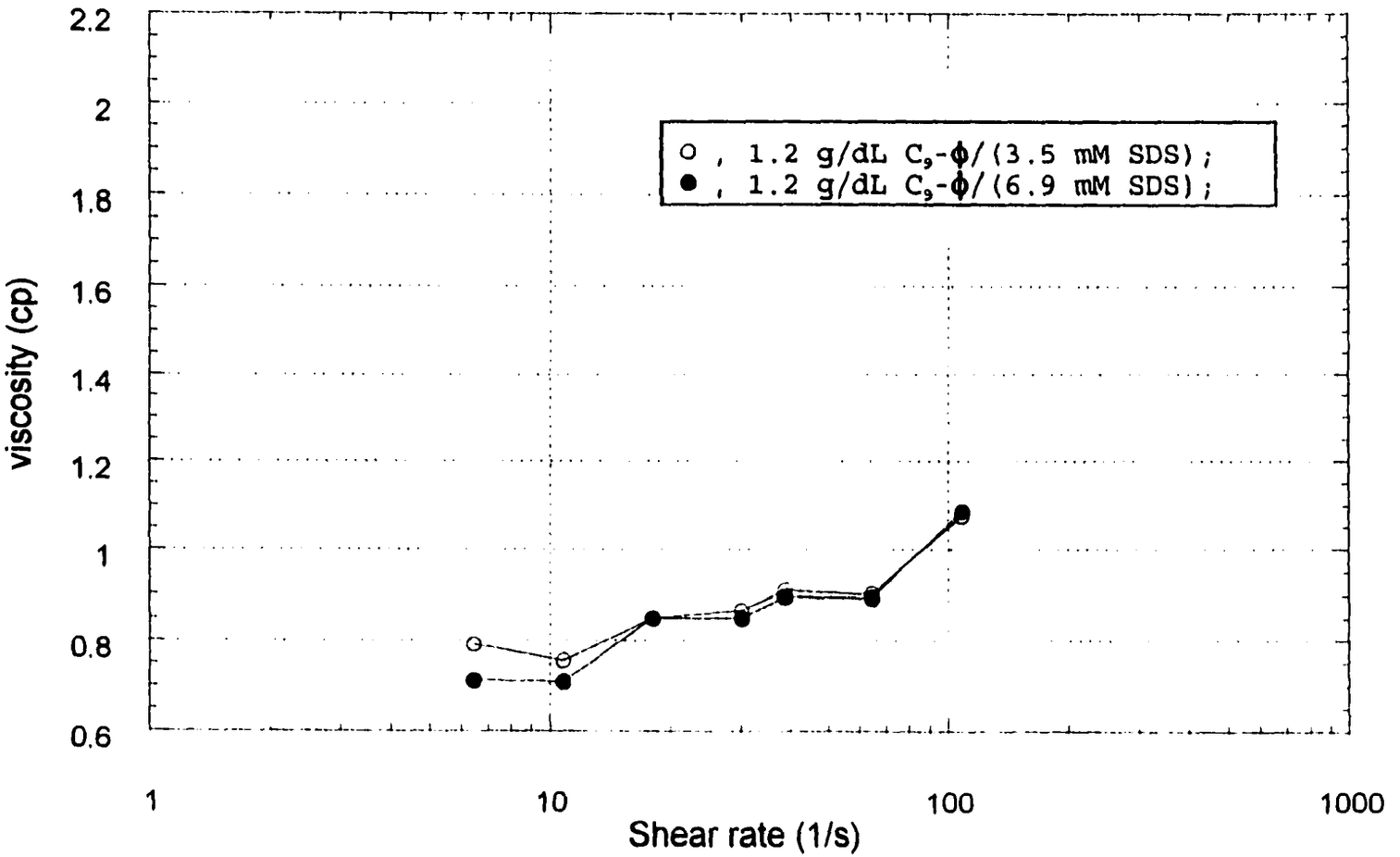

Figure 4.7 : Effect of bulk polymer concentration on polymer concentration in the gel phase of C_8/SDS systems.

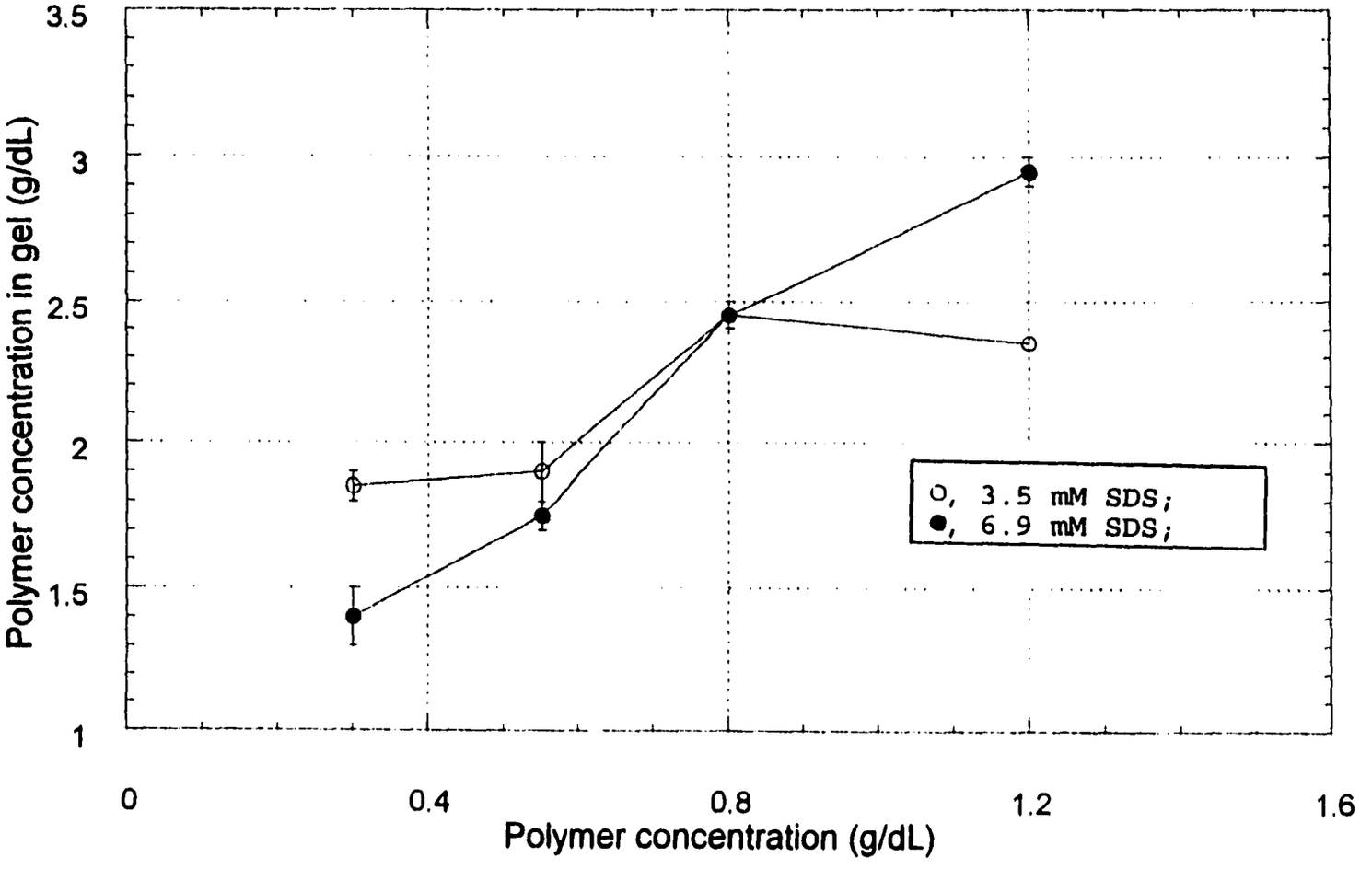

Figure 4.8 : Effect of bulk polymer concentration on polymer concentration in the gel phase of C_9-ϕ/SDS systems.

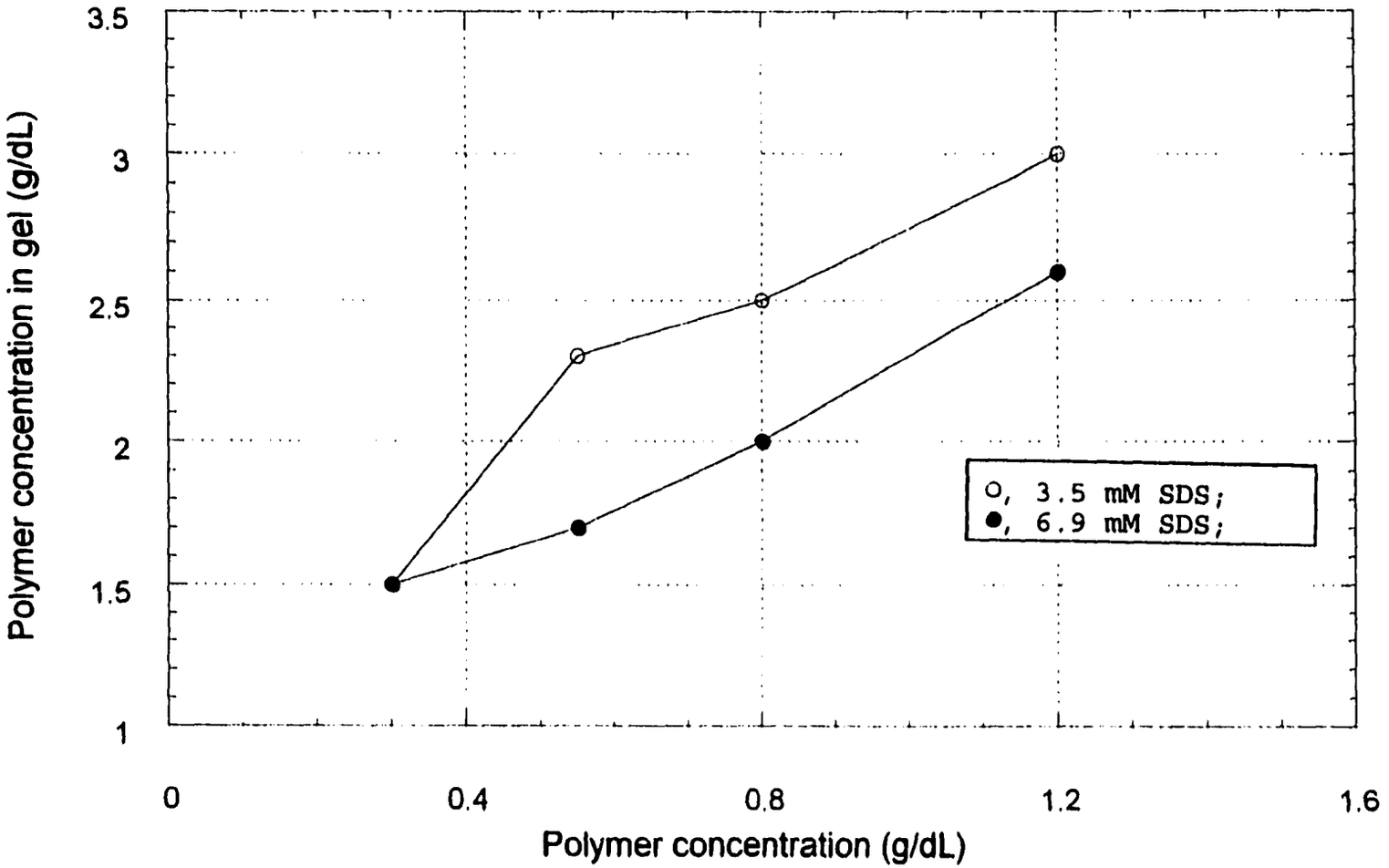

Figure 4.9 : Effect of bulk composition (N) on polymer concentration in the gel phase. Open symbols 3.5 mM SDS, closed symbols 6.9 mM SDS systems.

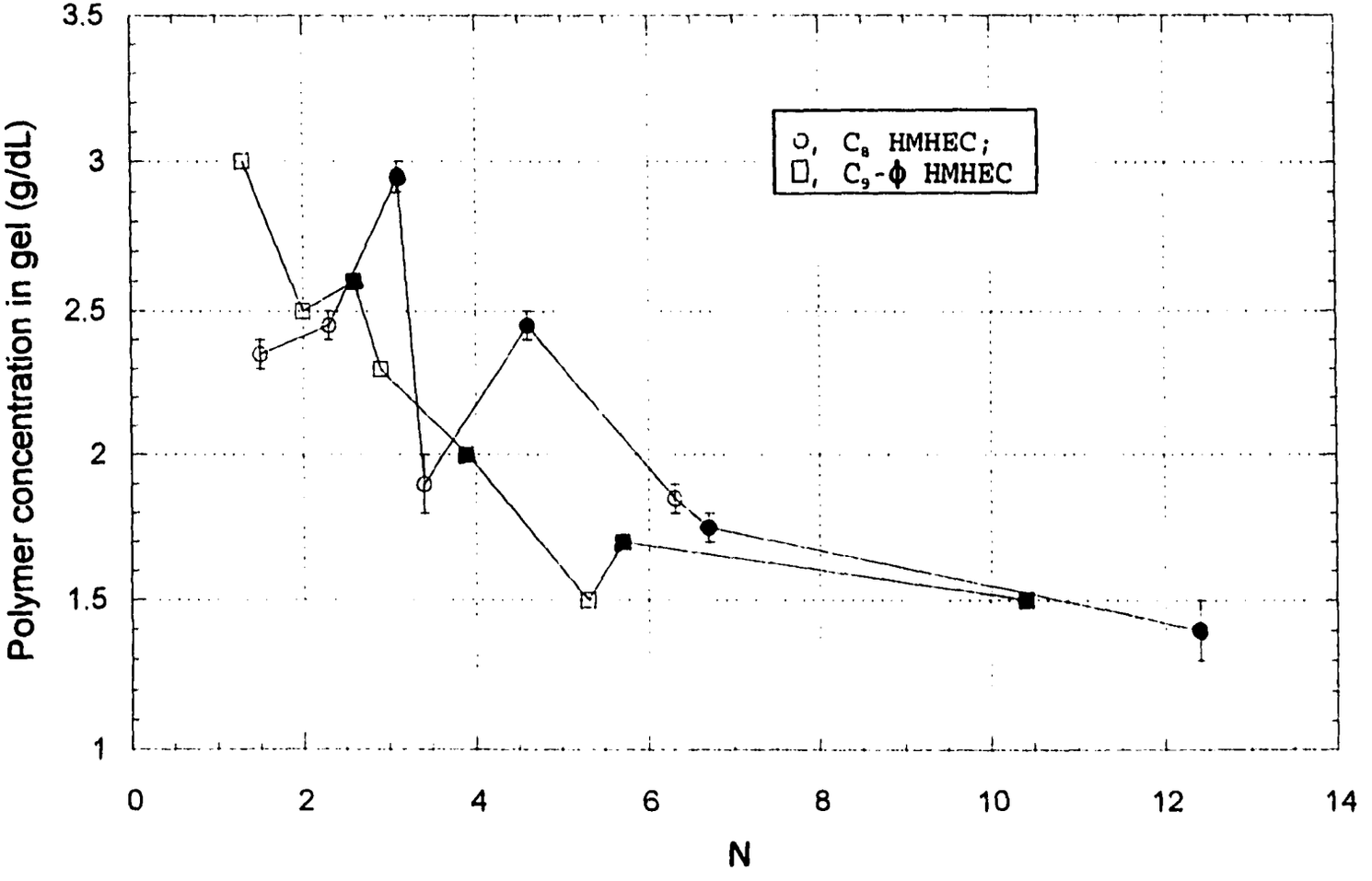

Figure 4.10 : Effect of bulk polymer concentration on gel volume of C_8 HMHEC/SDS systems.

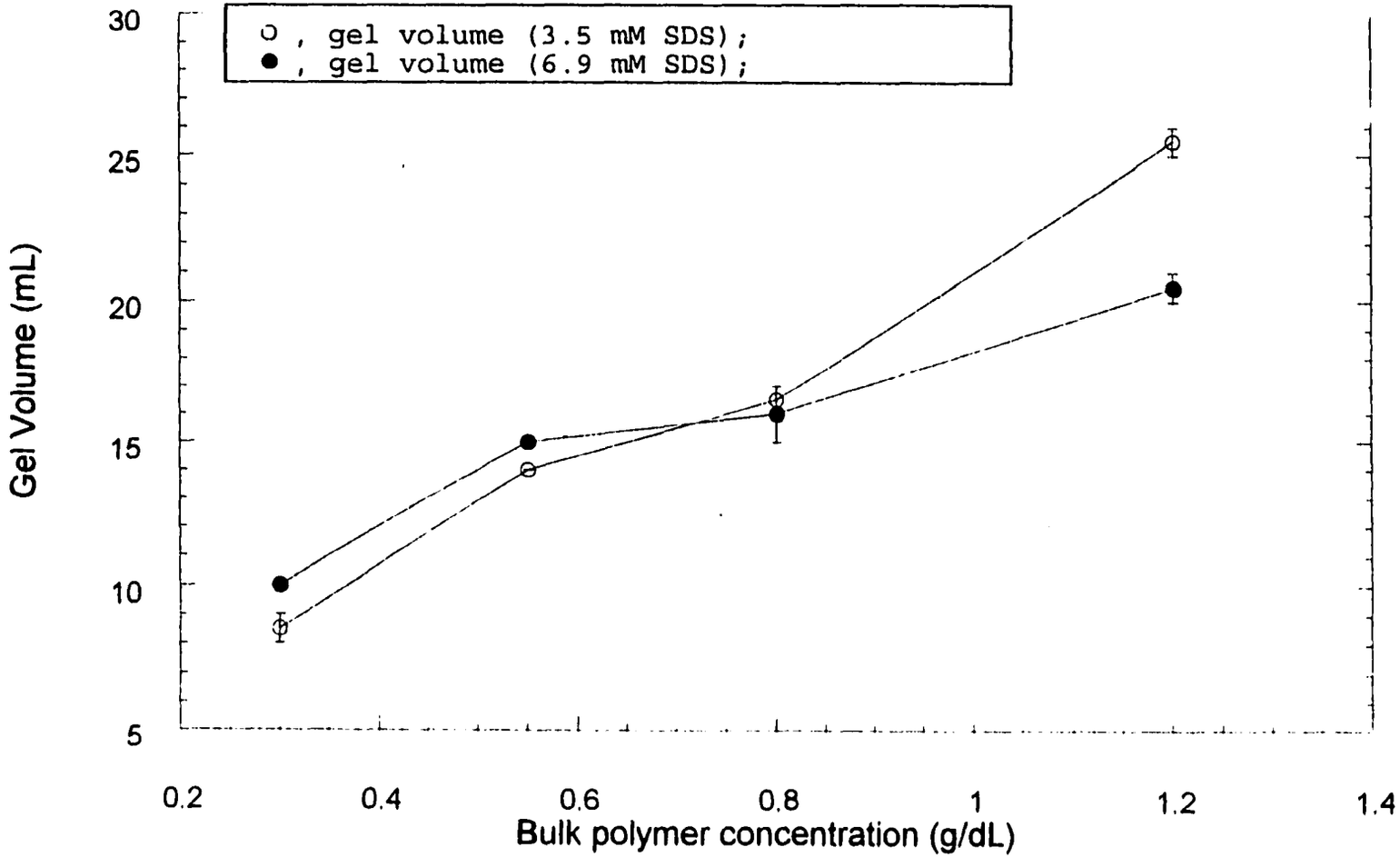

Figure 4.11 : Effect of bulk polymer concentration on gel volume of C_9-ϕ HMHEC/SDS systems.

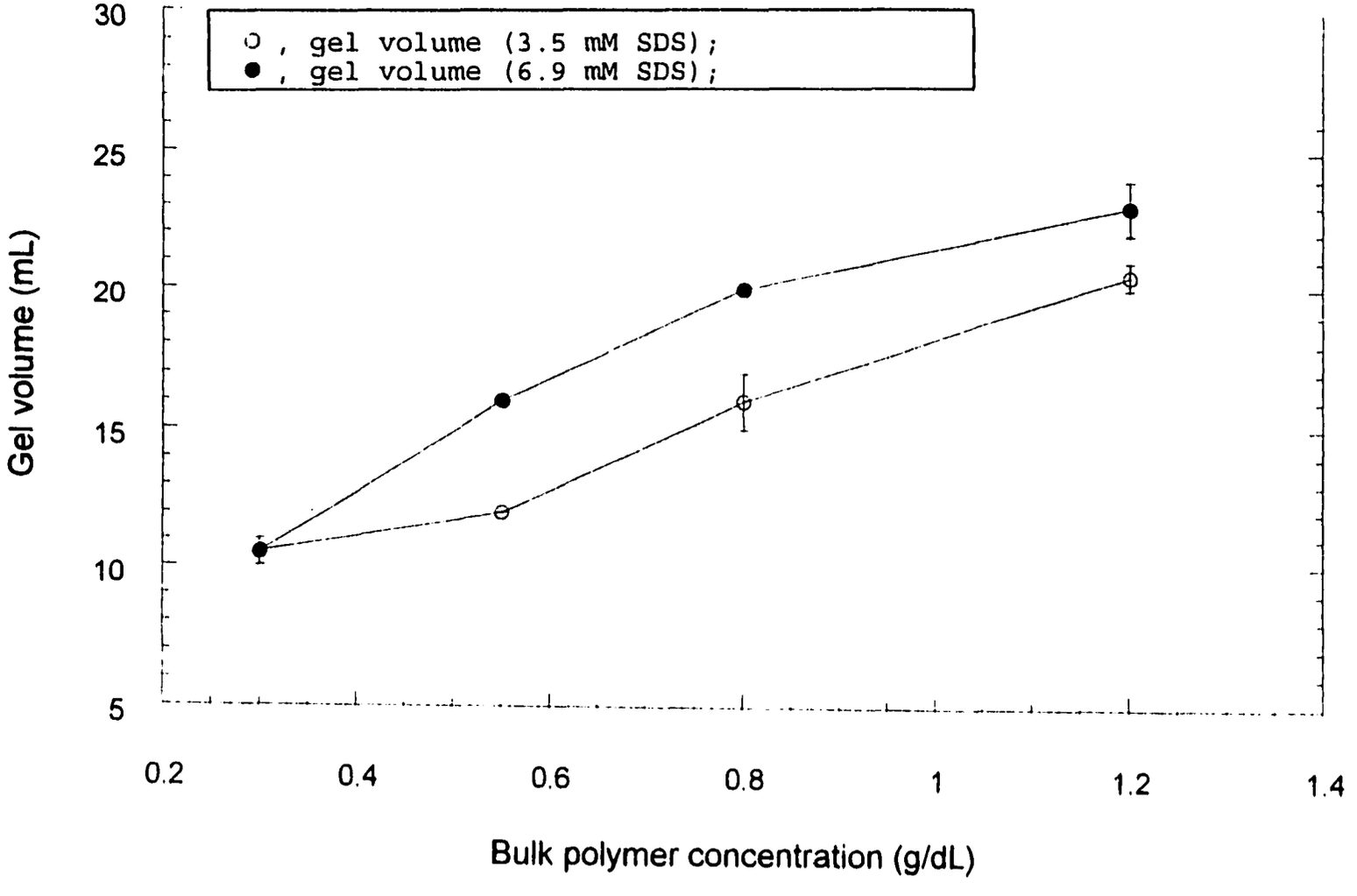

Figure 4.12 : Gel volume vs N. Open symbols 3.5 mM SDS, closed symbols 6.9 mM SDS systems.

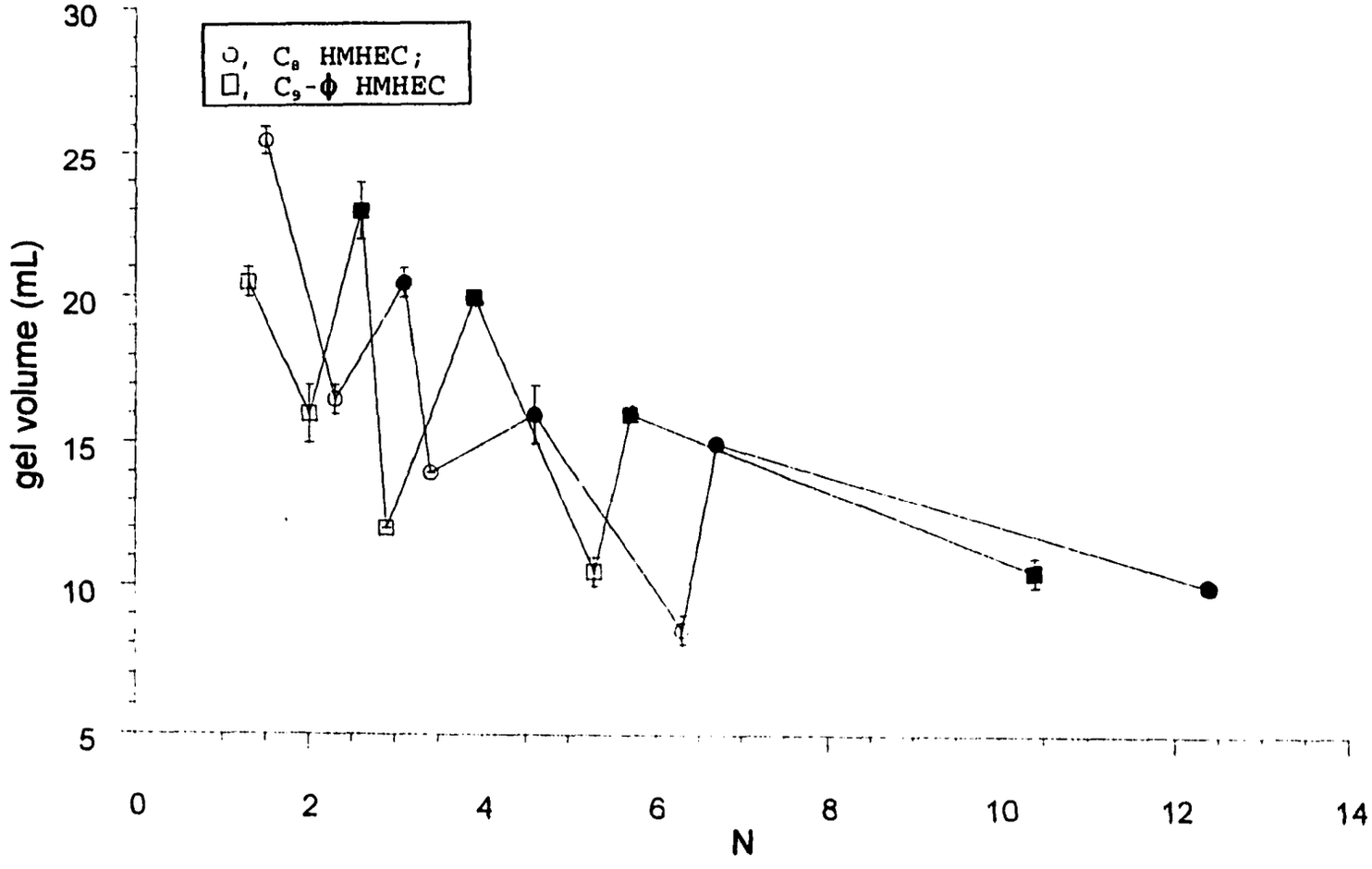

Figure 4.13: Rheological spectra of hydrogel of (0.3 % C_8 HMHEC)/(3.5 mM SDS) system.

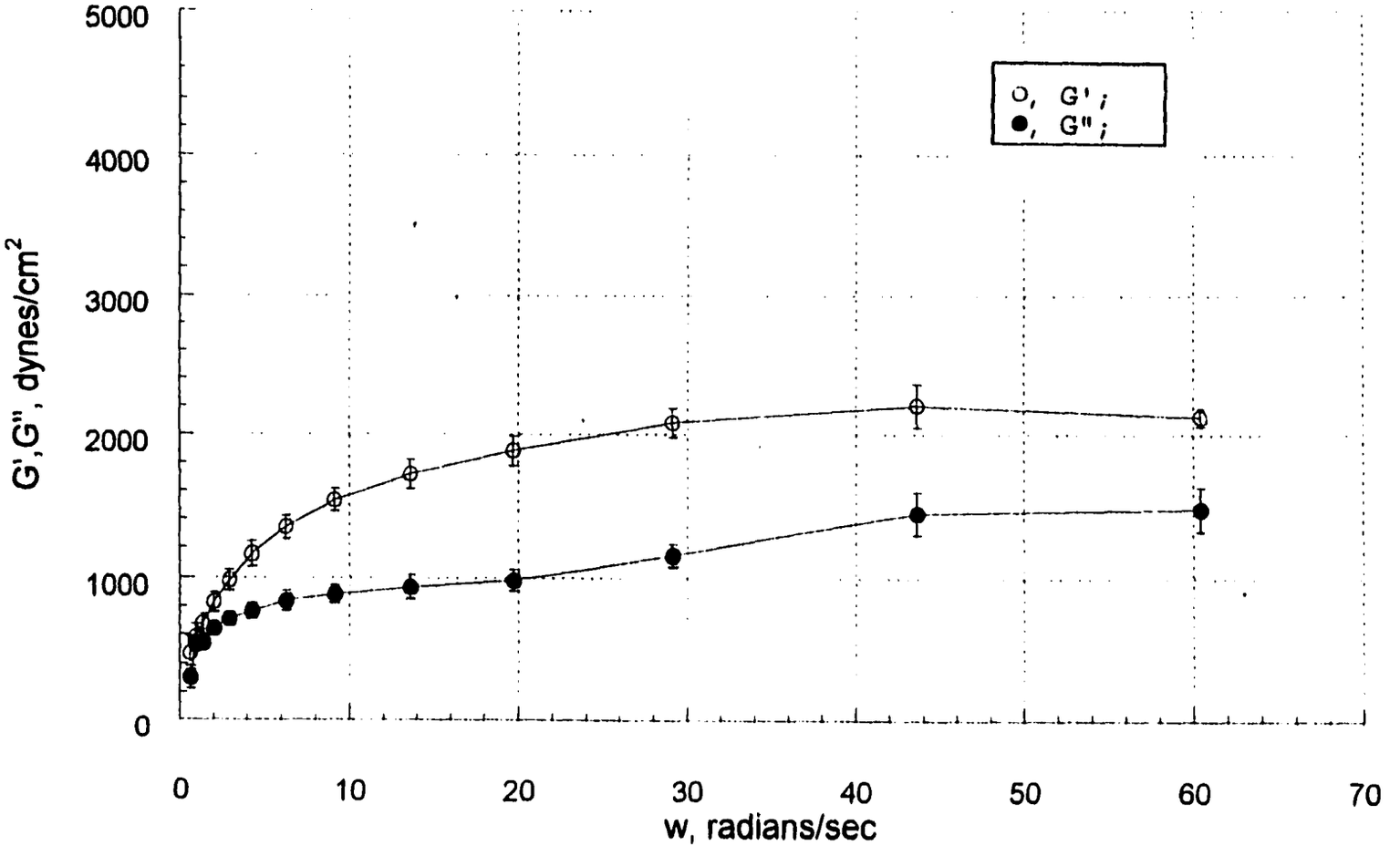

Figure 4.14: Rheological spectra of hydrogel of (0.55 % C_8 HMHEC)/(3.5 mM SDS) system.

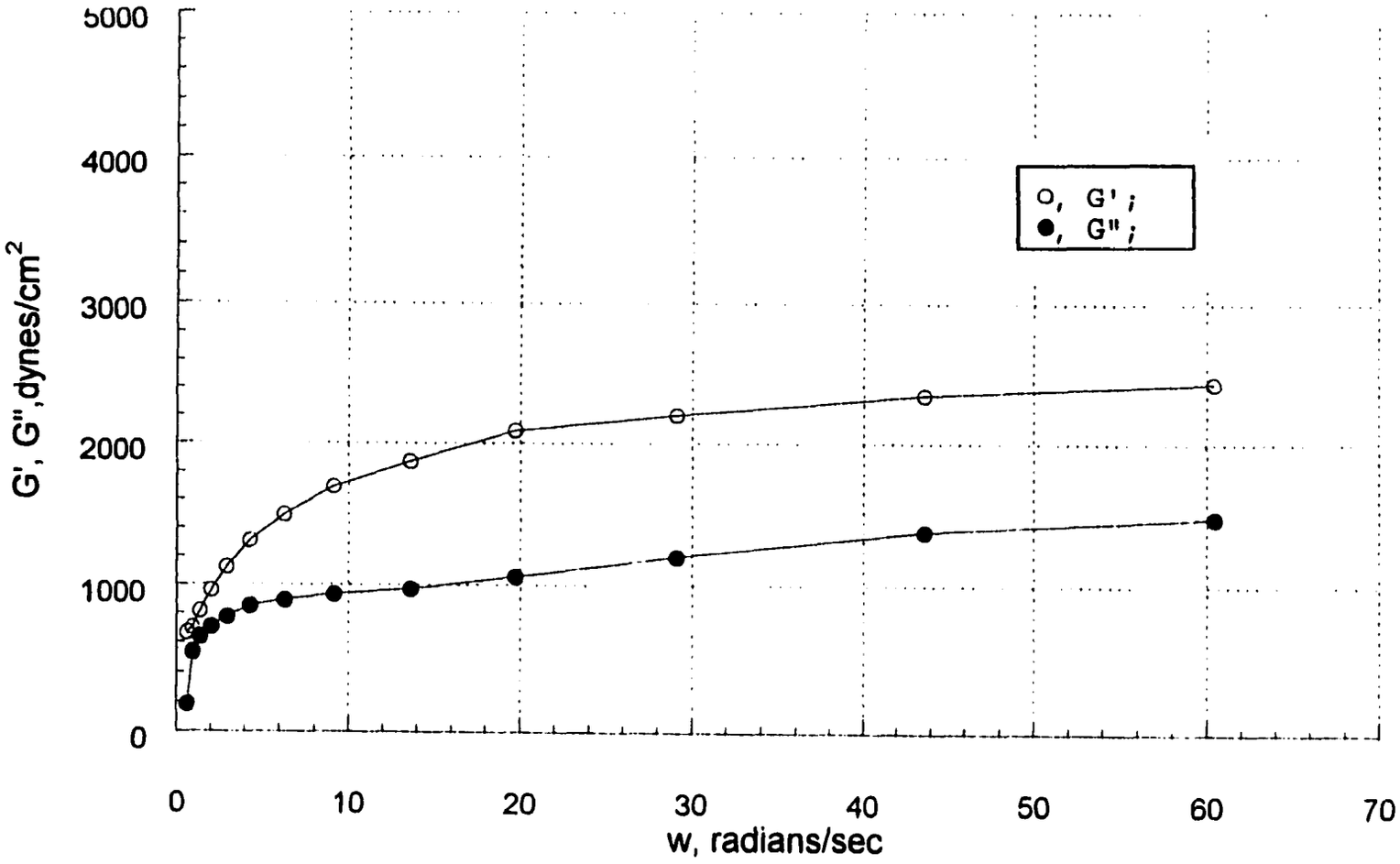

Figure 4.15: Rheological spectra of hydrogel of (0.8 % C_8 HMHEC)/(3.5 mM SDS) system.

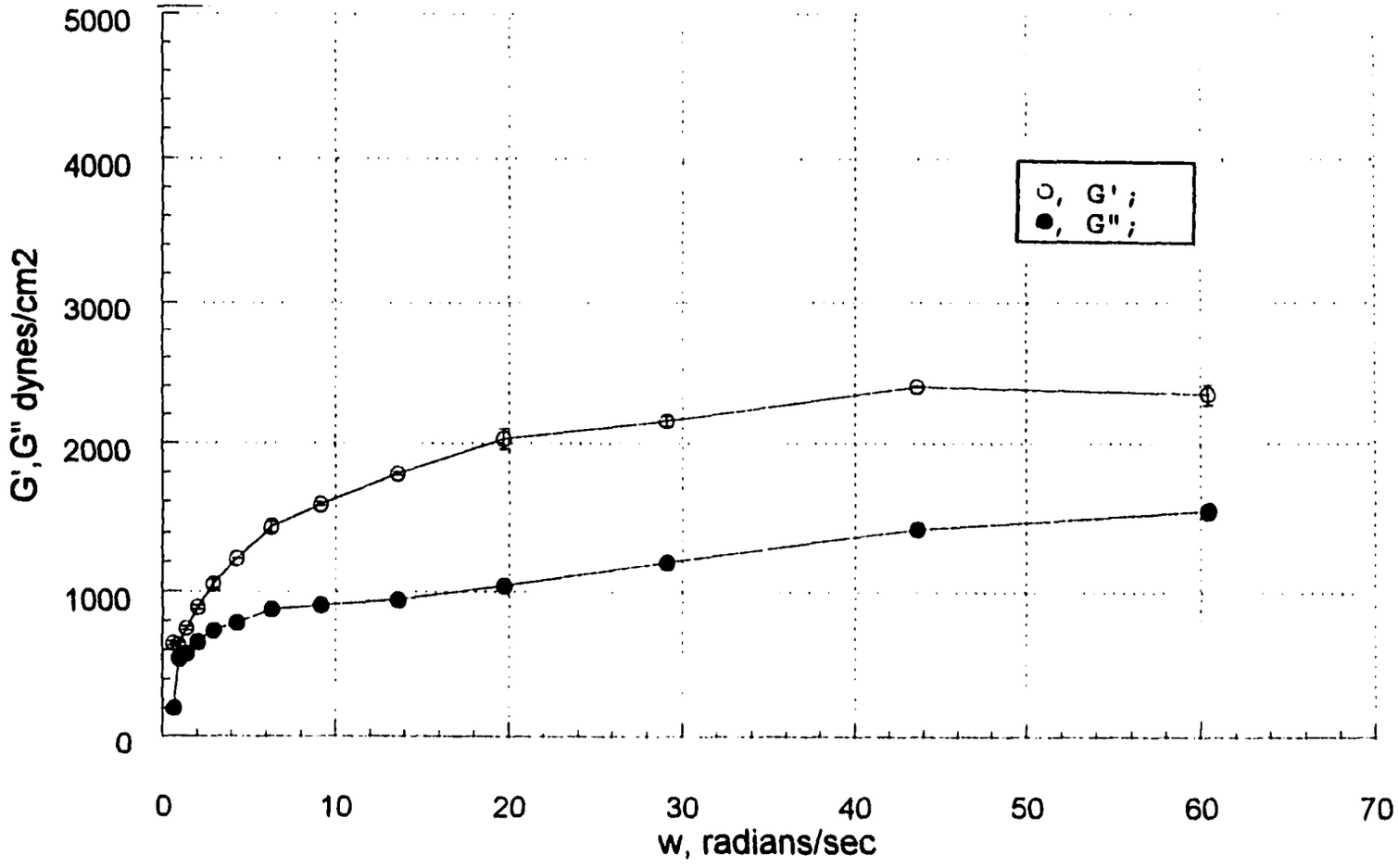

Figure 4.16: Rheological spectra of hydrogel of (1.2 % C_8 HMHEC)/(3.5 mM SDS) system.

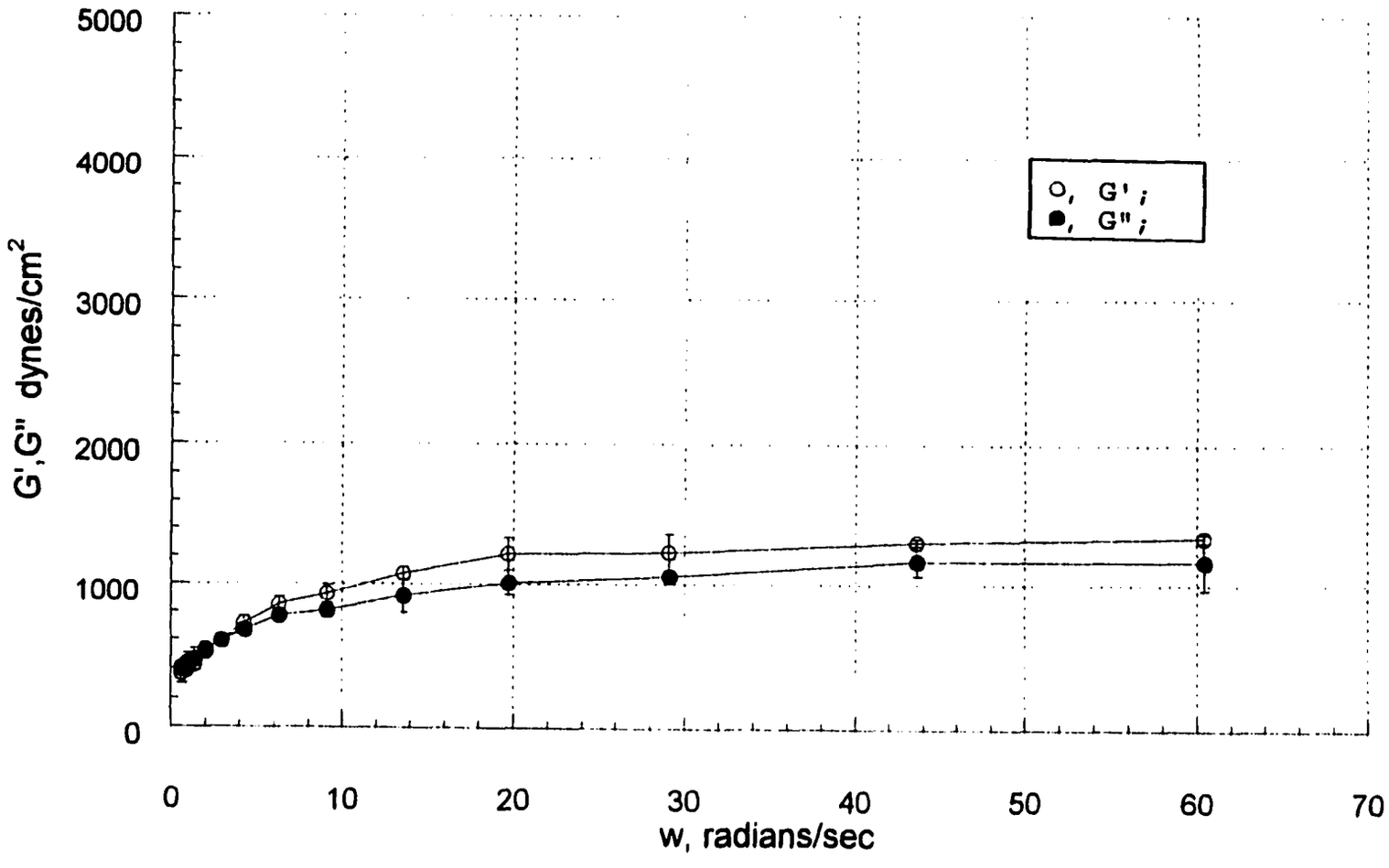

Figure 4.17: Rheological spectra of hydrogel of (0.3 % C8 HMHEC)/(6.9 mM SDS) system.

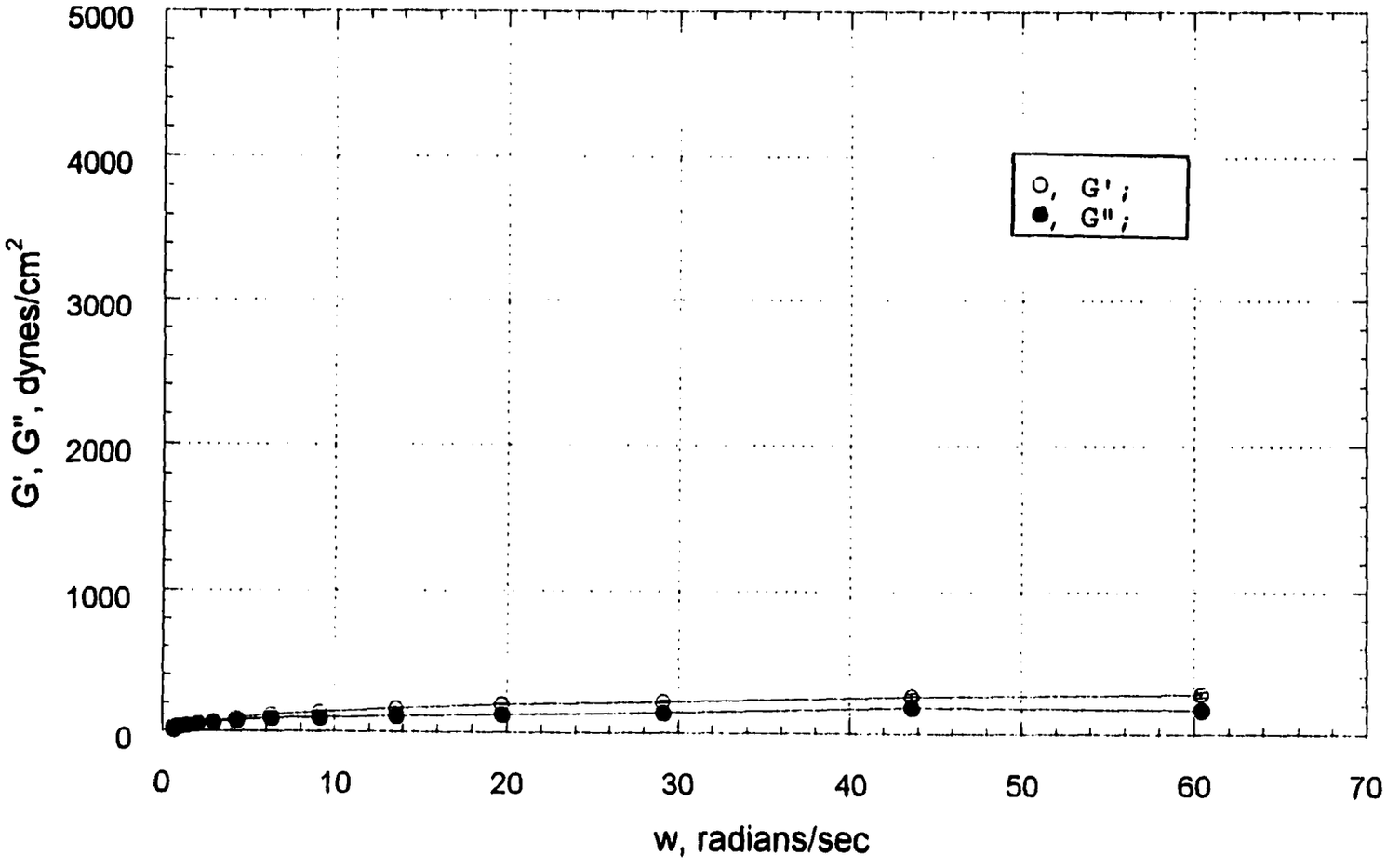

Figure 4.18: Rheological spectra of hydrogel of (0.55 % C8 HMHEC)/(6.9 mM SDS) system.

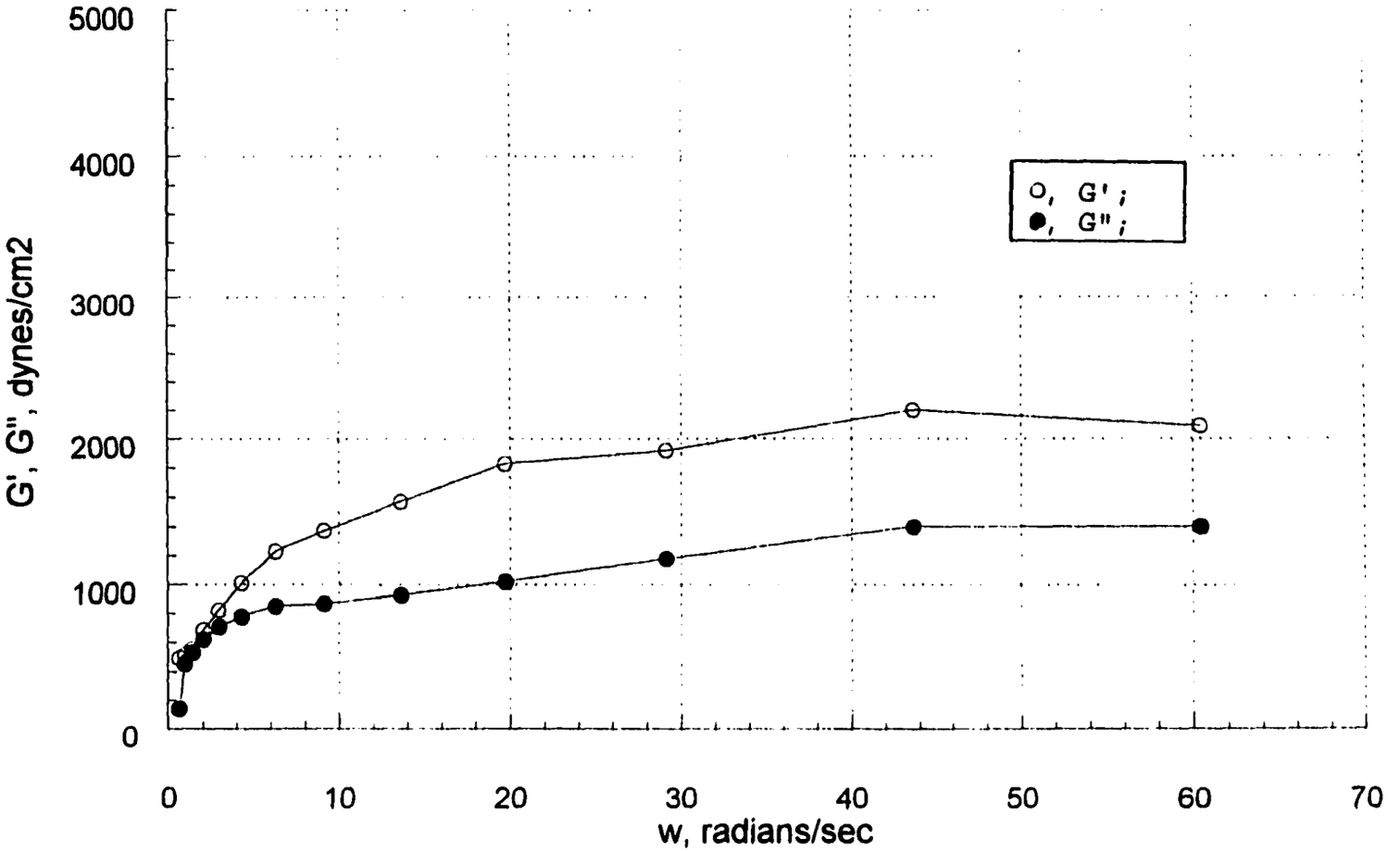

Figure 4.19: Rheological spectra of hydrogels of (0.8 % C8 HMHEC)/(6.9 mM SDS) system.

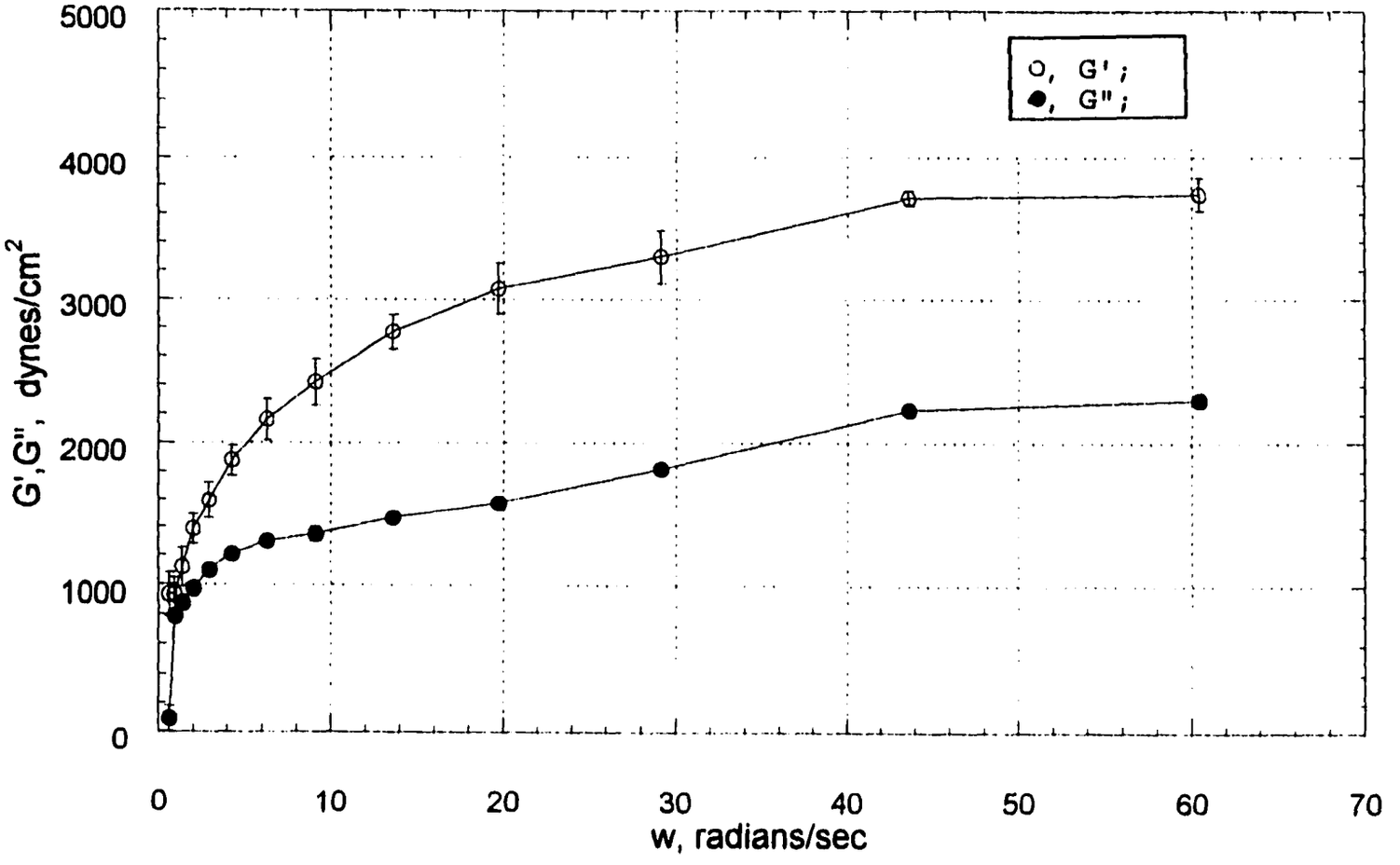

Figure 4.20: Rheological spectra of hydrogel of (1.2 % C8 HMHEC)/(6.9 mM SDS) system.

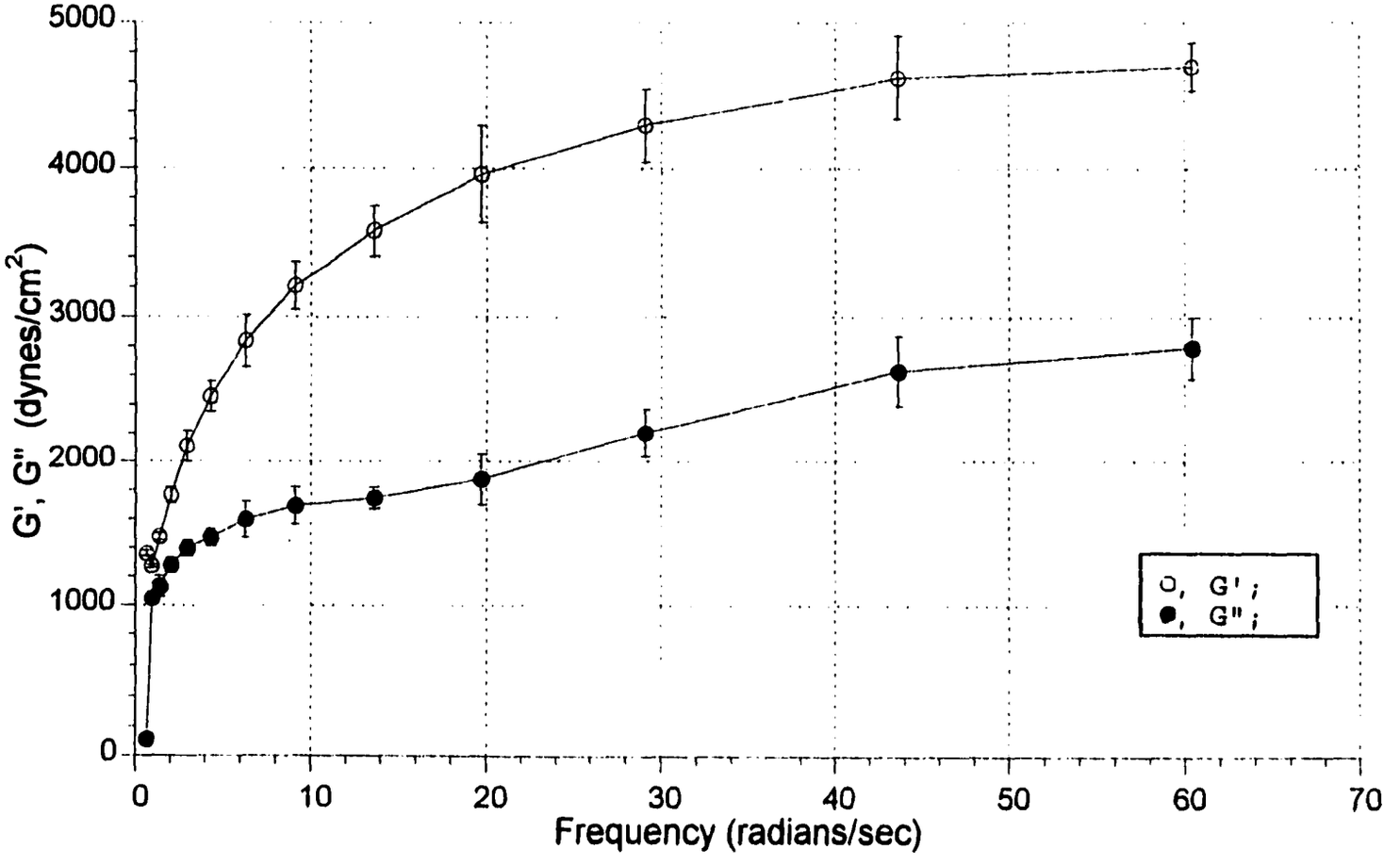

Figure 4.21: Effect of system composition on G'_o of hydrogels of C_8 HMHEC/SDS systems.

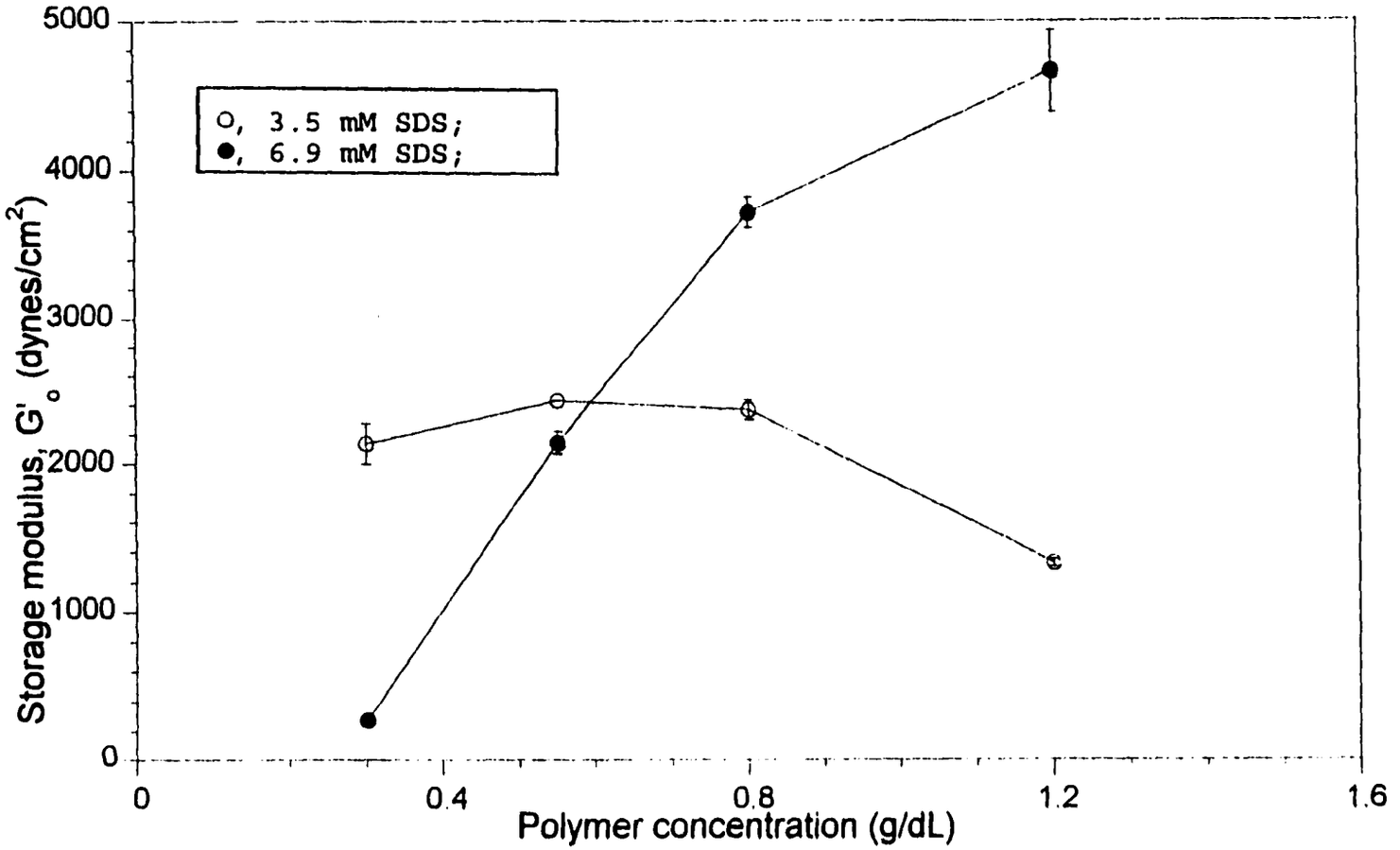

Figure 4.22: Effect of polymer concentration in the gel phase on G'_o of hydrogels of C_8 HMHEC/SDS systems.

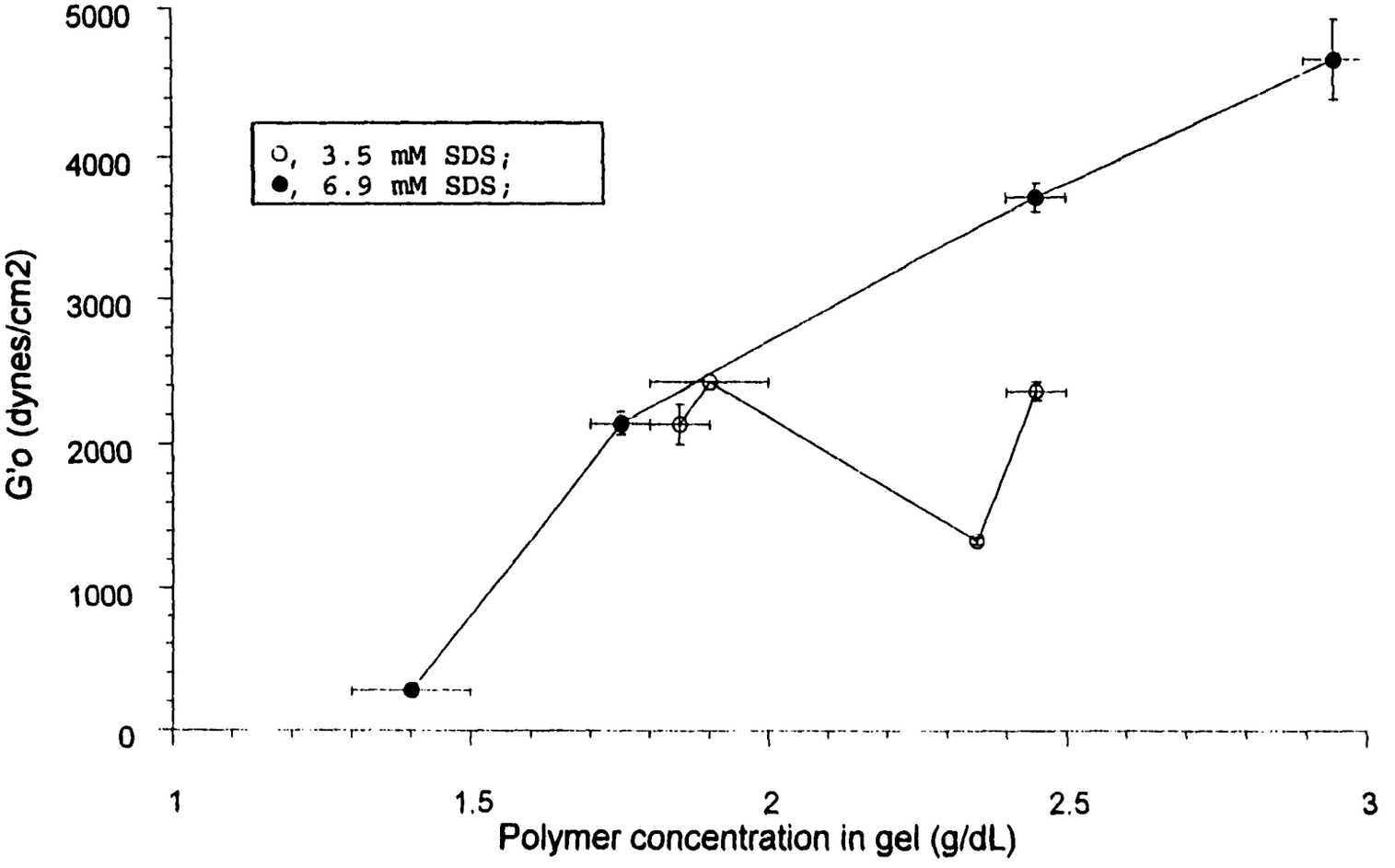

Figure 4.23: Sensitivity of G'_o to N. Open symbols 3.5 mM SDS, closed symbols 6.9 mM SDS systems.

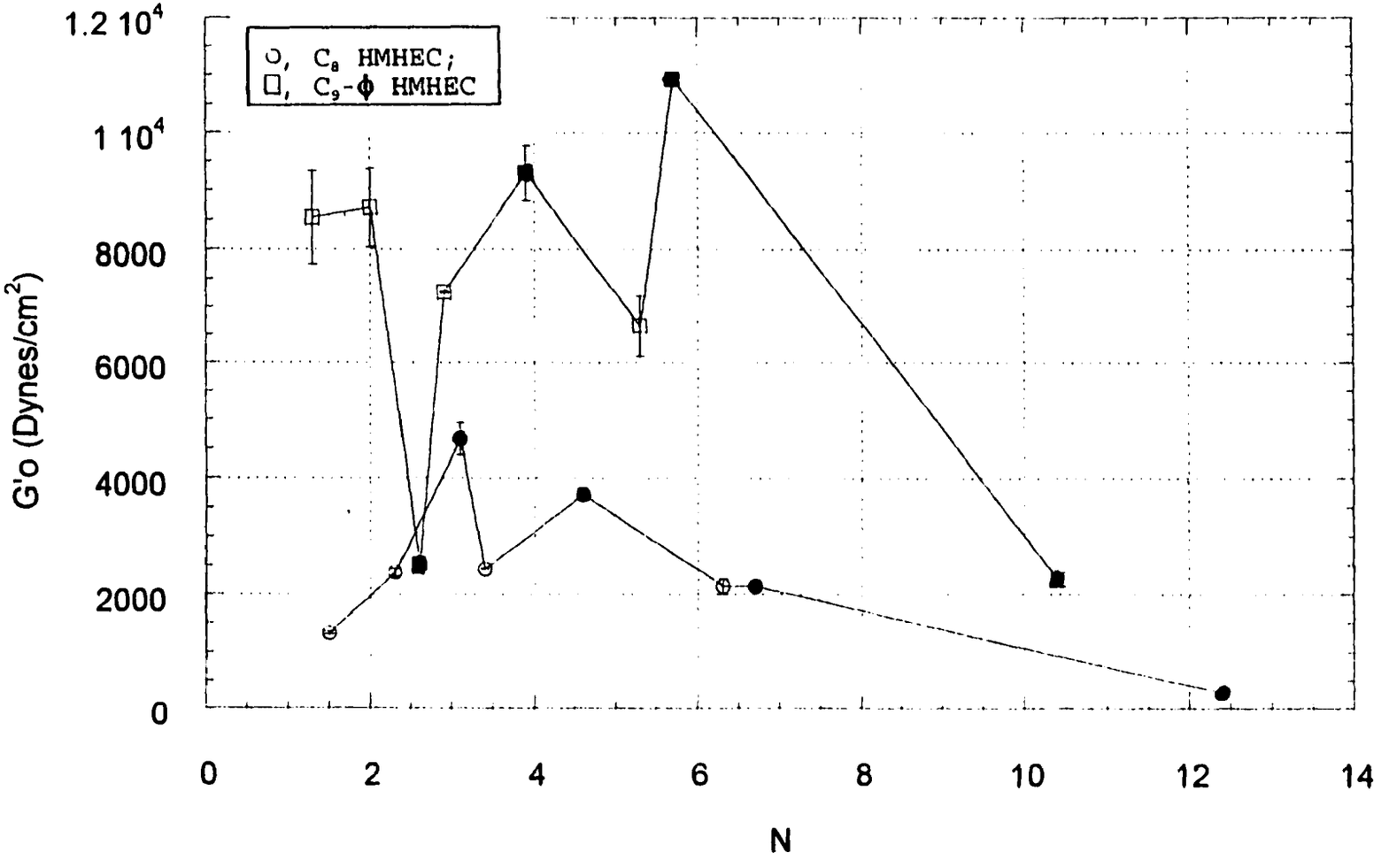

Figure 4.24: Sensitivity of G'_o to N_{gel}. Open symbols 3.5 mM SDS, closed symbols 6.9 mM SDS systems.

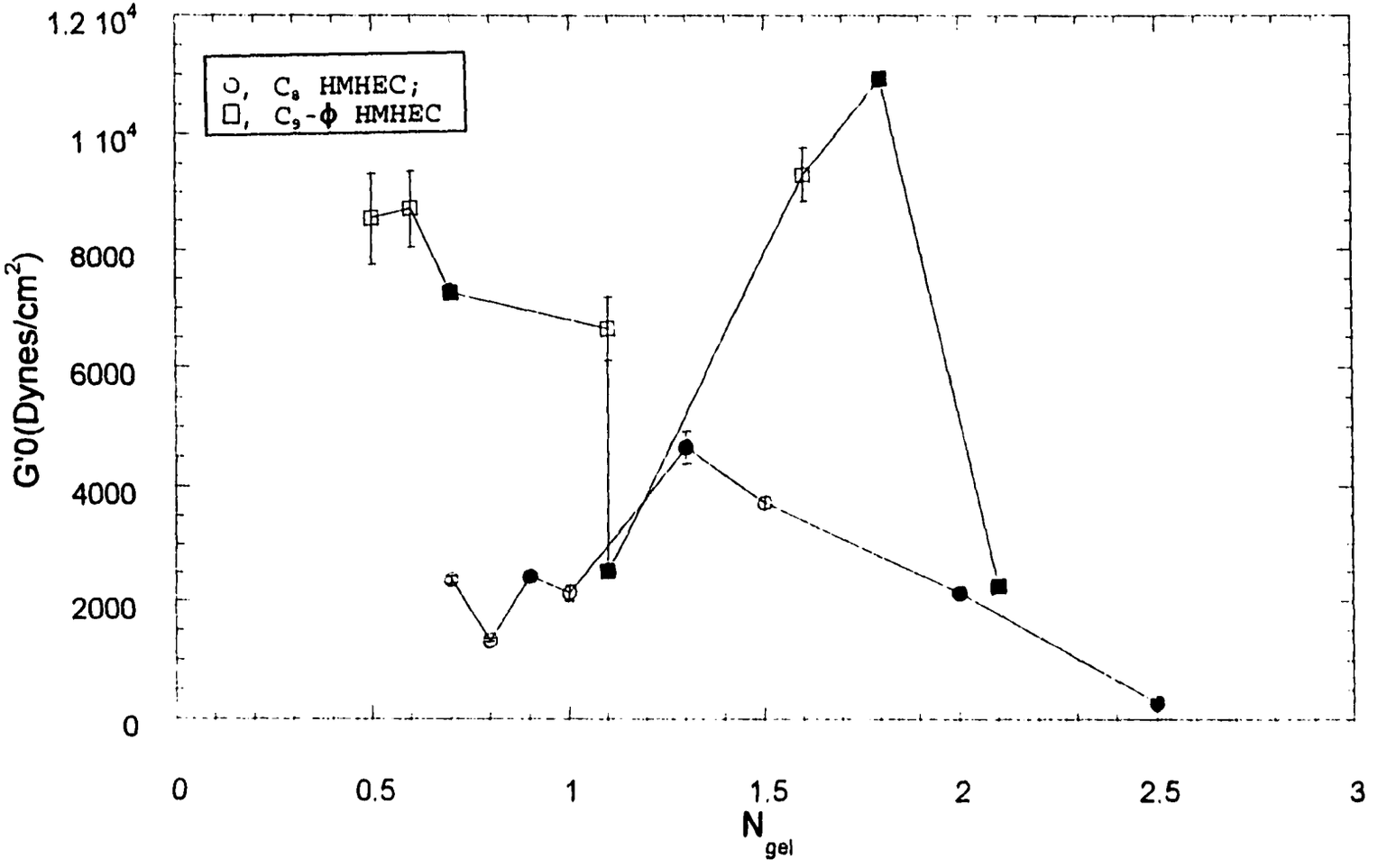

Figure 4.25: Rheological spectra of hydrogel of (0.3 % C_9-ϕ HMHEC)/(3.5 mM SDS) system.

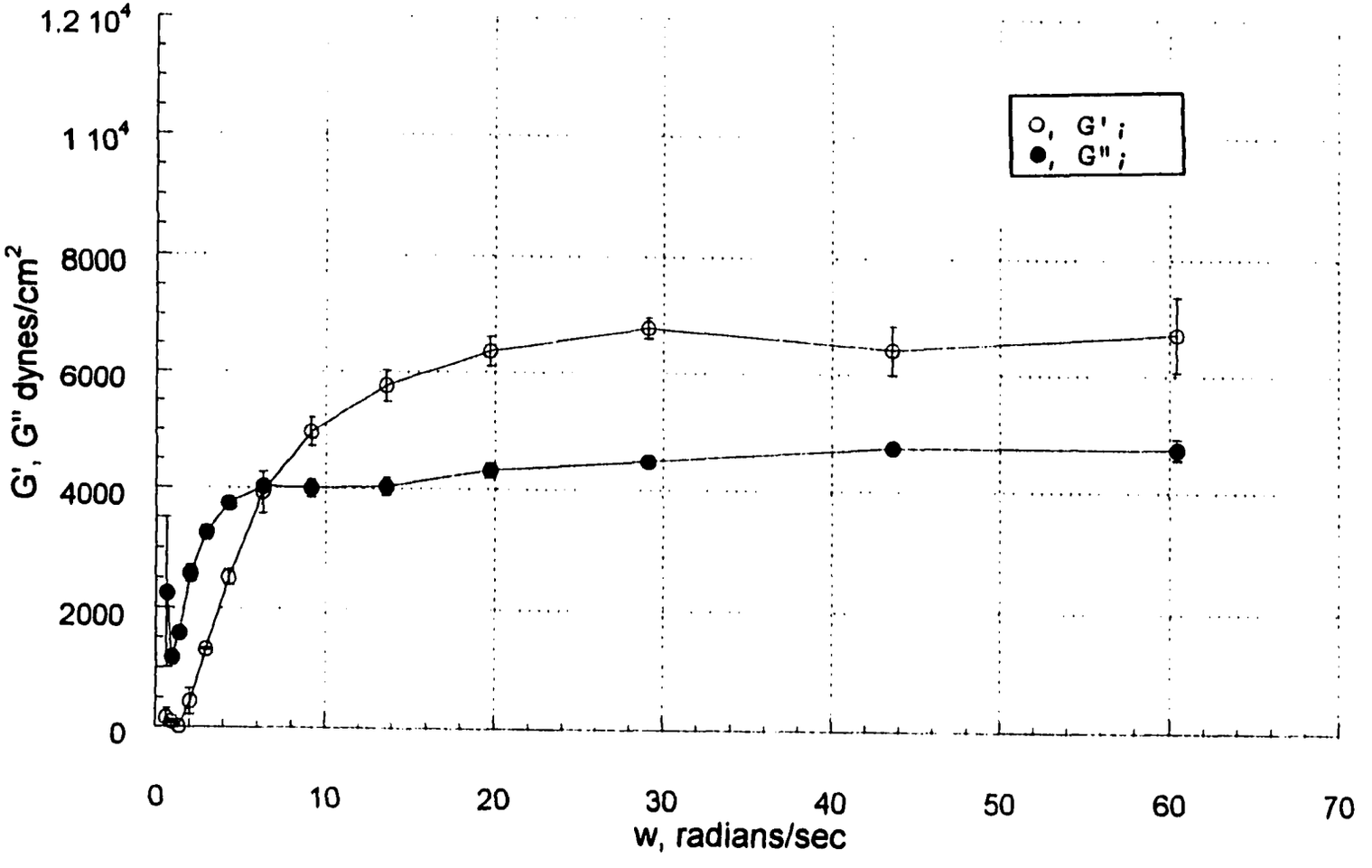

Figure 4.26: Rheological spectra of hydrogel of (0.55 % C_9-ϕ HMHEC)/(3.5 mM SDS) system.

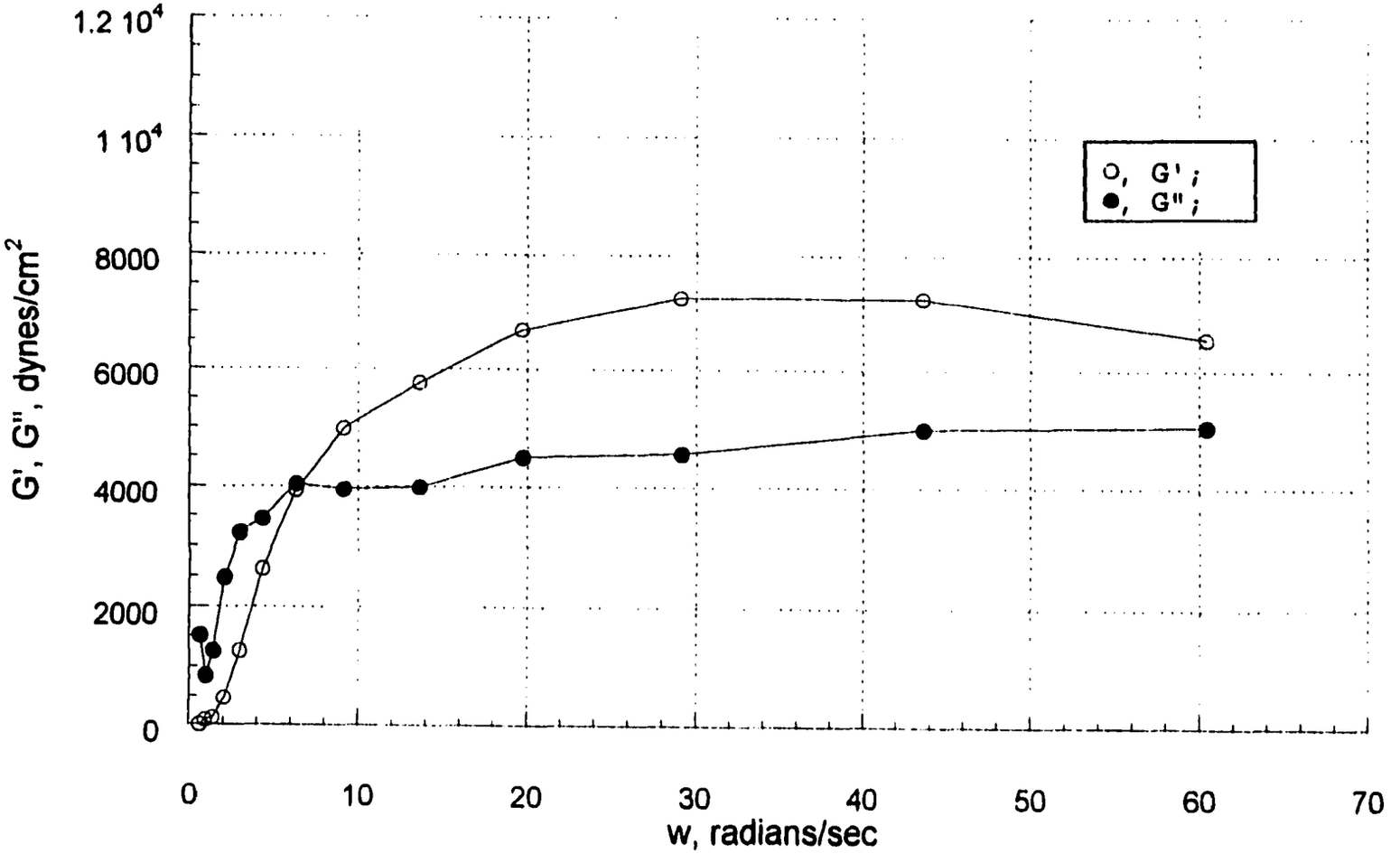

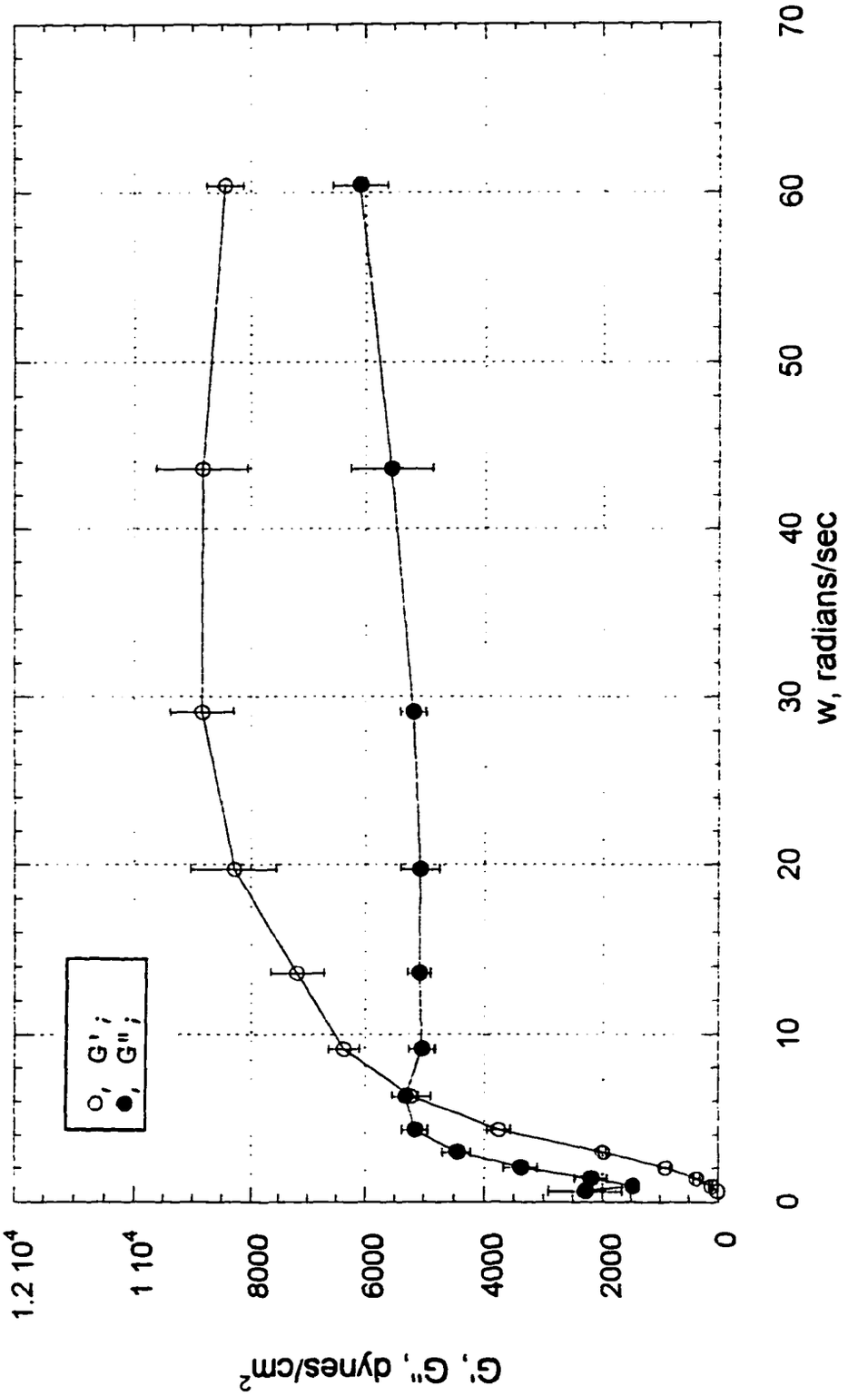

Figure 4.27: Rheological spectra of hydrogel of (0.8 % C_9-ϕ HMHEC)/(3.5 mM SDS) system.

Figure 4.28: Rheological spectra of hydrogel of (1.2 % C_9-ϕ HMHEC)/(3.5 mM SDS) system.

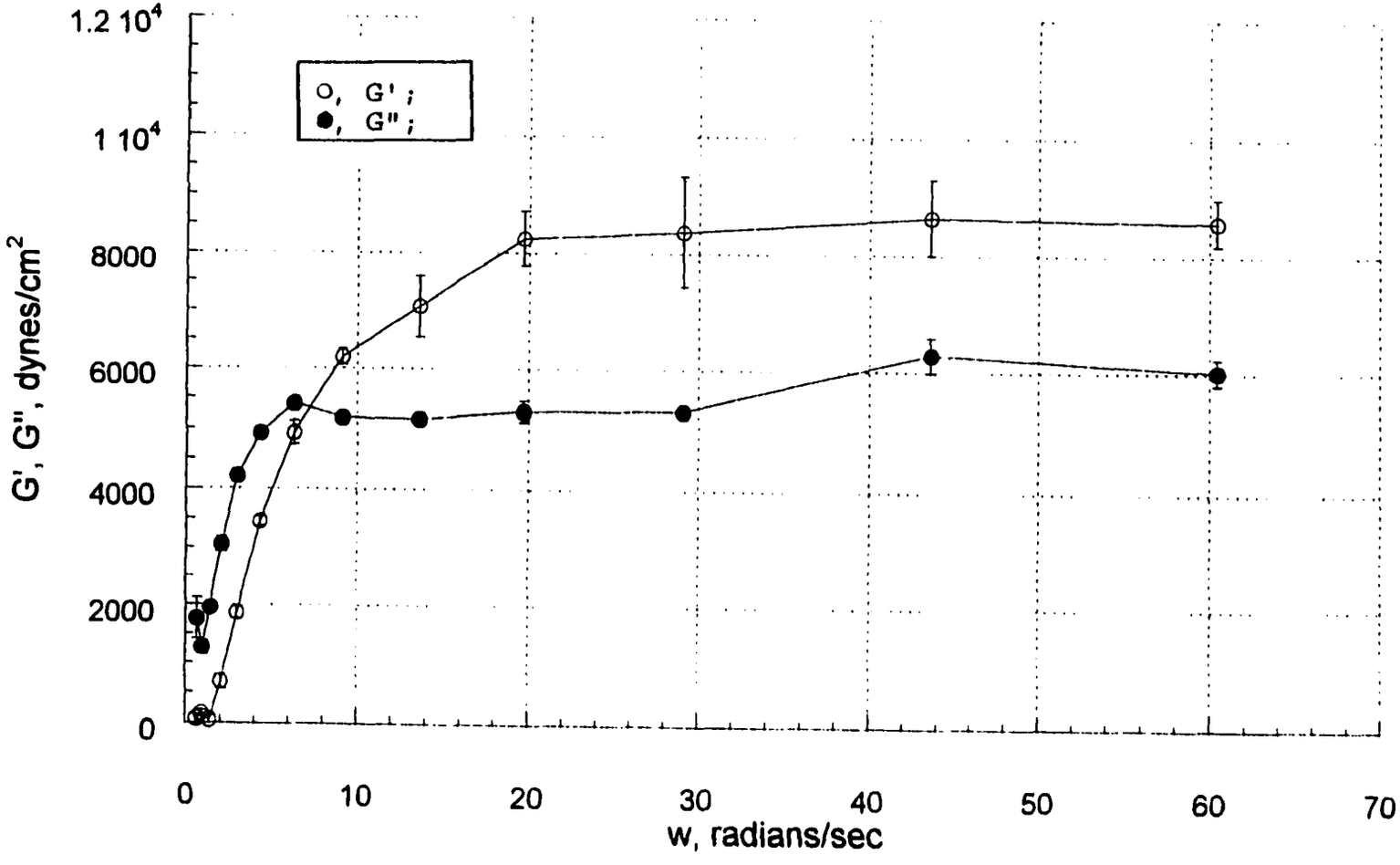

Figure 4.29: Rheological spectra of hydrogel of (0.3 % C_9-ϕ HMHEC)/(6.9 mM SDS) system.

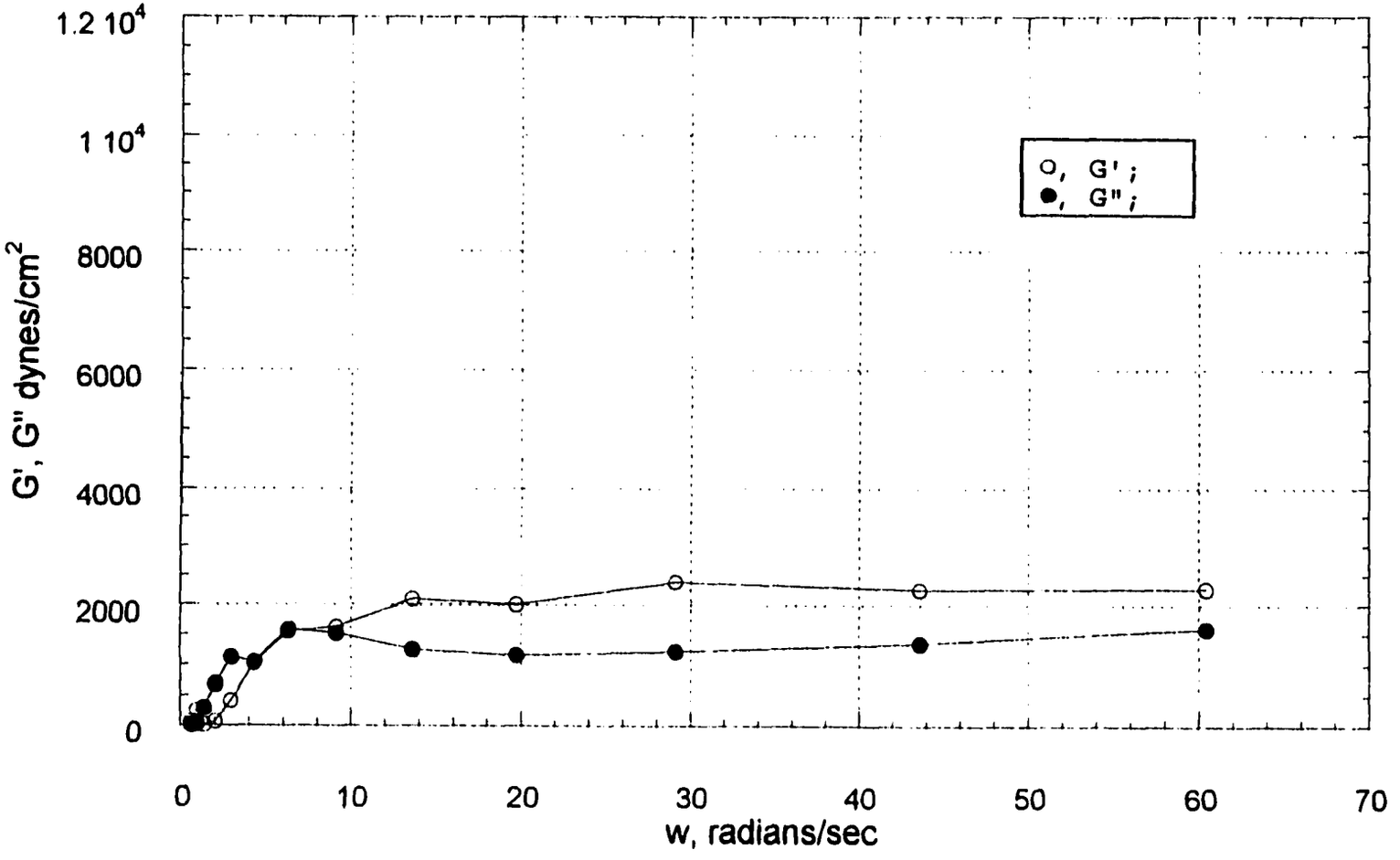

Figure 4.30: Rheological spectra of hydrogel of (0.55 % C_9-ϕ HMHEC)/(6.9 mM SDS) system.

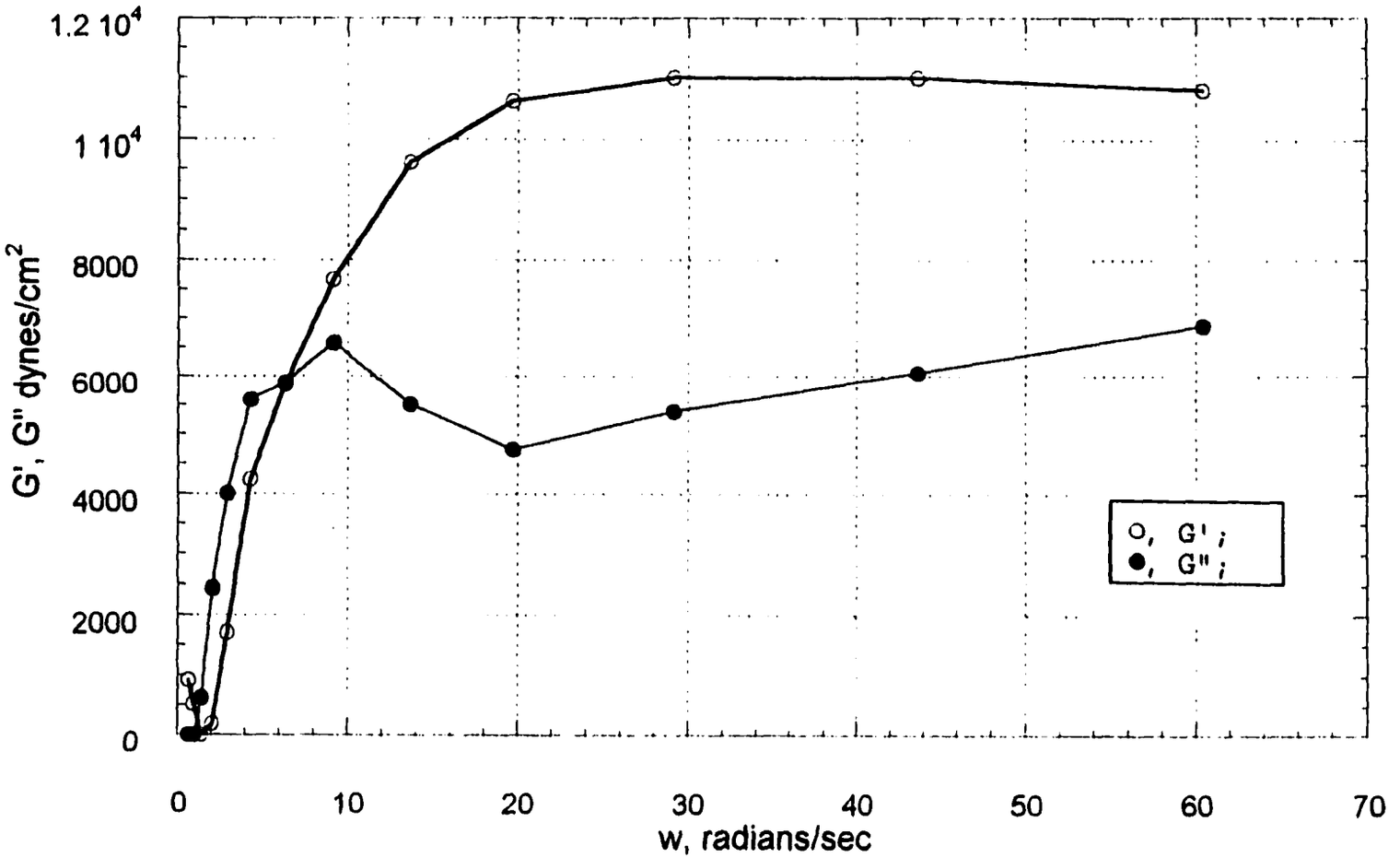

Figure 4.31: Rheological spectra of hydrogel of (0.8 % C_9-ϕ HMHEC)/(6.9 mM SDS) system.

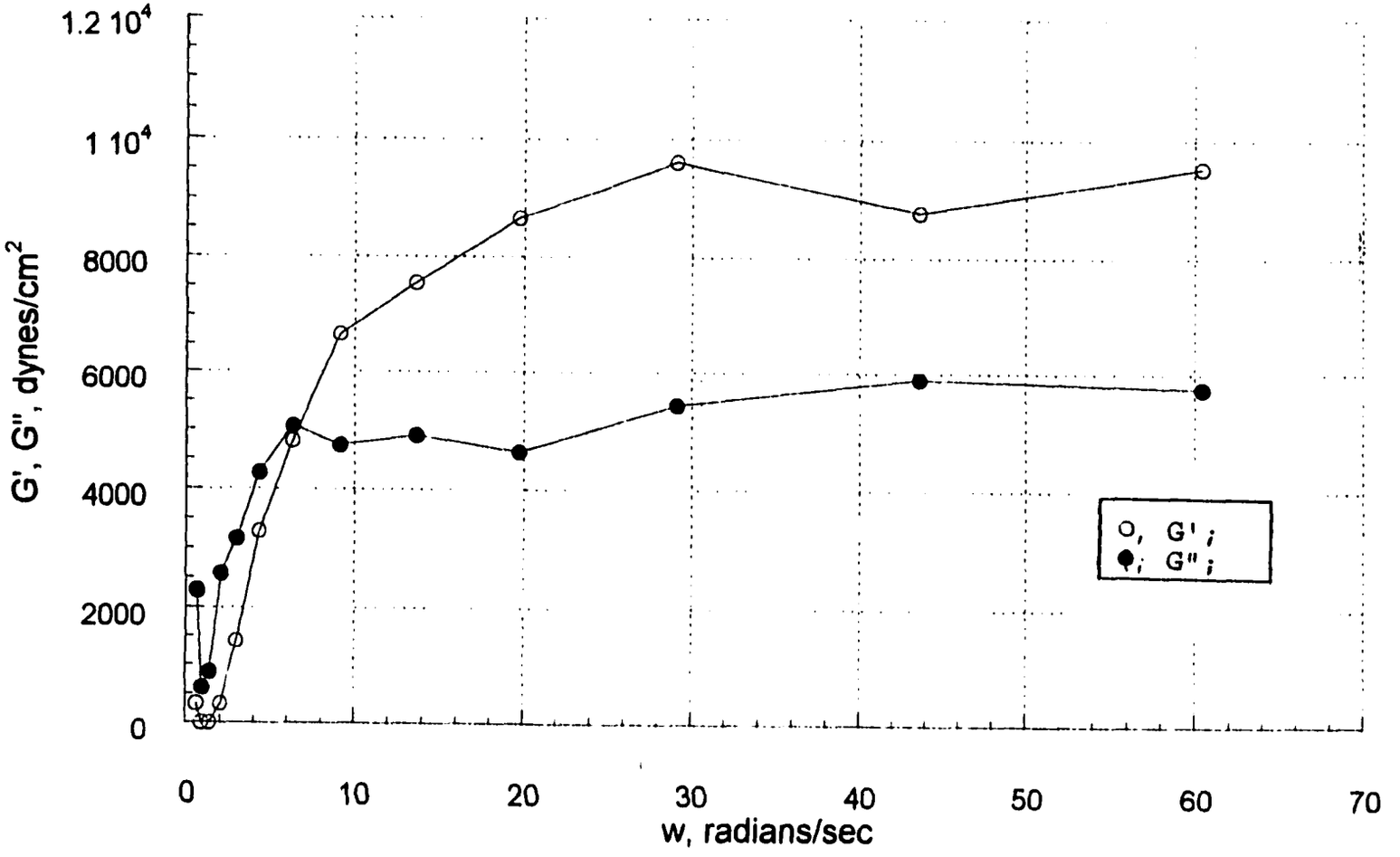

Figure 4.32: Rheological spectra of hydrogel of (1.2 % C_9-ϕ HMHEC)/(6.9 mM SDS) system.

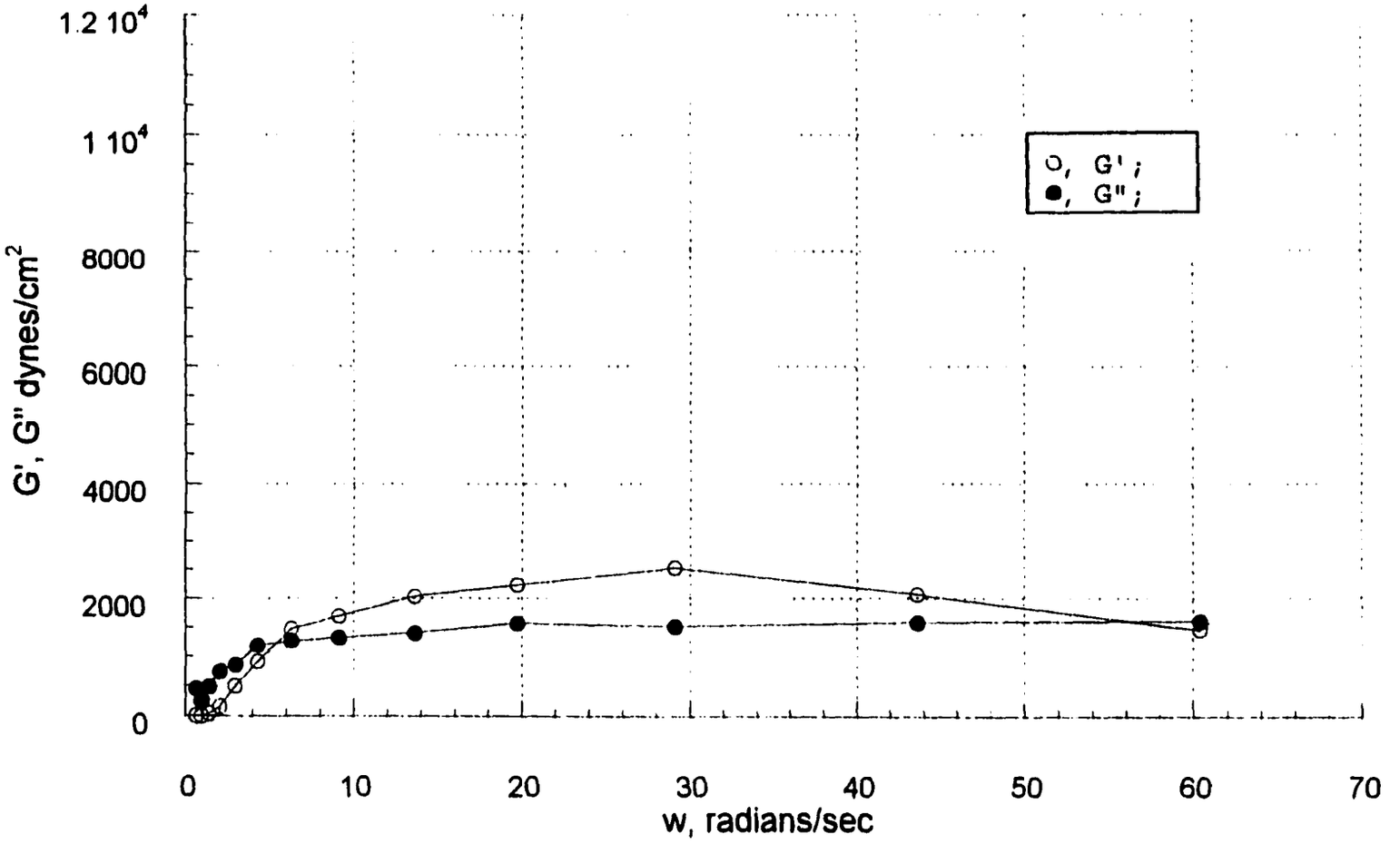

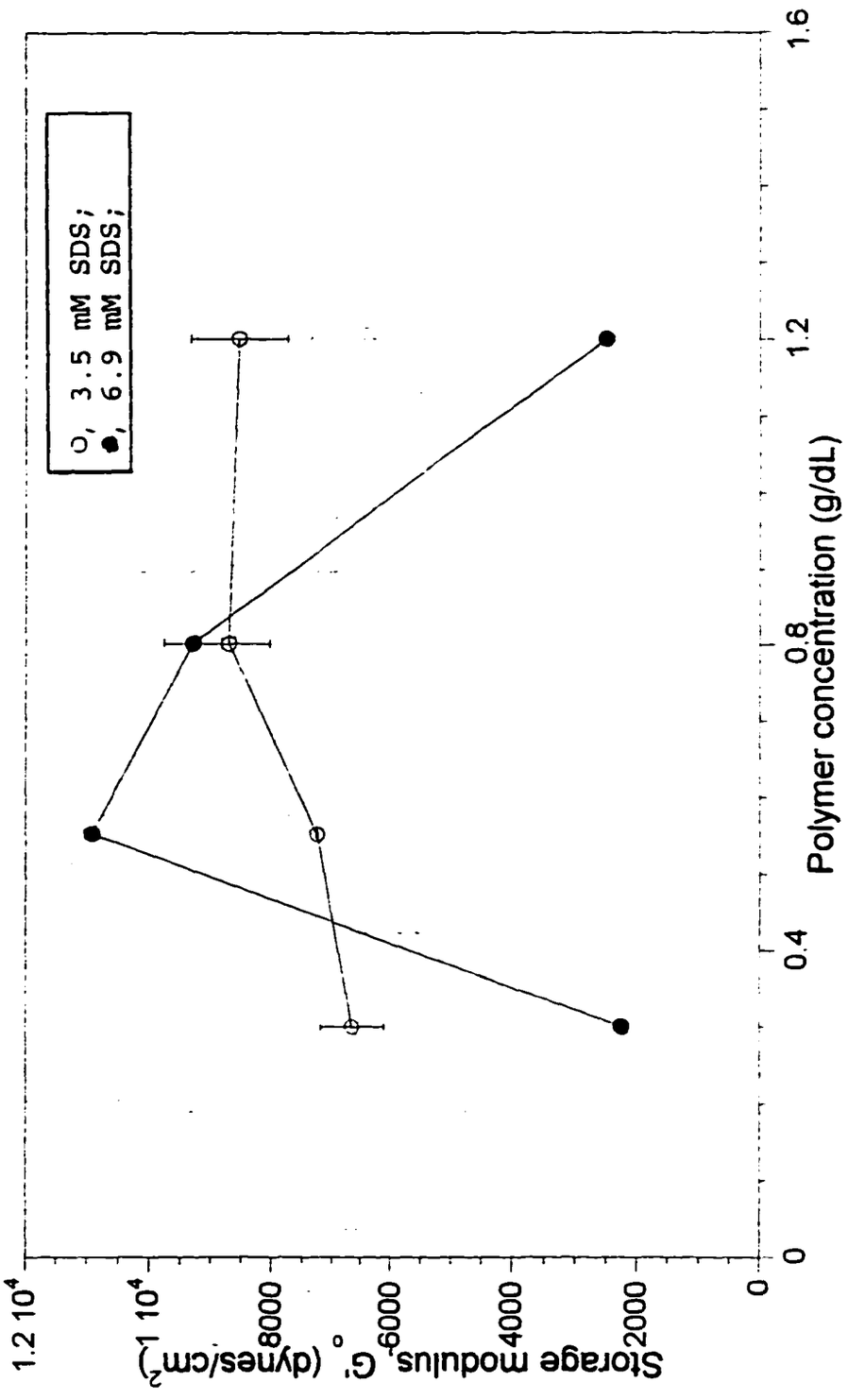

Figure 4.33: Effect of system composition on G'$_o$ of hydrogels of C_9-ϕ HMHEC/SDS systems.

Figure 4.34: Effect of polymer concentration in the gel phase on G'_o of hydrogels of C_9-ϕ HMHEC/SDS systems.

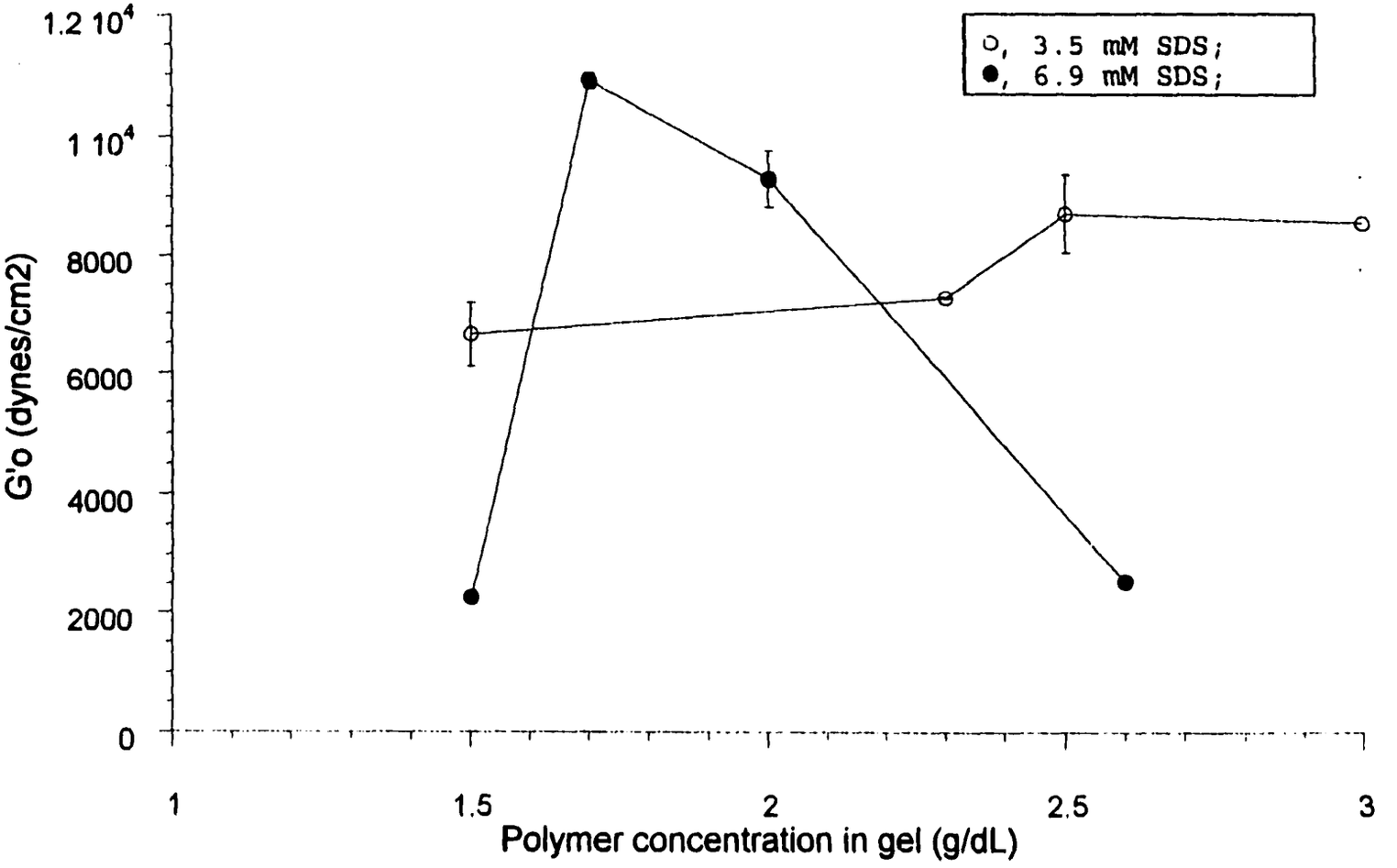

Figure 4.35: Fluorescence spectra of pyrene present in low DP HEC/water solution.

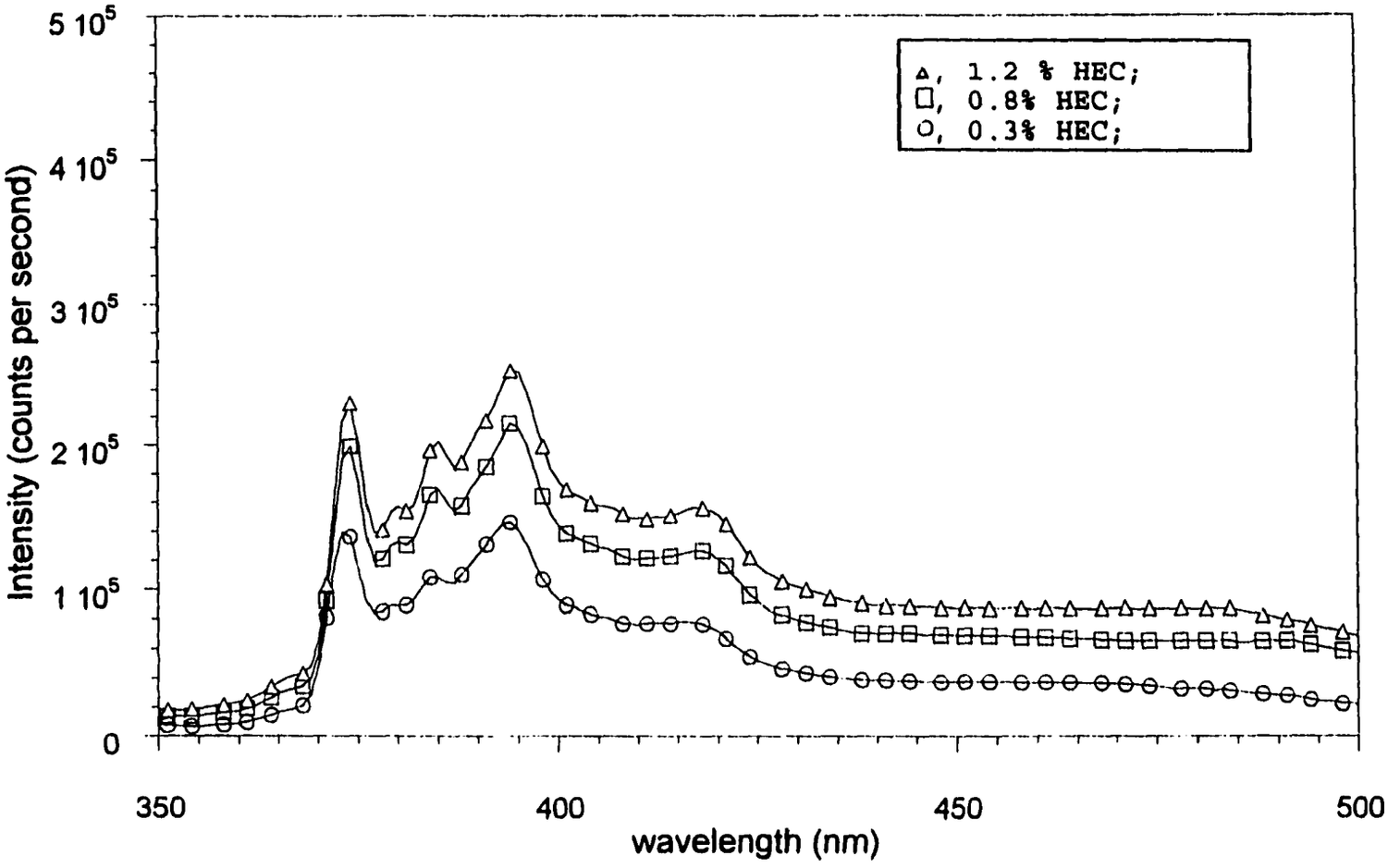

Figure 4.36: Fluorescence spectra of pyrene present in low DP HEC/3.5 mM SDS solution.

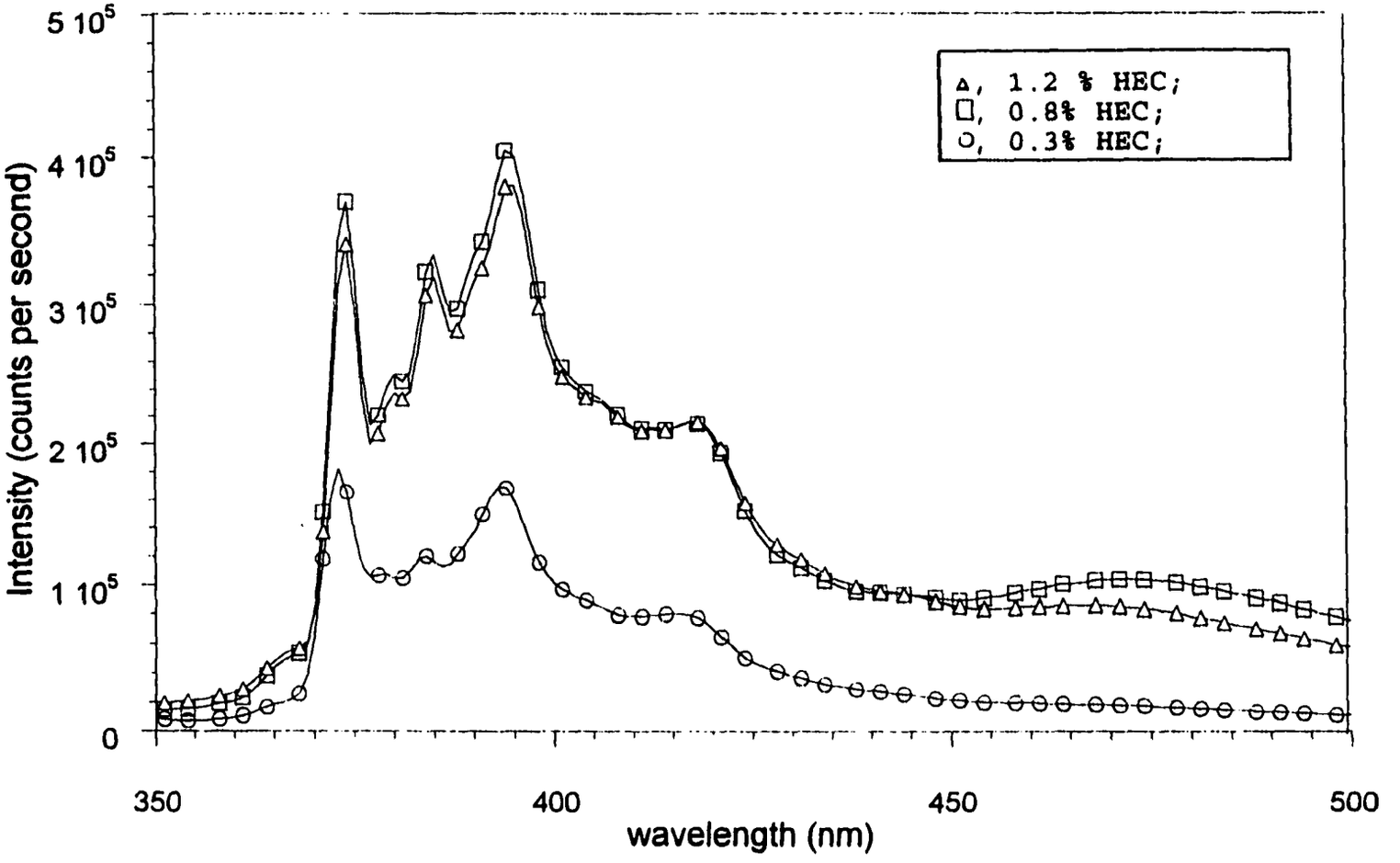

Figure 4.37: Fluorescence spectra of pyrene present in low DP HEC/6.9 mM SDS solution.

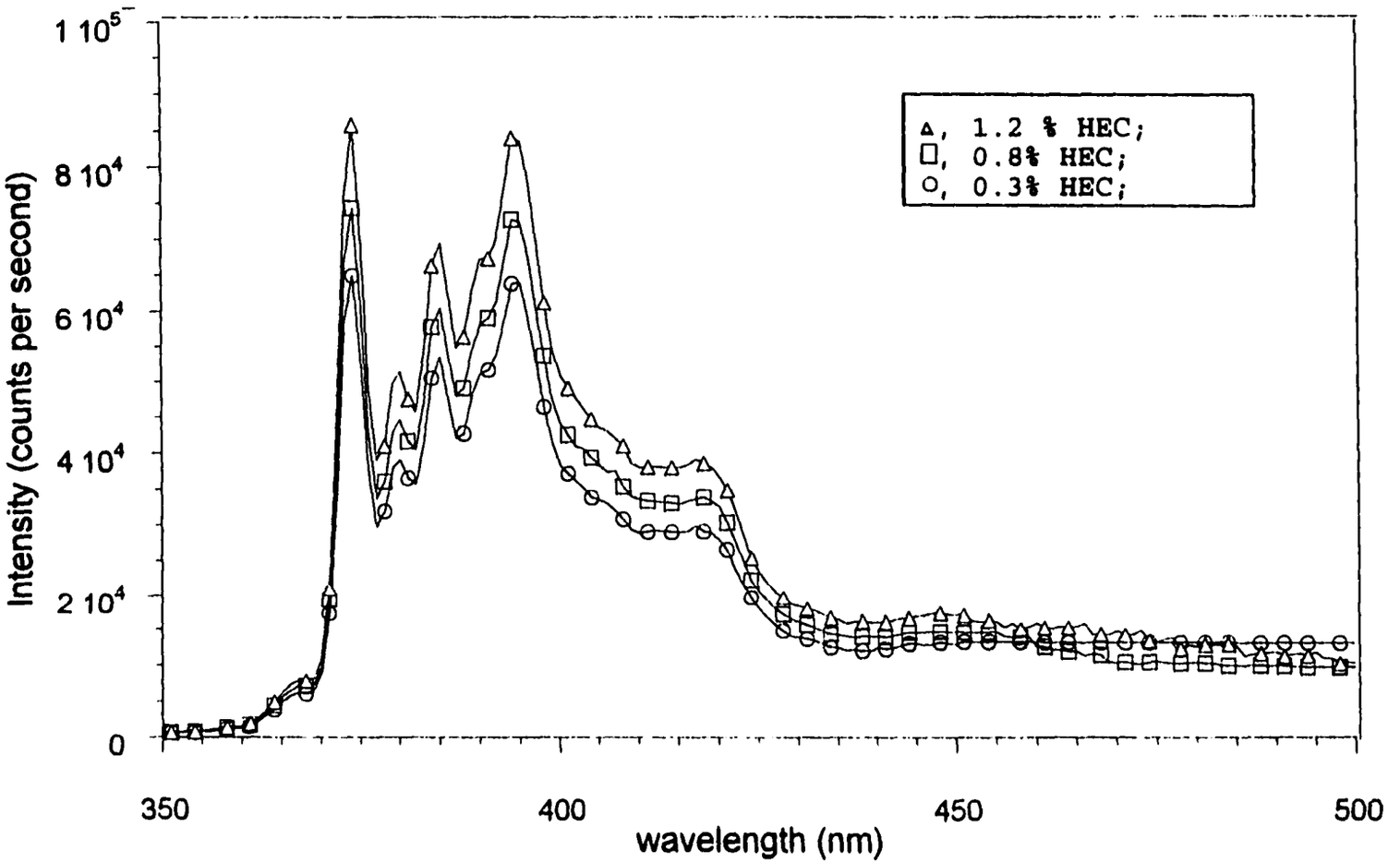

Figure 4.38: Fluorescence spectra of pyrene present in the gel phase of C_8 HMHEC/(3.5 mM SDS) systems.

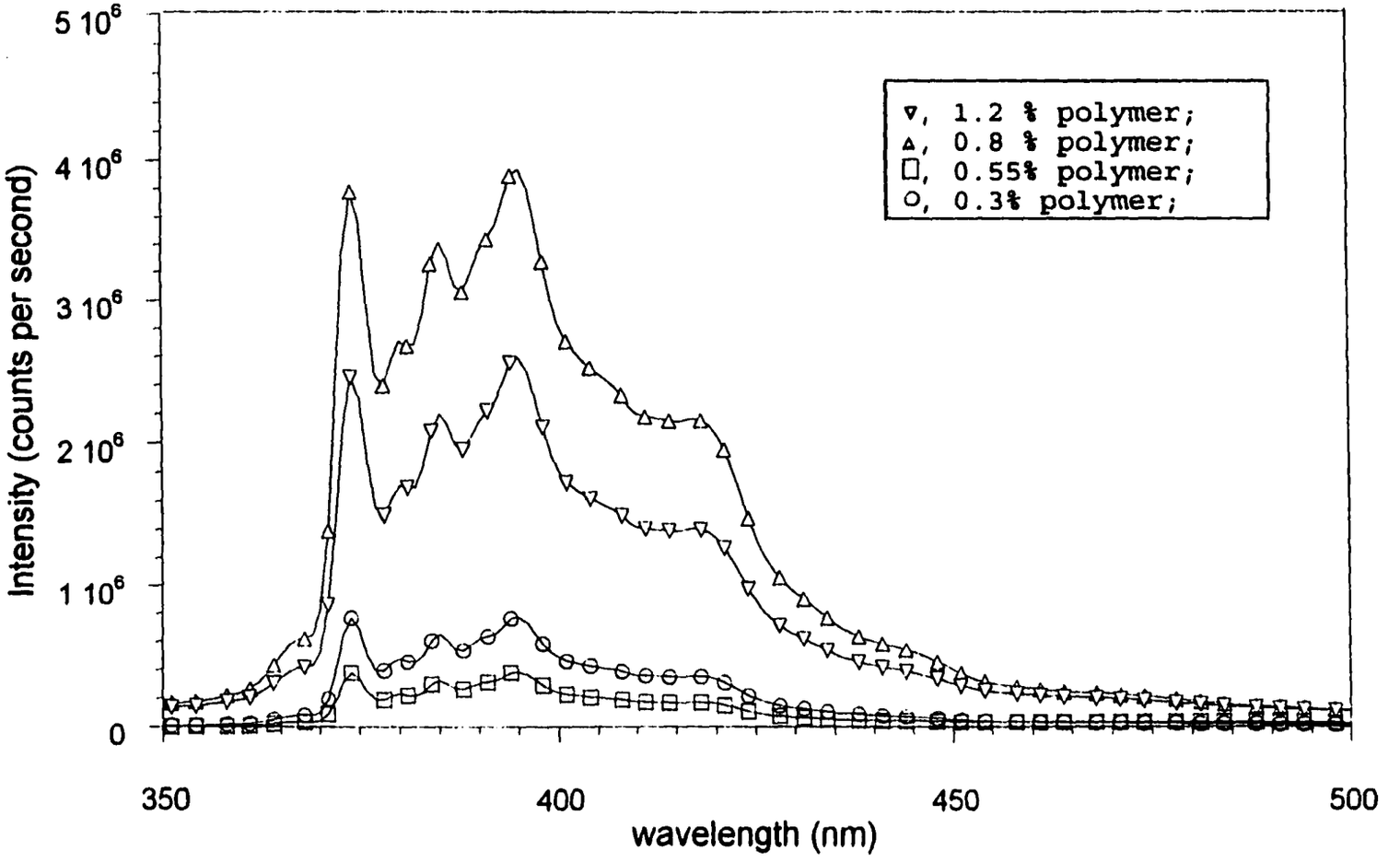

Figure 4.39: Fluorescence spectra of pyrene present in the gel phase of C_8 HMHEC/(6.9 mM SDS) systems.

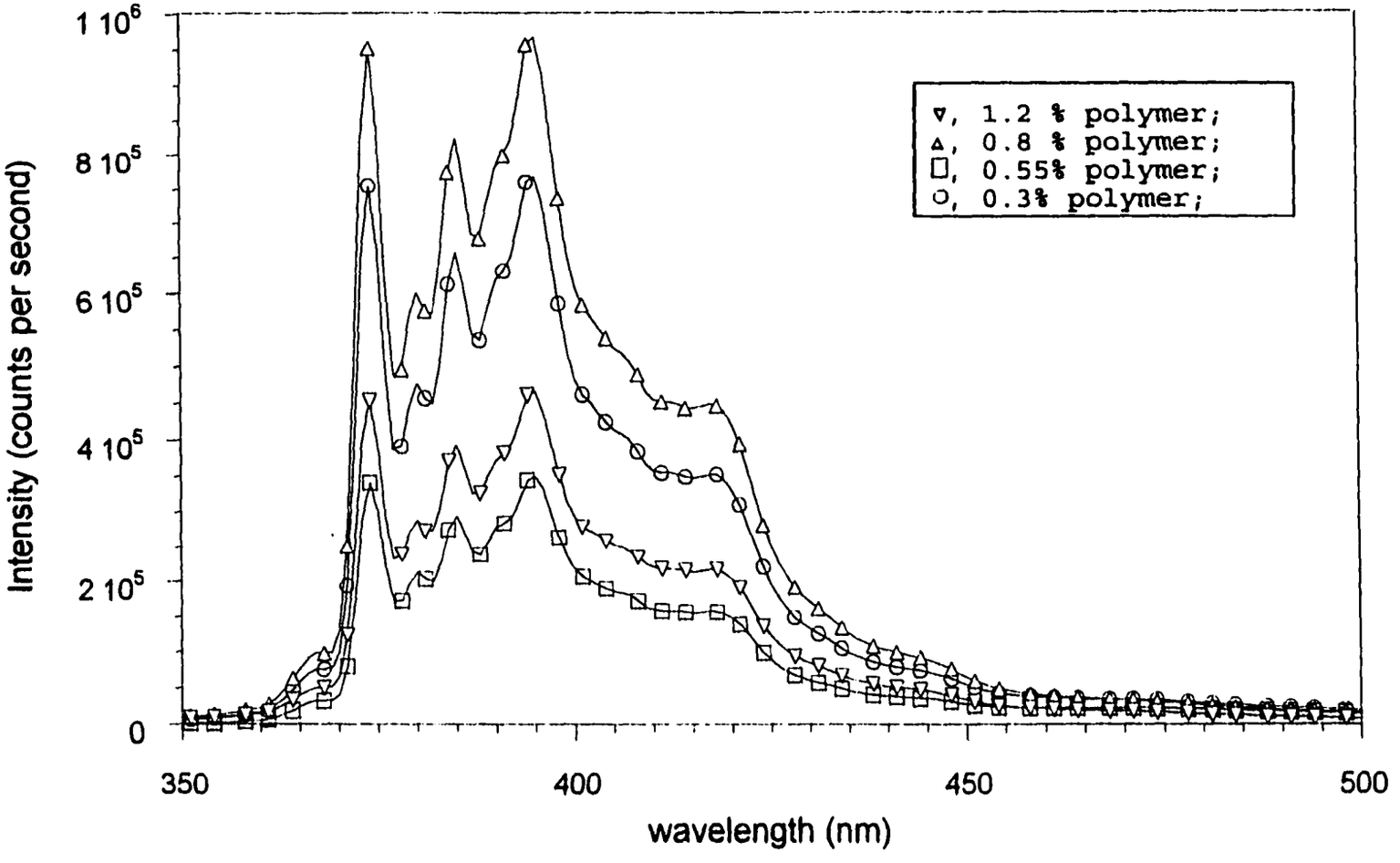

Figure 4.40: Fluorescence spectra of pyrene present in the gel phase of C_9-ϕ HMHEC/(3.5 mM SDS) systems.

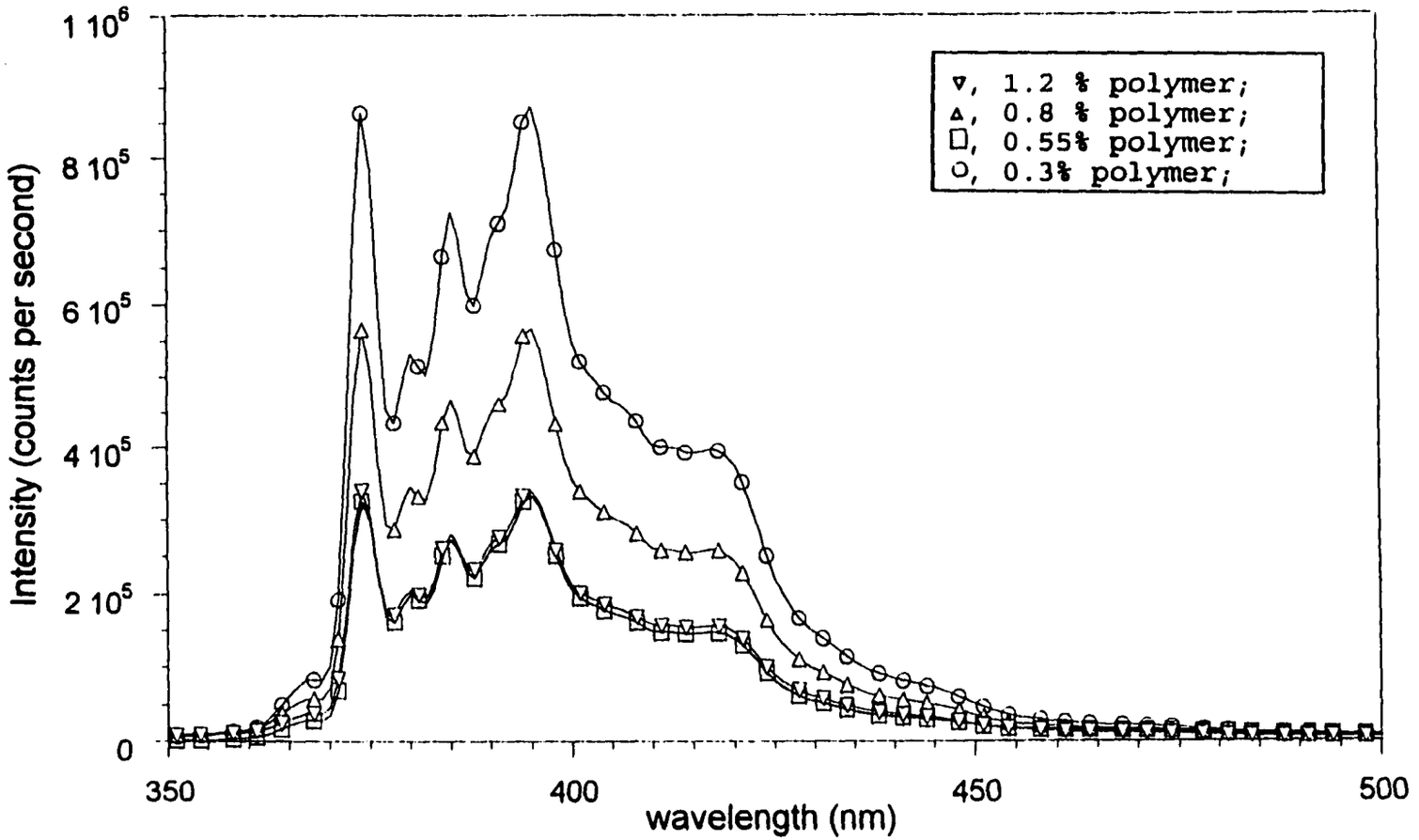

Figure 4.41: Fluorescence spectra of pyrene present in the gel phase of C_9-ϕ HMHEC/(6.9 mM SDS) systems.

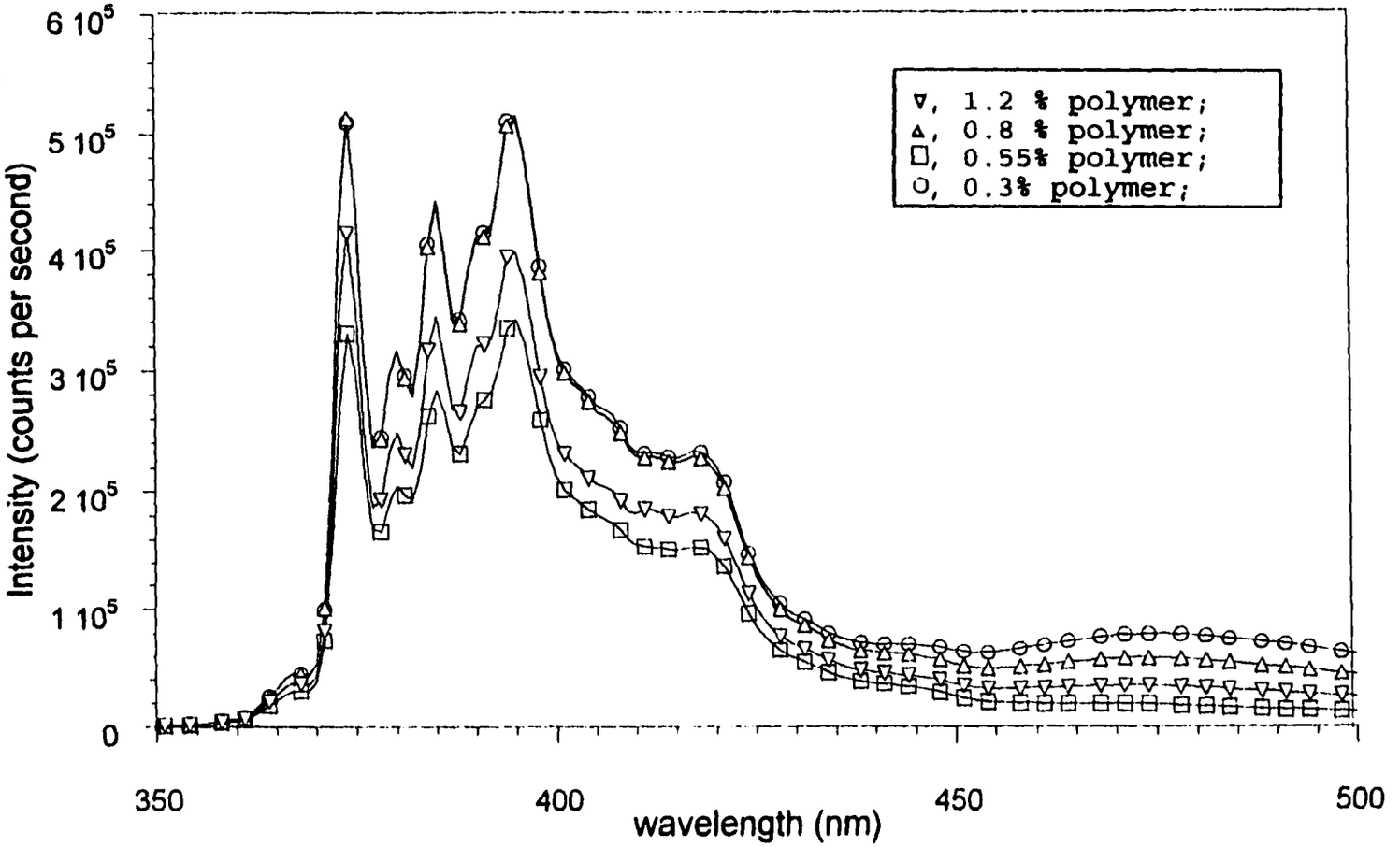

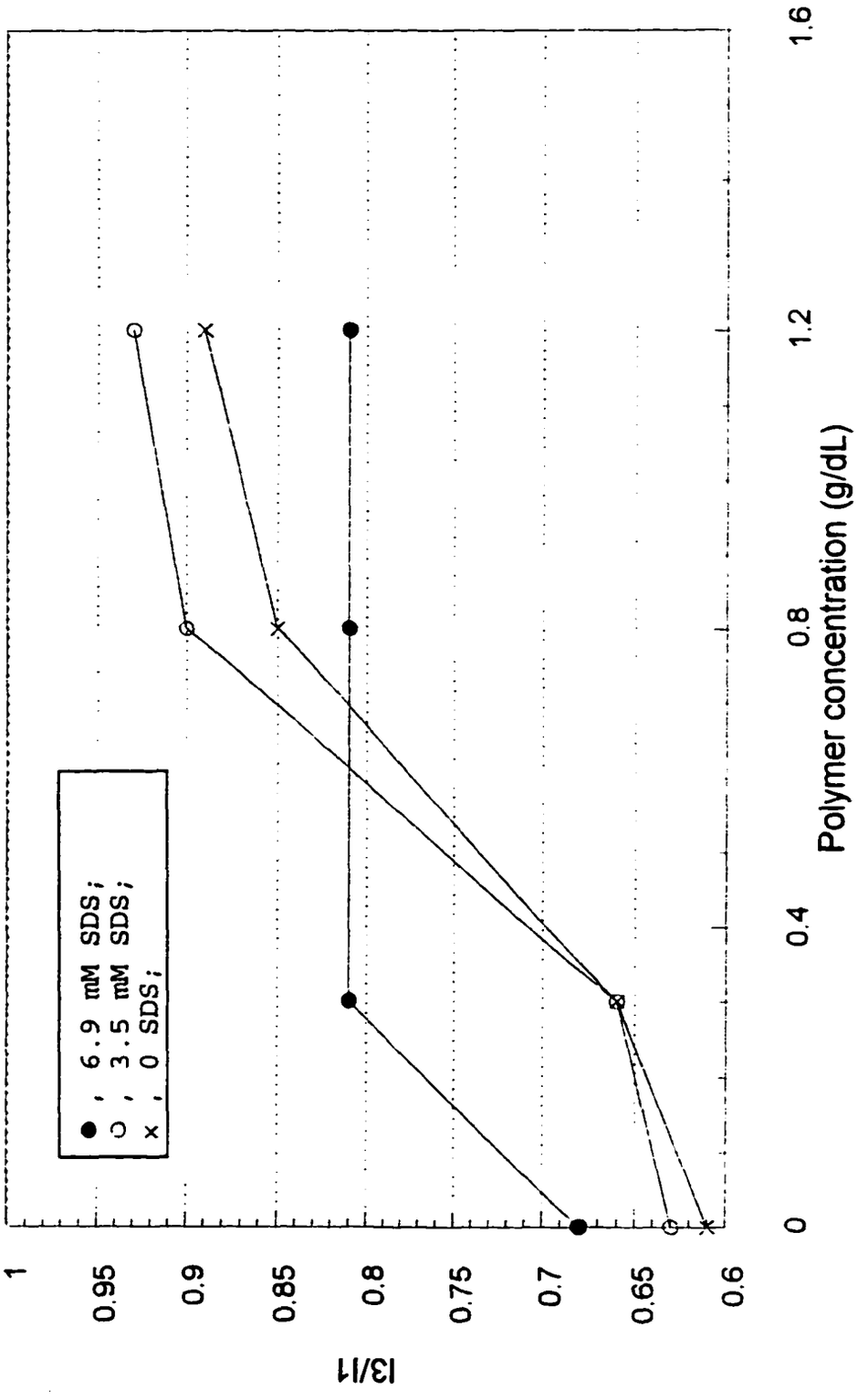

Figure 4.42: Hydrophobicity of control polymer solutions.

Figure 4.43: Effect of bulk polymer concentration on I3/I1 of pyrene present in the gel phase of C_8 HMHEC/SDS systems.

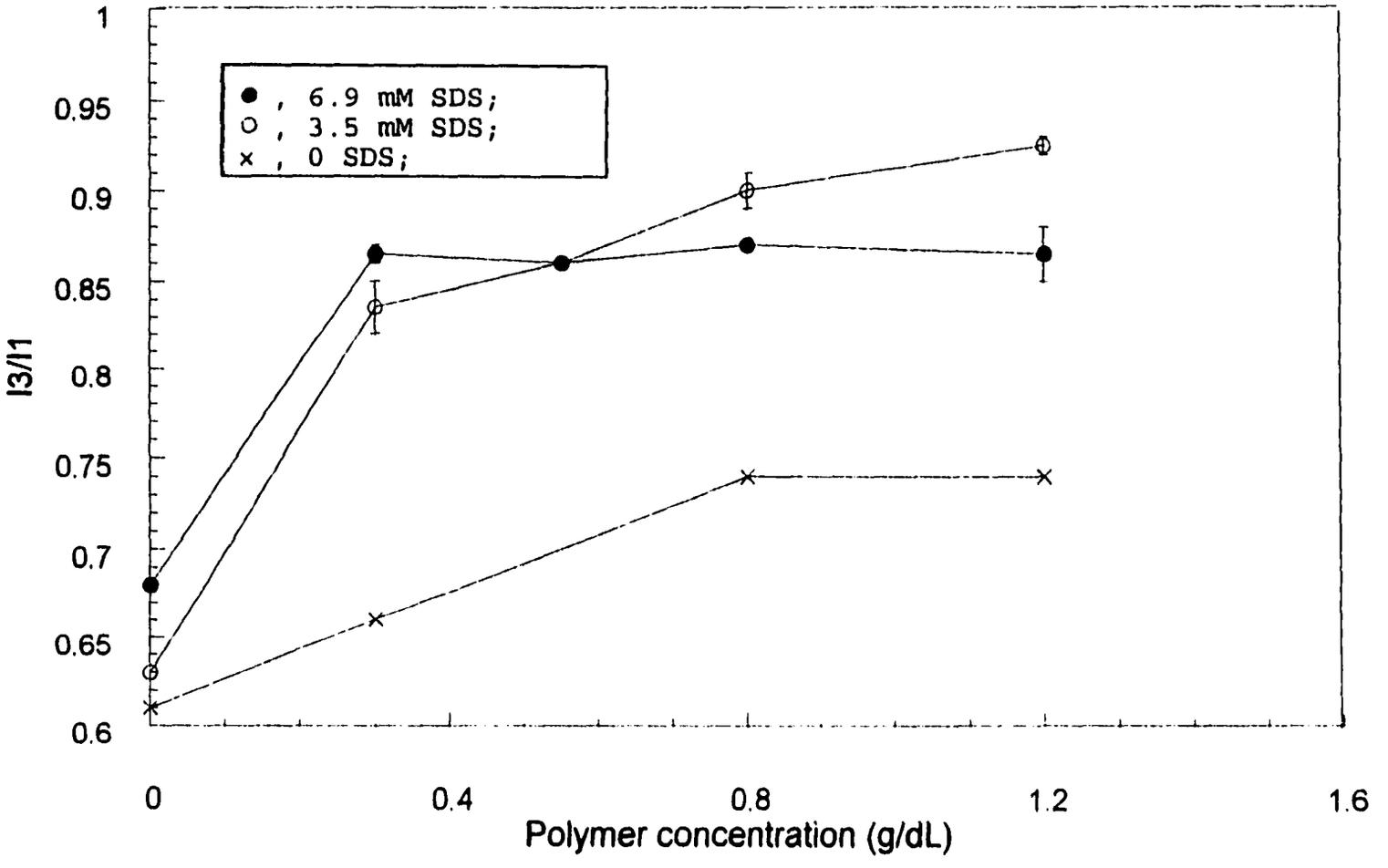

Figure 4.44: Effect of bulk polymer concentration on I3/I1 of pyrene present in the gel phase of C_9-ϕ HMHEC/SDS systems.

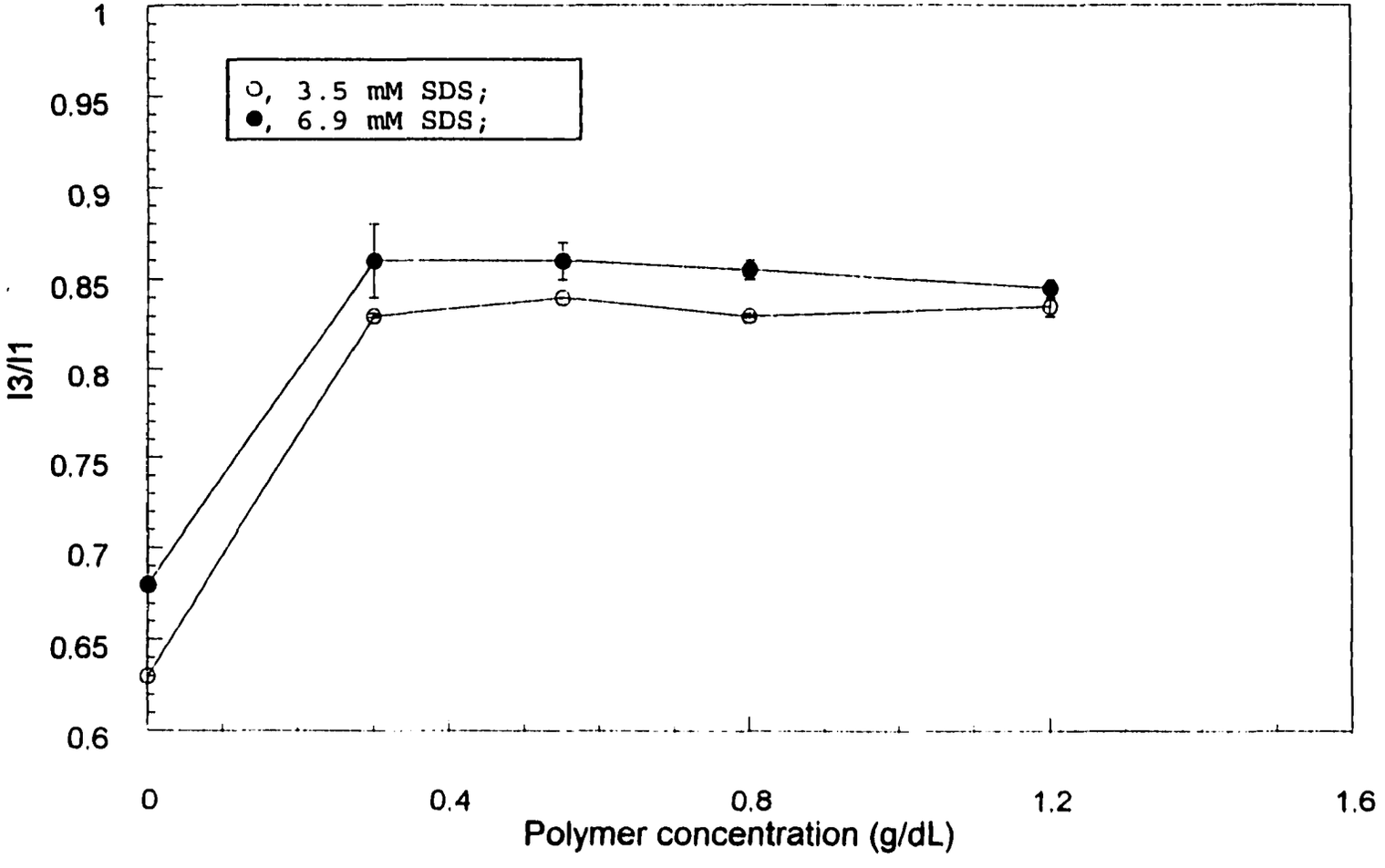

Figure 4.45: Effect of polymer concentration in the gel phase on I3/I1 of pyrene present in hydrogels of C_8 HMHEC/SDS systems.

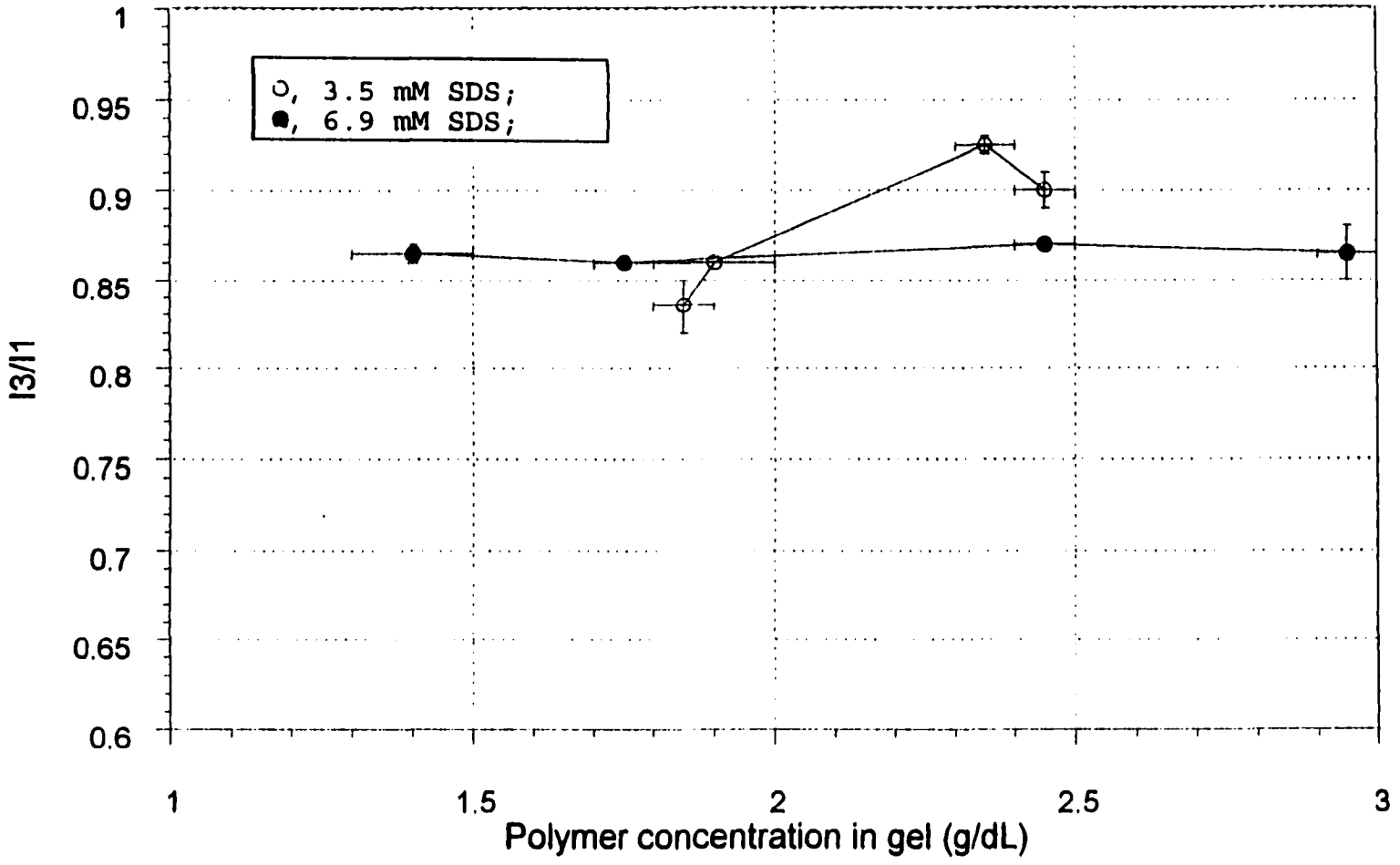

Figure 4.46: Effect of polymer concentration in the gel phase on I3/I1 of pyrene present in hydrogels of C_9-ϕ HMHEC/SDS systems.

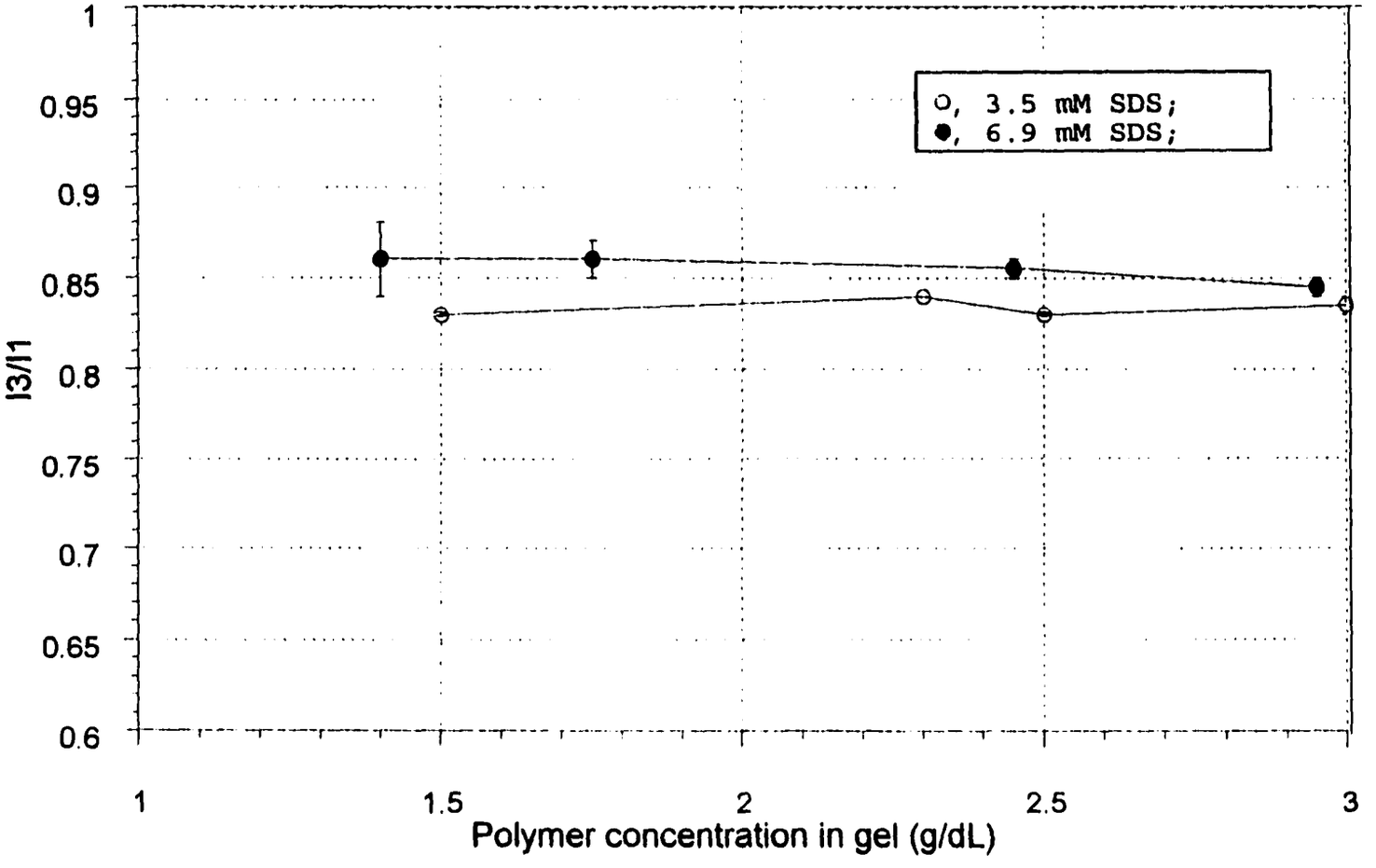

Figure 4.47: Sensitivity of I3/I1 of pyrene present in the gel to N. Open symbols 3.5 mM SDS, closed symbols 6.9 mM SDS systems.

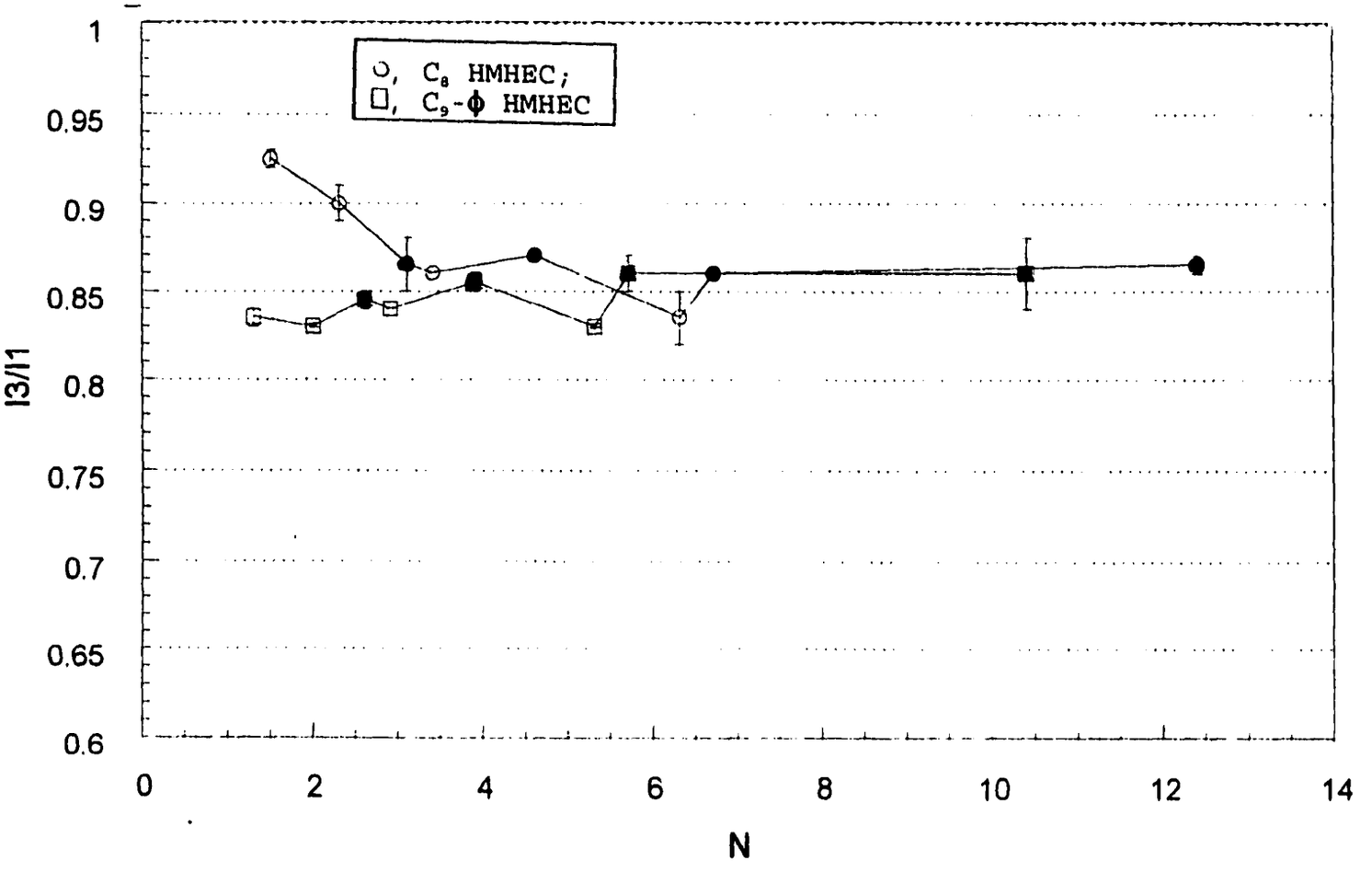

Figure4.48 Phase behavior of polymer H in: ○, SDS; □, SOS; ▽, SS × represents the behavior of control polymer (low DP HEC)in each in of the three surfactants.

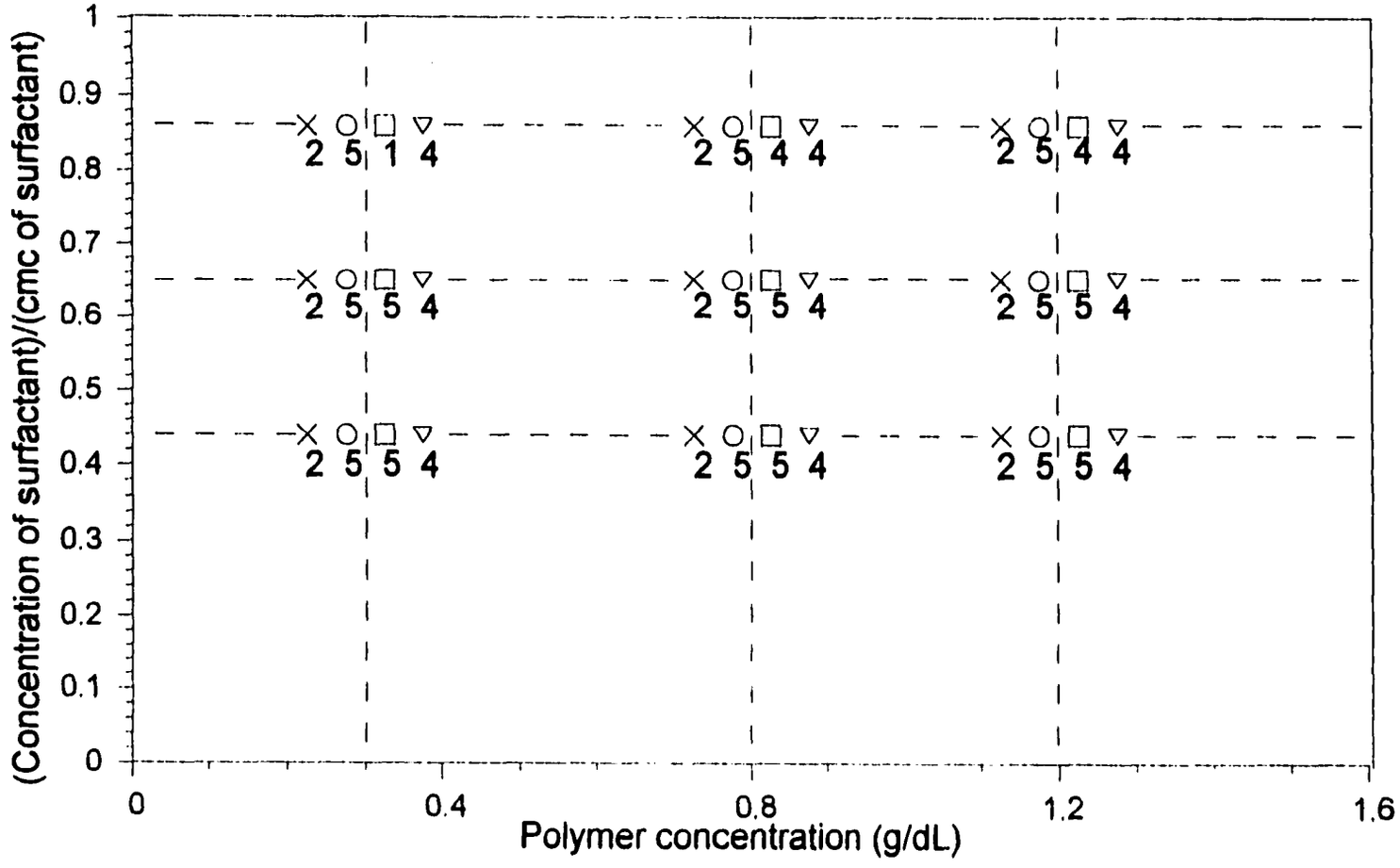

Chapter 5

Summary, conclusions and recommendations for future work

In summary, we have identified several important structure/property relationships governing phase separation and gel formation in HMHEC/surfactant systems. First, hydrogels form in unmicellized SDS solutions from polymers containing 80-210 side chains/backbone; polymers with >390 side chains are incompatible with SDS. For a constant molar substitution of side chain, gel quality improves with the molecular weight of the polymer and with the compatibility of the side chain with solvent. The quality of HMHEC/surfactant hydrogels improves with increasing surface activity of the surfactant, at least for anionic surfactants.

The composition dependence on gel properties was examined in terms of the ratio N=(number of surfactant molecules)/(number of side chains). N was found to be a very good indicator with regard to the quality of gels - intact gels are favored at intermediate values of N while "easily breakable" gels form when N is very high or very low. However, no correlation was found between N and other properties, viz. gel volume and gel hydrophobicity. One parameter which might be responsible for dictating the gel properties is the ratio of the number of SDS molecules in the gel to the number of polymer side chains in the gel. Of the two numbers needed to evaluate the above parameter, in this work I have developed a method to determine the number of

polymer side chains in the gel. Information on the number of SDS molecules in the gel can be obtained by determining the SDS concentration in the supernatant phase and then doing a mass balance over the (gel+supernatant) system. I suggest using spectroscopic methods such as Atomic Absorption (AA) and Fourier Transform Infra-red (FTIR) to determine the concentration of SDS molecules in the supernatant. AA would involve determining the concentration of counterions of surfactant (= concentration of surfactant) in the supernatant. FTIR would involve determining the absorbance of a molecular species present in the surfactant molecules and then converting the absorbance to surfactant concentration using a calibration. For instance, one can determine the absorbance of the $-CH_2-$ asymmetric peak (~ 2920 cm^{-1}) and convert the absorbance to surfactant concentration using a calibration (Part II, reference # 32).

A more detailed study of effect of surfactant concentration on the gel properties (such as gel strength) is needed. This is so since it has been shown that viscosity exhibits a peak with surfactant concentration in solutions. Thus there might exist a surfactant concentration at which the gel strength is maximized.

This study has identified some polymer/surfactant systems which form good gels. I recommend testing these systems for the proposed application of the hydrogels, viz. drug delivery. To start with one should use low molecular weight drugs such

as those used by Varelas et al [26]. It should be kept in mind that since many drugs are amphiphilic in nature, the drug molecules will tend to adsorb at the polymer side chains just as the surfactant molecules. Hence the microdomain and thus rheology properties of the gels are expected to be different with and without the drug molecules. Thus it might be advisable to determine the strength of the drug loaded gels and compare with my results. While conducting the drug release studies, it should be kept in mind that not just the drug molecules but the surfactant molecules as well will be diffusing out of the hydrogel into the reservoir. Thus composition of the microdomains and hence the mechanical strength of the gel will change as the drug release experiment proceeds. This point should be kept in mind during data interpretation. A good control experiment would be to study how the mechanical strength of the "unloaded" gel, viz. with no drug molecules in the gel, changes with time when the gel is contacted with the reservoir. Now, it is not possible to measure the mechanical strength of the gel in-situ since the technique of oscillatory rheology is sample destructive. Thus one will have to prepare various gels of the same composition , contact them with the solvent reservoir for different periods of time and then measure their mechanical strength to evaluate the effect of long-term exposure to flowing solvent on the rheological properties of the gels.

PART 2

CHAPTER 6

INTRODUCTION

The ability to make aqueous solutions spread over hydrophobic surfaces is the key step in the herbicide, fabric, adhesion and superabsorbancy industries. Water does not normally spread on a hydrophobic surface mainly due to the very high surface tension of water.

Insight into the mechanism of spreading can be obtained by differentiating Young's equation,

$$\frac{d(\gamma_{V/L}\cos\theta)}{d(\ln C)} = \frac{d(\gamma_{V/S} - \gamma_{S/L})}{d(\ln C)} \qquad \ldots\ldots\ldots\ldots 6.1$$

and substituting Gibb's equation,

$$\Gamma = -\frac{1}{RT}\frac{d\gamma}{d\ln C} \qquad \ldots\ldots\ldots\ldots 6.2$$

for each of the three interfaces. One obtains,

$$\frac{d\cos\theta}{d\ln C} = \frac{RT[\Gamma_{V/L}\cos\theta + \Gamma_{S/L} - \Gamma_{V/S}]}{\gamma_{V/L}} \qquad \ldots\ldots\ldots\ldots 6.3$$

where γ (force/distance) and Γ(moles/area) refer to the surface tension and concentration of adsorbed surfactant respectively and subscripts V/L, V/S and S/L refer to the vapor/liquid, vapor/solid and solid/liquid interfaces. θ is the contact angle of a drop of solution having a surfactant concentration C. A surfactant enhances spreading only if the contact angle decreases with C, i.e if the derivative $d\cos\theta/d\ln C$ is positive. Hence the right hand side of the equation should also be positive. In addition, the denominator of the right hand side of equation, $\gamma_{V/L}$, should be low to enable a substantial decrease in the contact angle, hence superspreading. Of the three terms in the numerator of the above equation the first term is negative (as $\theta > 90$, and thus $\cos\theta < 0$) and so is the third term. Hence to make the right hand side positive, one has to make the second term of the numerator, viz. $\Gamma_{S/L}$ as large as possible. Thus the surfactant being used should be able to pack very densely at the solid/water interface.

The focus of this work is to study the packing characteristics of surfactants at the solid/water interface. Previous experiments done by our group [19] have shown that some hydrocarbon based ethoxylated surfactants, for instance $C_{14}E_1$, pack very tightly (~20 A^2/molecule) at the air/water interface. One of the objectives of this work is to find out if those surfactants can pack tightly at the hydrophobic surface/water interface as well.

The focus of this study was to use nonionic surfactants, specifically polyethylene glycol monoalkyl ethers $CH_3(CH_2)_{m-1}$-$(OCH_2CH_2)_n$-OH (designated C_mE_n), to modify the wetting characteristics of planar hydrophobic surfaces. In addition the dynamics of surfactant adsorption onto hydrophobic surfaces was investigated as well.

Visual and quantitative evidence of close packing of the ethoxylated surfactants at the hydrophobic/water interface is provided. Visual evidence was obtained using the fluorescence microscopy and quantitative evidence was obtained by using attenuated total reflection Fourier transform infrared spectroscopy (ATR-FTIR). This is the first flow study for C_mE_n adsorption on a solid surface ever to be reported. The hydrophobic surface used was octadecyltrichlorosilane (OTS) modified silicon. The film of OTS produced on silicon is very hydrophobic (water contact angle ~ 107 degrees) and is characterized by high physical and chemical stability. The C_mE_n used was $C_{14}E_1$. The data obtained was compared with kinetic data of $C_{14}E_6$ adsorption on hydrophobic surfaces. Such a comparison enabled us to determine the effect of length of polar group on the kinetics of adsorption.

The work presented here is divided into different chapters. Chapter 7 is a literature review and deals with 'superspreading' and adsorption characteristics of siloxane based and C_mE_n surfactants. Chapter 8 deals with the materials, experimental techniques and procedures that were

employed in this study. The results and discussions are included in chapter 9. Chapter 10 contains recommendations for future work.

CHAPTER 7

Literature review

Spreading of aqueous solutions over hydrophobic surfaces

Spreading of water on hydrophobic surfaces is extremely important in the herbicide [1, 2], cosmetics [3] and coatings [4] industry. Water is unable to spread on hydrophobic surfaces. This can be explained by taking a force balance at the water, solid and vapor contact point (refer Figure 7.1 where a drop of water is placed on a hydrophobic solid),

$$\gamma_{v/s} - \gamma_{v/L}\cos\theta = \gamma_{s/L} \qquad \ldots\ldots\ldots\ldots 7.1$$

Equation 7.1 can be re-written as,

$$\cos\theta = (\gamma_{v/s} - \gamma_{s/L})/\gamma_{v/L} \qquad \ldots\ldots\ldots\ldots 7.2$$

The symbols $\gamma_{v/s}$, $\gamma_{s/L}$ and $\gamma_{v/L}$ refer to the vapor/solid, solid/liquid and vapor/liquid interfacial tensions respectively and θ refers to the contact angle.

Hydrophobic surfaces have very low $\gamma_{v/s}$, and when water is placed over them the $\gamma_{s/L}$ is very high due to dissimilar polarities of the solid and water. As a consequence, the

numerator in equation 7.2 is negative and thus the contact angle is > 90. Thus spreading of water over hydrophobic surfaces is inhibited. Previous research has demonstrated that some siloxane based surfactants can promote complete spreading ($\theta \sim 0$ degrees), termed 'superspreading', of aqueous solutions over hydrophobic surfaces such as parafilm [5-9]. These surfactants have been used as wetting agents for water-based insecticides on plant leaves [1, 10].

7.1 Spreading ability of Siloxane based surfactants

The structure of siloxane based surfactants is shown in Figure 7.2. These surfactants consist of a compact hydrophobic part, in which methyl (CH_3) groups are linked to a siloxane backbone, and an extended hydrophilic part which consists of an ethoxylate chain $(-OCH_2CH_2)_n$ with an end group R. The value of n is 4, 5, 7.5 (commercially available mixture of various $(-OCH_2CH_2)_n$), 8, 12, 16 or 18 and R is -H, $-CH_3$ or $-C(C=O)CH_3$.

The spreading behavior of the homologous series (n=5 to 18) of the above surfactants was examined by He et al. [8]. For concentration of 1 wt %, for a variety of end-caps 'R', the n = 5, 7.5 and 8 member solutions spread on parafilm (water contact angle, θ = 97 degrees). However, the n = 12, 16 and 18 member solutions do not promote spreading.

Recent work by Stoebe et al. [6] has shown that

superspreading can be achieved even by the non-spreading members (n =12, 16 and 18) but on surfaces more hydrophilic than parafilm (θ < 90). The spreading characteristics of a homologous series of the siloxane surfactants (n = 4, 8 and 12) were studied over substrates with different hydrophobicity (θ ranging from 0 to 114 degrees). As expected from the work of He et al [8], the lower member of the homologous series (n=4, which was not studied by He et al. and n=8) were superspreaders on highly hydrophobic surfaces (θ > 90). In addition, the n = 12 member of the homologous series, which is a non-spreader on highly hydrophobic surfaces (θ > 90), is a superspreader for less hydrophobic surfaces (θ < 90).

The mechanism involved in superspreading is unclear. Ananthpadmanabhan et al [9] proposed that when a drop of a solution of a spreading surfactant is placed on a hydrophobic surface, a primary film (precursor film) spreads ahead of the surfactant drop. The surfactant present on the surface of the precursor film starts getting depleted due to the transfer of surfactant to the solid/water interface (see Figure 7.3). The transfer of surfactant to the solid/water interface is highly favorable due to the geometry of the siloxane surfactant, viz. a highly hydrophobic and compact hydrophobic part and a long hydrophilic part. Due to this transfer, the surface of the precursor film has a lower surfactant concentration and thus a higher surface tension as compared to the rest of the drop. The surface tension gradient drives the water flow in the

direction of increasing tension, viz. towards the precursor film. The drawback of this description is that the issue of how and why the precursor film is formed has not been addressed. In addition, this mechanism does not explain the variation of the spreading characteristics of the homologous series of the surfactants with surface hydrophobicity.

7.2 Proposed mechanism for superspreading

Recall, as proposed in the previous chapter (equation 6.3), one way to enhance spreading is to use a surfactant which has $\Gamma_{s/L}$ as large as possible. The packing density of the surfactant at the hydrophobic solid/water interface depends on the structure of the surfactant. The concentration of surfactant at the solid/water interface (at least for an ethoxylated surfactant and a hydrophobic surface), for a given hydrophobic group, is expected to decrease with an increase in the number of ethoxy groups present in the surfactant. This can be explained as follows. When a surfactant adsorbs onto a hydrophobic surface, the surfactant must configure itself so as to develop some hydrophobic interaction with the nonpolar surface or itself so that it can shield the hydrophobic part from water. The configuration must allow the polar groups to remain in contact with water. If this energy lowering does not occur there is no free energy gain on adsorption, and adsorption of surfactant onto the solid/water interface will be minimal. With large polar groups, the chains cannot stack

very close together and hence the surface concentration at the surface is limited.

We postulate that the reason why the highly hydrophilic trisiloxane surfactants (n = 12, 16 and 18) do not superspread on parafilm is because they cannot achieve a high enough surface concentration to make the right hand side of equation 6.3 positive. However, in case of a surface having a lower hydrophobicity ($\theta < 90$), $\Gamma_{v/L}Cos\theta$ in the numerator of the right hand side of equation 6.3 is positive, hence the right hand side can become positive for a lower $\Gamma_{v/L}$ (as compared to the case of a surface with $\theta > 90$). Hence it is possible for the higher members (n = 12, 16 and 18) to exhibit superspreading on a surface with $\theta < 90$.

7.3 Spreading ability of hydrocarbon based surfactants

Hydrocarbon based polyethoxylated surfactants (for structure refer Figure 7.4) were also shown to be superspreaders for surfaces which are less hydrophobic than parafilm [6]. The authors studied the homologous series of $C_{12}E_n$ (n=4, 5, 6). The results were similar to those for the siloxane based surfactants. Increased length of the hydrophilic part results in poorer spreading. This result can once again be explained in terms of a decrease in the concentration of the surfactant at the solid/water interface with an increase in n. The dependence of surface concentration on the surfactant structure has been studied by various authors [13-17]. It has been shown that the

equilibrium adsorbed amount of a C_mE_n surfactant on a hydrophobic surface increases with an increase in the ratio m/n. This is because the C_mE_n surfactants are composed mostly of methylene groups, significant hydrophobic interaction at an interface can only be obtained by stacking the chains perpendicular to each other. This degree of interaction increases with an increase in the number of methylene groups per molecule, hence m. However, with an increase in n the chains cannot stack together due to the presence of bulky headgroups and thus the degree of hydrophobic interaction and hence the amount adsorbed decreases.

In this work we plan to identify and study spreading characteristics of certain C_mE_n surfactants that exhibit superspreading behavior on very hydrophobic surfaces ($\theta > 90$). The identification of the appropriate C_mE_n surfactants will be based on the rationale discussed above. As noted there are two key factors which determine the spreading ability of surfactants, viz. a high packing density of the surfactant at the solid/water interface and a low air/water surface tension. This work focusses on one of the two factors involved in superspreading, viz. high packing density at the solid/water interface. Previous experiments done by our group [19] have demonstrated that $C_{14}E_1$ packs very tightly at the air/water interface. Hence the main objective of this work is to find out if $C_{14}E_1$ can pack tightly at the hydrophobic surface/water interface as well.

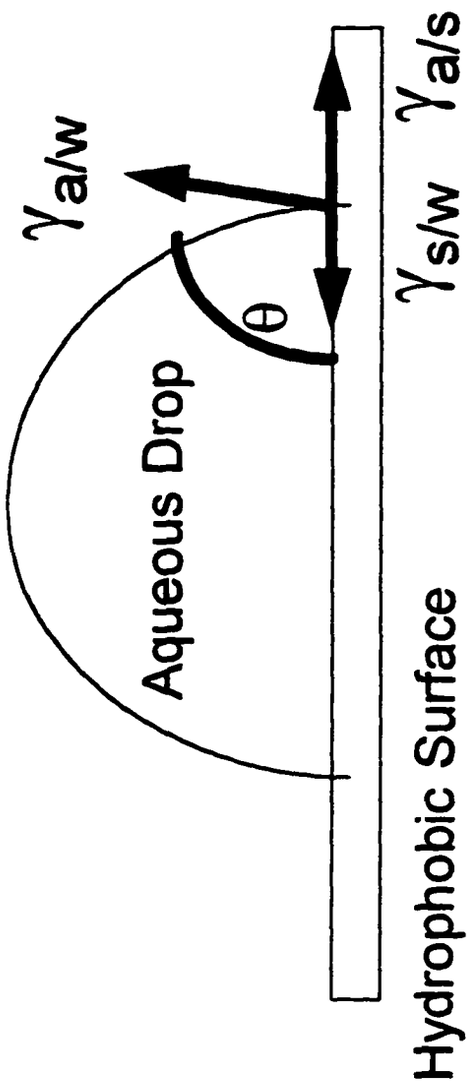

Figure 7.1: Aqueous drop placed on a hydrophobic surface.

Figure 7.2: Structure of Siloxane based surfactants.

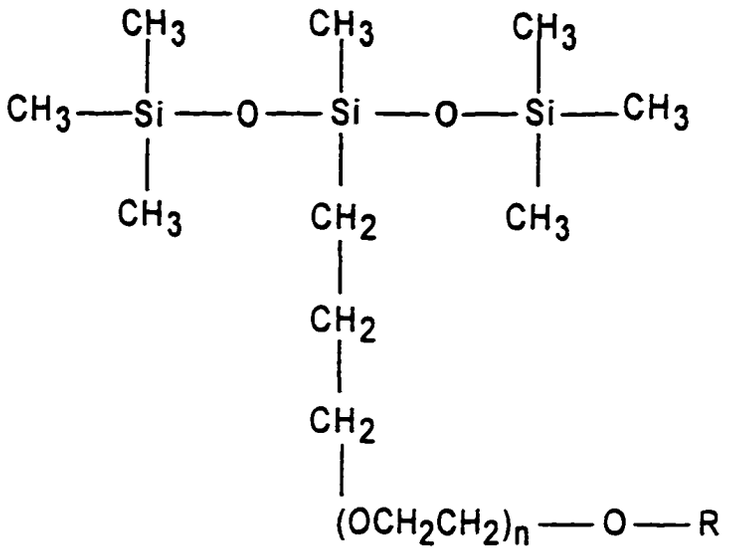

Figure 7.3: A schematic depiction of the transfer of surfactant molecules from the air/water interface to hydrophobic surface/water interface. (reference # 9)

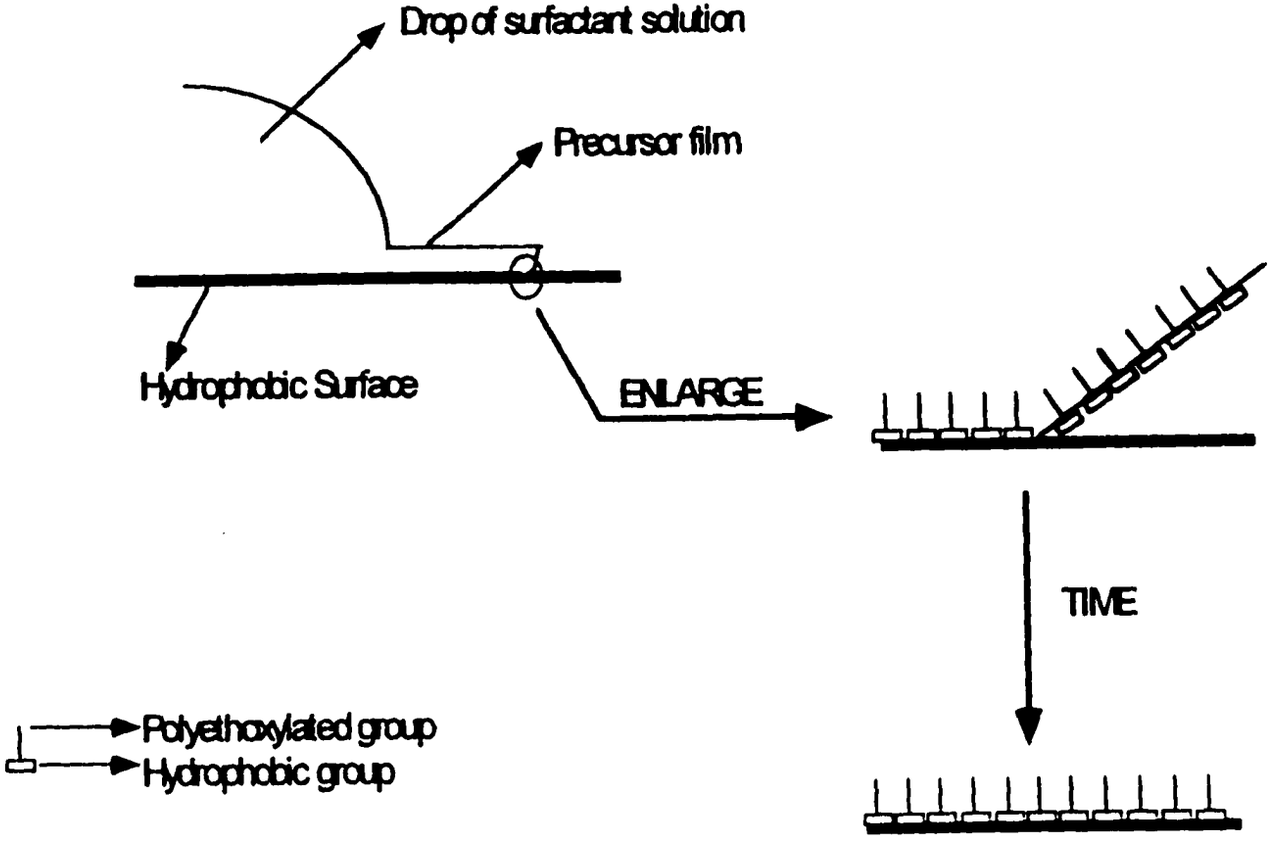

Figure 7.4: Structure of hydrocarbon polyethoxylated surfactants.

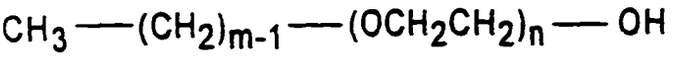

CHAPTER 8

Experimental section

8.1 Materials

Ethyleneglycol mono n-tetradecyl ether ($C_{14}E_1$) (>99.9 %) and hexa-ethyleneglycol mono n-tetradecyl ether ($C_{14}E_6$) (>99.9%) were supplied by Nikko Chemicals Ltd., Tokyo, Japan. 4-(hexadecylamino)-7-nitrobenz-2-oxa-1,3-diazole) (NBD-HDA) used for fluorescence observation was supplied by Molecular Probes, Eugene, OR. Octadecyltrichlorosilane (OTS) (95%), chloroform (>99.9%), carbon tetrachloride (>99.9%) and hexadecane (99%) were purchased from Aldrich. All surfactants and solvents were used as received. Sulfuric acid (95-98%, Fisher Scientific) and Nochromix crystals (Aldrich) were also used as received. The silicon Internal Reflection Element (IRE) used in this study had dimensions of 50*10*3 mm with the bevelled edge cut at 45 degrees. The IRE was obtained from Aldrich. Water used for our experiments was obtained by passing tap water through a Milli-Q filter system fit with an Organex-Q column to remove trace surface active impurities (Millipore, Marlborough, MA).

8.2 Methods

8.2.1 Cleaning protocol

This sub-section describes in detail the cleaning protocol followed for conducting our experiments to remove

impurities, especially the surface active ones. All glassware (including glass cover-slips) was first sonicated in freshly prepared Nochromix (active agent ammonium bisulfate) solution (Nochromix crystals dissolved in sulfuric acid) for 30 minutes. This was followed by rinsing the glassware with water and subsequent sonication in water for 15 minutes. Cleaning the Teflon beaker (for fluorescence imaging experiment) and the flow cell for in-situ flow experiments involved two modifications over the glassware procedure. First the time for sonication in Nochromix solution was reduced to 10 minutes. This was done to avoid absorption of sulfuric acid by Teflon. The problem of absorption exists over long exposure times. Second, after Teflon was sonicated in water it was treated in a plasma cleaner (Harrick Scientific Corporation, model PDC-32G) for 10 minutes. The plasma treatment was performed using argon at a power of 100 W. Cleaning of the Silicon IRE involved two steps. The first is the same as that used for cleaning glassware. In the second step each side of the IRE was treated in the plasma cleaner for 10 minutes. The rubber O-rings used in the flow cell were sonicated in ethanol for 15 minutes, rinsed with water and then sonicated in water for 15 minutes. The aluminum foils used in the flow cell, to shield Teflon from the IR beam, were cleaned by plasma treating each side for 10 minutes. The ZnSe windows used in the liquid cell for taking FTIR spectra in transmission mode, were sonicated in acetone

for 15 minutes and then each side was plasma treated for 15 minutes. Clean Si IRE, flow cell and all accessories were handled using Teflon tweezers which had been cleaned prior to use following the protocol given above for cleaning Teflon surfaces.

All glassware that comes in contact with OTS has to be pre-treated with OTS. This treatment is necessary as OTS reacts with the Si-OH groups present on the glass surface, and as a consequence the bulk concentration of OTS is reduced. The pre-treatment method involves allowing the OTS to react with all the Si-OH groups on the glass surface. The glass surface was contacted with 30 mM solution of OTS in chloroform for 14 hours. These conditions are more than sufficient for all Si-OH groups on the surface to react [20]. In fact there exists the possibility of some physisorbed OTS on top of the chemisorbed layer. To remove this physisorbed layer we sonicated the glassware twice in fresh chloroform. Each sonication was done for 30 minutes. This was sufficient time to remove all physisorbed OTS, as evidenced by the absence of all hydrocarbon related peaks in the FTIR spectrum of residue from the sonicated chloroform. The FTIR spectrum was taken in transmission mode using ZnSe liquid cell. 150 μl of sonicated chloroform was spread on one ZnSe cell and allowed to evaporate. After 10 minutes, which was sufficient for chloroform to evaporate, the other ZnSe window was placed on top of the first one and the spectrum taken.

8.2.2 Preparation of hydrophobic surfaces

Hydrophobic surfaces were prepared using a method proposed by Sagiv et. al. [21-24]. The reaction scheme proposed by Sagiv is shown in Figure 8.1. A 2 mM solution of OTS was prepared in a ternary solvent of composition (by volume) - 80% hexadecane, 8% chloroform and 12 % carbon tetrachloride. 45 minutes after preparing this solution the substrate (glass coverslip or Si IRE) was immersed in it. The substrate was kept immersed for 10 minutes. After that the substrate was removed from the solution and the physisorbed layer of OTS was removed by sonicating the substrate in fresh chloroform twice. Each sonication was done for 30 minutes. The degree of hydrophobicity of the substrates was determined by measuring the contact angle of water drops measured using a Goniometer NRL C.A. (Rame-Hart, Inc., Mountain Avenue, NJ). The measurements were performed at room temperature and contact angles were measured immediately after placing the water drop on the substrate. Contact angles were taken at 5 to 6 spots on the substrate and the values averaged. All contact angles were within ±3 degrees.

8.2.3 Surface pressure isotherm of Octadecyltrichlorosilane (OTS)

The surface pressure isotherm of octadecyltrichlorosilane (OTS) was determined by using a Langmuir film balance (Lauda Model D, Lauda Konigshofen, Germany). The trough of the Langmuir was filled with water

(Millipore water, 18 MΩ). The water had a pH of 5.7 and was maintained at a temperature of 18.6 C. Next a 0.3±0.003 mg/mL solution of OTS in chloroform was prepared. Immediately after preparation of the stock solution, 200 μl was spread onto the water present in the Langmuir trough. The initial area per molecule (when the barriers were fully expanded) of OTS on the water surface was 100 A^2/molecule. The compression of the monolayer was started one minute after the OTS stock solution was spread (to allow the chloroform to evaporate). The compression of the monolayer was stopped when the area per molecule of OTS reached 16 A^2/molecule. The surface tension of water was recorded continuously as the monolayer was compressed. The surface pressure was obtained by subtracting the surface tension of the water from the surface tension of pure water. A plot of surface pressure versus area per molecule of OTS (surface area of subphase)/(concentration of OTS stock solution*volume of stock solution spread onto the subphase*Avogadro number) gave the surface pressure isotherm.

8.2.4 Fluorescence imaging of air/water and hydrophobic solid/water interface

A schematic of the fluorescence set-up is shown in Figure 8.2. The main components are a light source for excitation of the fluorescent dye at the interface, an optical filter to isolate the fluorescence emission, and a camera to view and record the interface fluorescent contrast. The water

insoluble dye used in this study, NBD-HDA, has its absorbance and emission bands with maxima at 468 nm and 523 nm, respectively. To excite the NBD-HDA molecules we used a 10 mW Argon ion laser, λ = 488 nm (Ion Laser Technology, Salt Lake City, UT), impinging the interface obliquely from above using an adjustable mirror. The fluorescence emission passed through a microscope objective and an emission filter with a lower cutoff wavelength of 515 nm (Omega optical, Brattleboro, VT), to a camera (Hamamatsu model C2741-08, Hamamatsu-City, Japan).

The fluorescence experiments were conducted in a Teflon trough (surface area~34 cm^2, height~2 cm). This trough was not equipped for compression and thus allowed only constant area observation. The experiment involved observation of a fluorescently doped, spread monolayer of $C_{14}E_1$ at air/water interface in the liquid condensed (LC)/liquid expanded (LE) region and then transfer of this monolayer to a hydrophobic solid/water interface. A stock solution with 8.9 mM $C_{14}E_1$ and 0.5 mole % NBD-HDA (relative to $C_{14}E_1$) was prepared in chloroform. The air/water interface was aspirated to remove dust particles and then 2.7 μl of the $C_{14}E_1$ stock solution was spread on the interface, which corresponds to a surface concentration which lies in the LE/LC phase transition, viz. 24 A^2/molecule [19]. One minute was allowed for chloroform to evaporate and then the fluorescence image was recorded. Next the hydrophobic glass coverslip was held with tweezers and

brought face down onto the monolayer. Care was taken to avoid trapping any air bubbles between the coverslip and the monolayer. After 15 seconds the coverslip was pushed through the monolayer and placed on a holder resting at the bottom of the Teflon well. The holder along with the coverslip was then removed from the well and the water on top of the coverslip was removed by aspiration. Care was taken that the underside of the coverslip was always in contact with water. The fluorescence image of the coverslip/water interface was then recorded.

8.2.5 Flow experiments to study adsorption of surfactants onto hydrophobic surfaces

A schematic of the flow cell used for observing the adsorption of bulk-soluble surfactants onto the hydrophobic solid/water interface is shown in Figure 8.3 The flow cell consists of two Teflon blocks each having a flow cavity with dimensions 40*3*1 mm. The Si IRE is clamped between the two halves of the flow cell. Only one flow channel was used for the experiments. The flow was provided by using either peristaltic pumps (under suction) or syringe pumps. The inlet tube to the cell was connected to a Y-connector. The connector enabled us to flow either surfactant or water through the flow cell without having to interrupt the flow. A flow rate of ~1.2 mL/hour was used. This low flow rate was selected so as to minimize convective effects in the flow

cell. The hydrophobic surface was prepared by hydrophobically modifying the Si IRE using the procedure mentioned earlier. The angle of incidence at the Si IRE/OTS interface was 45 degrees. This is greater than the critical angle ($\sin^{-1}(1.33/3.42)$=23 degrees) (refer section 8.3.2). Typically we flowed water over the hydrophobic surface for a few hours before switching to surfactant. In case of $C_{14}E_1$ we used an over-saturated solution concentration (7 mg/L) since the solubility of $C_{14}E_1$ in water is very low (<0.1 mg/l). For a fair comparison of limiting surface coverage for $C_{14}E_1$ and $C_{14}E_6$ we used a $C_{14}E_6$ concentration of ~5 mg/L. This concentration is above cmc of $C_{14}E_6$ and from previous studies will thus give the highest possible surface coverage for $C_{14}E_6$ [17]. All the experiments were conducted at room temperature.

The adsorption of surfactant was monitored by the increase in the integrated absorbance of the asymmetric methylene stretch peak (2917-2926 cm^{-1}). Spectra were collected as interferograms using a Bio-rad (FTS-175) spectrometer at a resolution of 2 cm^{-1}, between 400 and 4000 cm-1. Each spectrum was the average of at least 100 scans. The signal to noise ratio is at least of order 10^{+4}. All interferograms were converted to absorbance spectra using air spectrum as the background. Typical spectra in the 3000-2800 cm^{-1} region, which includes the CH_2 asymmetric stretch, as a function of time are shown in Figure 8.4. The integrated absorbance of the surfactant adsorbed on the hydrophobic

surface was obtained by subtracting the integrated absorbance for surfactant flow from that for water flow. This subtraction was necessary to cancel the contribution of OTS to the integrated absorbance.

8.3 Experimental Theory

8.3.1 Fluorescence microscopy

Fluorescence microscopy is a useful technique for visual observation of the monolayer phase transitions, like liquid expanded (LE) and liquid condensed (LC). In fluorescence microscopy [25, 26], a small amount of a water insoluble fluorescent dye is spread onto the air/water interface along with the surfactant under study. The monolayer is illuminated at the excitation wavelength of the dye, and the fluorescence is filtered and observed. In the LE/LC coexistence phase, the dye is solubilized in the LE phase while it is expelled from the LC phase. The expulsion occurs because the LC phase is very tightly packed. Thus the fluorescence image shows the LE phase to be bright and the LC phase to be dark.

8.3.2 IR spectroscopy and its application to determine molar absorptivity and to monitor kinetics of surfactant adsorption.

Principles of transmission mode

In transmission mode IR spectroscopy the sample of

interest is placed in the path of the IR beam. The transmittance (T) of the sample is defined as the ratio I/I_0, where I_0 is the intensity of IR radiation entering the sample and I is the intensity transmitted by the sample. The fundamental equation governing the absorption of IR is,

$$T = I/I_0 = 10^{-\epsilon bc} \qquad \ldots\ldots\ldots \quad 8.1$$

where b is the sample cell thickness (cm), c is the concentration of the absorbing molecule (mol/cm^3) and ϵ is the molar absorptivity (cm/mol) and is characteristic for a specific compound at a specific wavelength. Equation 8.1 can be rewritten in terms of the absorbance, A of the molecule, defined as

$$A = \log(I_0/I) = \epsilon cb \qquad \ldots\ldots\ldots \quad 8.2$$

The absorption law, as shown in the above equation, is commonly referred to as the Beer-Lambert law.

Principles of Attenuated Total Reflectance (ATR)

We used the technique of ATR-FTIR to monitor the kinetics of adsorption of surfactants at the solid/water interface.

The principle behind this technique is explained below. When light strikes an interface between two media it is partially reflected and partially transmitted. When light strikes the interface from the denser medium the reflection is called internal reflection. Total internal reflection i.e., there is no transmitted portion of the incident beam takes place, takes place when the angle of incidence (θ) is greater than a critical angle(θ_c),

$$\theta_c=\sin^{-1}(\eta_{21})$$

..... 8.3

where η_{21} is the ratio of refractive index of the rarer medium to that the denser medium. Total internal reflection gives rise to a standing wave in the denser medium and an evanescent wave in the rarer medium [27]. The amplitude of the evanescent wave decreases exponentially from the interface and is given by,

$$E=E_0 e^{-z/d_p}$$

..... 8.4

E_0 is the amplitude of the electric field at the interface and can be calculated from the following equations,

$$E_{y0}=\frac{2\cos\theta}{(1-\eta_{21}^2)^{1/2}} \qquad \ldots\ldots\ldots \quad 8.5$$

$$E_{x0}=\frac{2(\sin^2\theta-\eta_{21}^2)^{1/2}\cos\theta}{(1-\eta_{21}^2)^{1/2}[(1+\eta_{21}^2)\sin^2\theta-\eta_{21}^2]^{1/2}} \qquad \ldots\ldots\ldots \quad 8.6$$

$$E_{z0}=\frac{2\sin\theta\cos\theta}{(1-\eta_{21}^2)^{1/2}[(1+\eta_{21}^2)\sin^2\theta-\eta_{21}^2]^{1/2}} \qquad \ldots\ldots\ldots \quad 8.7$$

where E_{x0}, E_{y0} and E_{z0} are the x, y and z components of the electric field amplitude at the interface. Thus d_p is the distance from the interface where the electric field is equal to E_0/e. d_p is given by the following equation,

$$d_p = \frac{\lambda_1}{2\pi (\sin^2\theta - \eta_{21}^2)^{1/2}}$$

..... 8.8

λ_1 is the wavelength of the incident beam in the denser medium, $\lambda_1 = \lambda/\eta_1$. λ is the wavelength of the IR beam in air.

A schematic of the flow cell used for the surfactant flow experiments is shown in Figure 8.3. An IR beam entering a Si IRE undergoes multiple total internal refections at the Si/SiO_2 interface before exiting the IRE. At each of the points of reflection an evanescent wave is created which propagates into SiO2, OTS, adsorbed surfactant and then into the bulk surfactant solution. If the beam undergoes N solution sensing reflections, then the total integrated absorbance is given by [28, 29],

$$A_{j,k} = \frac{N\eta_{21}E_0^2}{\cos\theta}\int_0^{\infty} \epsilon_{i,j,k} C_{i,j} e^{-2z/d_p} dz$$

..... 8.9

where,

$A_{j,k}$ is integrated absorption of 'j' group in 'k' vibrational

mode [1/cm],

$c_{i,j}$ is the concentration of 'j' group in 'i' layer [mol/cc]

$\epsilon_{i,j,k}$ is the molar absorptivity of 'j' group in 'k' vibrational mode in the 'i' layer, [cm/mol]

Equation 8.9 was integrated over a step-type concentration profile [28] at the OTS/surfactant interface: $c_{t2-\infty,j} = c_{ads,j} + c_{bulk,j}$ for $t_2<z<t_3$ and $c_{t2-\infty,j} = c_{bulk,j}$ for $t_3 < z < \infty$.

$$A_{j,k}=\frac{N\eta_{21}E_0^2}{\cos\theta}\left(\int_0^{t_1}\epsilon_{SiO_2,j,k}C_{SiO_2,j}e^{-2z/d_p}dz+\int_{t_1}^{t_2}\epsilon_{OTS,j,k}C_{OTS,j}e^{-2z/d_p}dz\right.$$

$$\left.+\int_{t_2}^{t_3}\epsilon_{ads,j,k}C_{ads,j}e^{-2z/d_p}dz+\int_{t_2}^{\infty}\epsilon_{bulk,j,k}C_{bulk,j}e^{-2z/d_p}dz\right)$$

..... 8.10

where t_i is the thickness of 'i' layer. For a hydrocarbon peak the first term in equation 8.10 does not exist. Doing an analysis for the CH_2 asymmetric peak,

$$A_{CH_2,a}=\frac{N\eta_{21}E_0^2}{\cos\theta}\left({}_{t_1}\int^{t_2}\epsilon_{OTS,CH_2,a}C_{OTS,CH_2}e^{-2z/d_p}dz\right.$$

$$\left.+{}_{t_2}\int^{t_3}\epsilon_{ads,CH_2,a}C_{ads,CH_2}e^{-2z/d_p}dz+{}_{t_2}\int^{\infty}\epsilon_{bulk,CH_2,a}C_{bulk,CH_2}e^{-2z/d_p}dz\right)$$

..... 8.11

where subscript a in $\epsilon_{bulk,CH2,a}$ refers to the asymmetric stretch of CH_2.

For water flow,

$$A_{CH_2,a}=\frac{N\eta_{21}E_0^2}{\cos\theta}\left({}_{t_1}\int^{t_2}\epsilon_{OTS,CH_2,a}C_{OTS,CH_2}e^{-2z/d_p}dz\right)$$

..... 8.12

Subtracting equation 8.12 from 8.11,

$$A_{CH_2,k}=\frac{N\eta_{21}E_0^2}{\cos\theta}\left({}_{t_2}\int^{t_3}\epsilon_{ads,CH_2,a}C_{ads,CH_2}e^{-2z/d_p}dz+{}_{t_2}\int^{\infty}\epsilon_{bulk,CH_2,a}C_{bulk,CH_2}e^{-2z/d_p}\right.$$

..... 8.13

To evaluate this integral we used the approximation

$e^{-t/dp} = 1 - t/dp$. This is valid for the conditions in our system because t_1, t_2, t_3 < 100 A [16, 30, 31] and d_p for CH_2 asymmetric peak ~ 2700 A. Evaluating the integral gives,

$$\frac{A_{CH_2,k}}{N} = \epsilon_{ads,CH_2,a}\left(2\frac{d_e}{d_p}\right)\left(C_{ads,CH_2}(t_3-t_2)\right) + \epsilon_{bulk,CH_2,a}C_{bulk,CH_2}d_e$$

$$= \epsilon_{ads,CH_2,a}\left(2\frac{d_e}{d_p}\right)\left(\Gamma_{ads,CH_2}\right) + \epsilon_{bulk,CH_2,a}C_{bulk,CH_2}d_e$$

..... 8.14

where,

$\Gamma_{ads,CH2}$ is the adsorbed amount of CH_2 groups on the adsorbed layer and

$$d_e = \frac{d_{e\parallel} + d_{e\perp}}{2}$$

..... 8.15

$$d_{e\parallel}=\frac{\eta_{21}E_{0\parallel}^2 d_p}{2\cos\theta}$$

..... 8.16

$$d_{e\perp}=\frac{\eta_{21}E_{0\perp}^2 d_p}{2\cos\theta}$$

..... 8.17

$$E_{0\perp}=E_{y0}$$

..... 8.18

$$E_{0\parallel}=(E_{x0}^2+E_{z0}^2)^{1/2}$$

..... 8.19

$E_{0\parallel}$ Electric field amplitude of parallel polarization

$E_{0\perp}$ Electric field amplitude of perpendicular amplitude

d_e Effective thickness (A)

$d_{e\parallel}$ Effective thickness, parallel polarization (A)

$d_{e\perp}$ Effective thickness, perpendicular polarization (A)

Equation 8.14 was used to evaluate the amount of surfactant adsorbing onto the substrate. More details are provided in the next chapter.

Figure 8.1: Chemisorption of Octadecyltrichlorosilane (OTS) on glass or Silicon. (reference # 24)

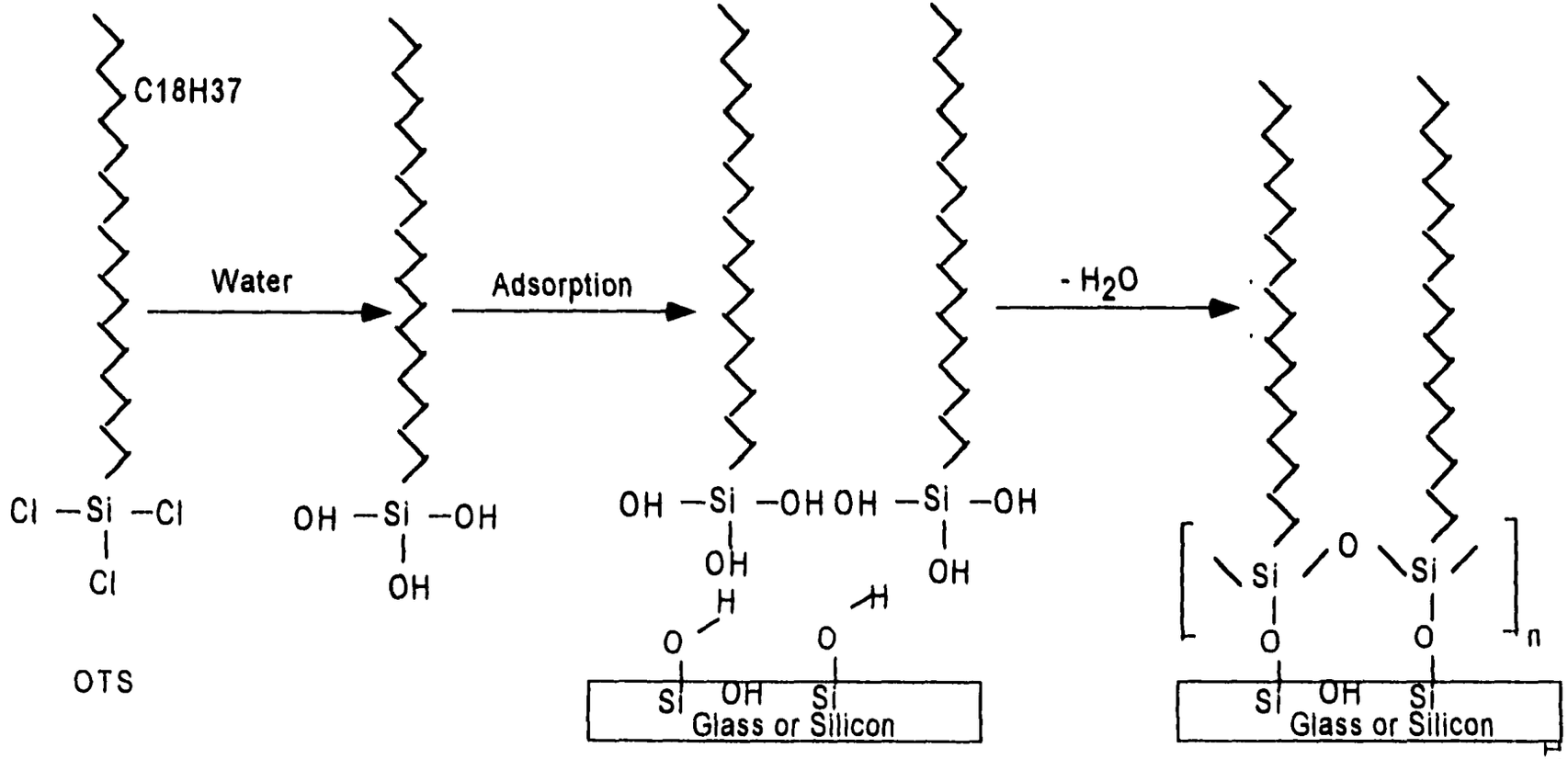

Figure 8.2: Schematic of Fluorescence microscope setup. (Also shown is structure of the dye NBD-HDA).

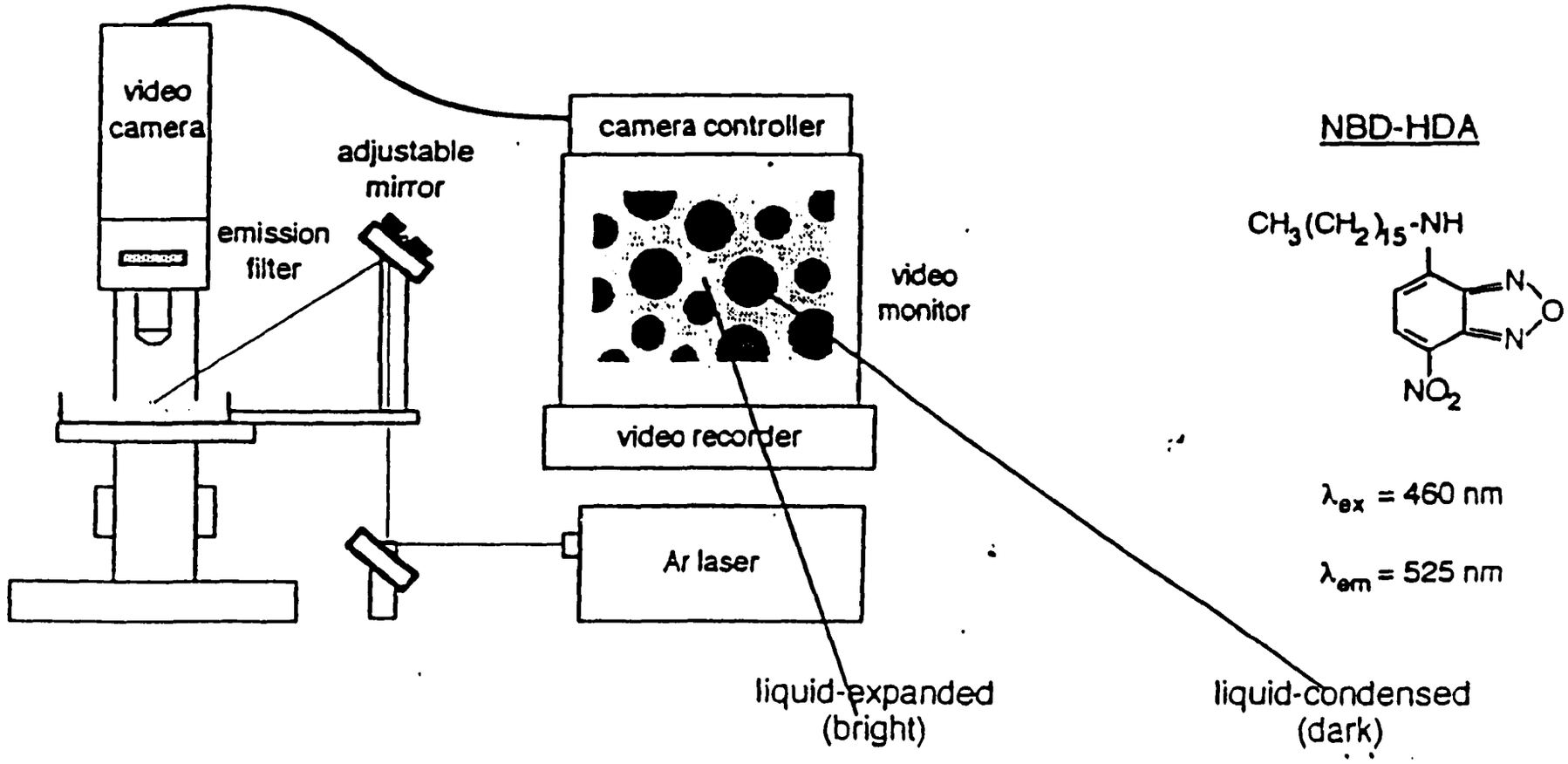

Figure 8.3: Schematic of the flow cell used to monitor the surfactant adsorption process in-situ.

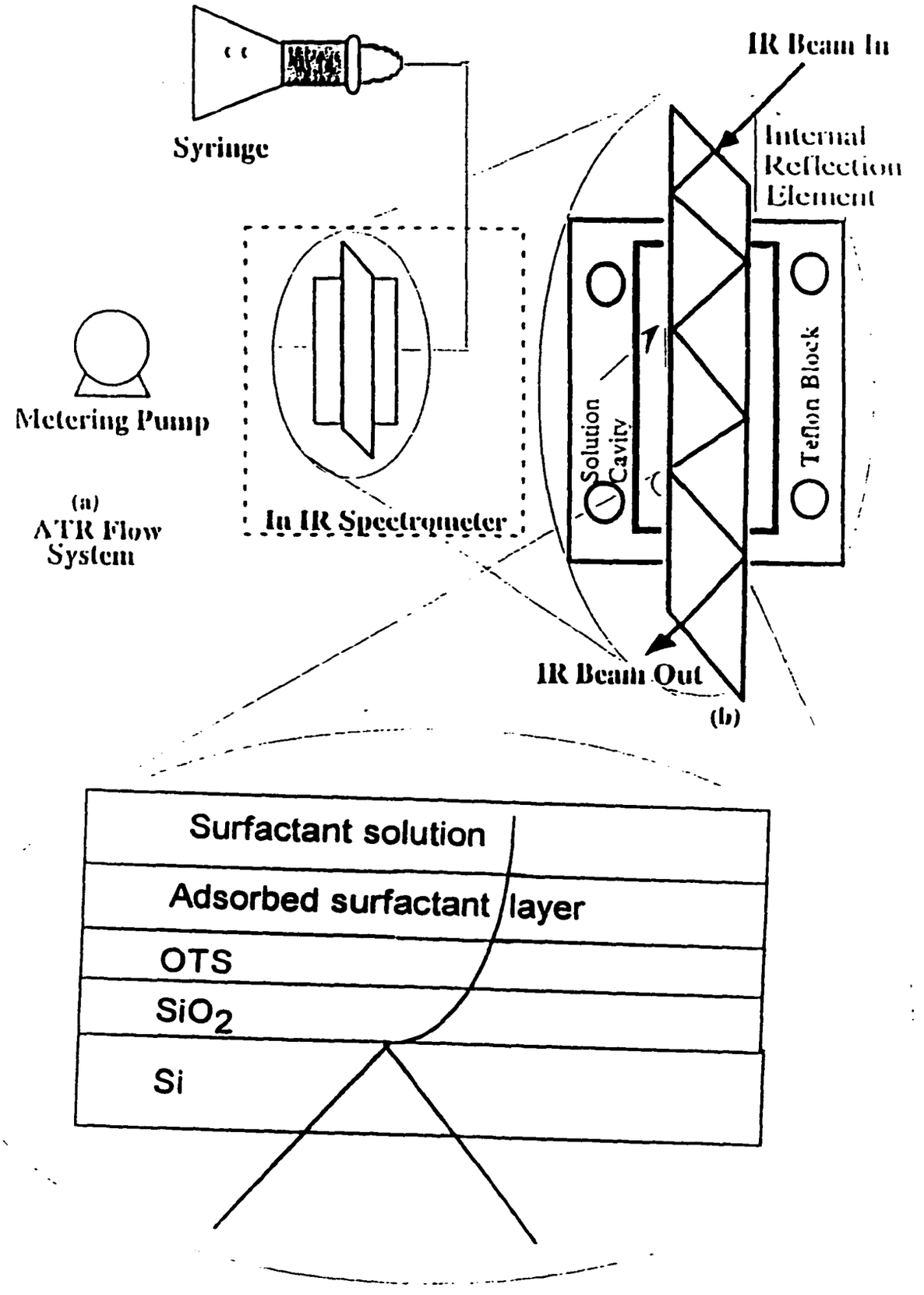

Figure 8.4: Typical FTIR spectra during surfactant adsorption showing the increase in hydrocarbon peaks with time.

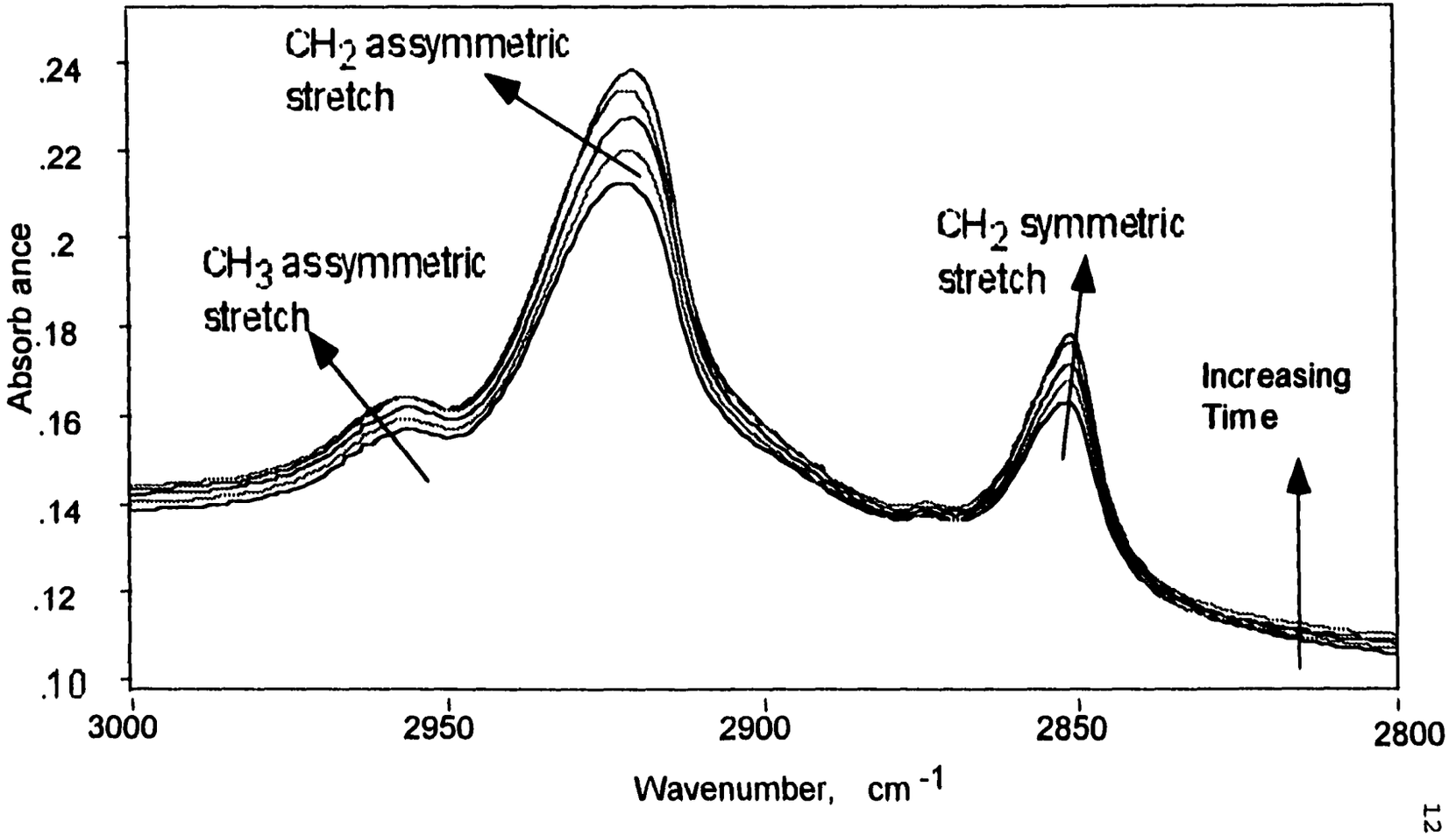

CHAPTER 9

RESULTS AND DISCUSSION

Surface pressure isotherms of $C_{14}E_1$ and $C_{14}E_6$ at 22.5 C are shown in Figure 9.1 [19]. $C_{14}E_1$ exhibits liquid expanded (LE) and liquid condensed (LC) phases and a LE/LC phase transition while $C_{14}E_6$ exhibits only a LE phase. This has been attributed to the difference in the size of headgroup of the two surfactants. The small headgroup, in case of $C_{14}E_1$, allows $C_{14}E_1$ molecules to pack so tightly (~ 20 A^2/molecule) at the air/water interface that a LE/LC phase transition results. In contrast the large headgroup, in case of $C_{14}E_6$, does not allow the molecules to pack tightly at the interface. Our objective in this study was to see if it is possible to transfer tightly packed $C_{14}E_1$ molecules onto hydrophobic solid and if so to study the kinetics of the adsorption process.

9.1 Visual evidence of close packing of $C_{14}E_1$ at the hydrophobic solid/water interface

Fluorescence images of the air/water and hydrophobic glass/water interfaces for $C_{14}E_1$ are shown in Figures 9.2 (a) and (b). The image at the air/water interface was recorded at a $C_{14}E_1$ area per molecule of 24 A^2/molecule. Recall from section 8.2.3 that after imaging the air/water interface the hydrophobic glass was pushed face down through the interface

and the hydrophobic glass/water interface was imaged. The image of the air/water interface, viz. LC domains dispersed in a LE phase, is as expected from previous studies [19]. The image of the hydrophobic solid/water interface is similar to that at the air/water interface. This shows that $C_{14}E_1$, existing in the LE/LC phase coexistence region, has been transferred from the air/water interface to the hydrophobic solid/water interface. Thus this provides us with visual evidence that it is possible to have a closely packed monolayer of $C_{14}E_1$ at the hydrophobic solid/water interface. Having established that we moved onto quantification of the adsorption process.

9.2 Quantitative evidence of close packing of $C_{14}E_1$ at the hydrophobic solid/water interface

We studied the adsorption kinetics of $C_{14}E_1$ onto a hydrophobic surface. In addition a similar study was conducted for $C_{14}E_6$ for a comparative analysis. The technique used to monitor the kinetics was ATR-FTIR. The experimental details and theory of this technique were discussed in the previous chapter. From the experimental data we obtained the integrated absorbance of the CH_2 asymmetric peak ($A_{CH2,a}$) as a function of time. To convert the $A_{CH2,a}$ to number of adsorbed CH_2 groups, and hence number of adsorbed surfactant molecules, equation 8.14 was used. In this equation the second term of the right hand side is negligible in our experiments. This is

because $C_{bulk,CH2}$ is of the order of micromolar, $\epsilon_{bulk,CH2,a}$ is $1.1*10^6$ cm/mol (as determined from another study by our group [20]) and d_e is of the order of $2.6*10^3$ A (equations 8.5 - 8.8, 8.15 - 8.19). Hence the order of magnitude of the second term is 10^{-8} - 10^{-6} cm^{-1}. The order of magnitude of the left hand side of equation 8.14, viz. $A_{CH2,a}/N$ for our experiments is 10^{-3} to 10^{-2} cm^{-1}. We therefore neglected the second term of the right hand sided of equation 8.14 for our calculations.

In order to evaluate the first term of equation 8.14 we had to determine $\epsilon_{bulk,CH2,a}$. To calculate $\epsilon_{bulk,CH2,a}$ a novel calibration of $A_{CH2,a}$ versus adsorbed number concentration of CH_2 groups was conducted [32]. The calibration involved spreading a monolayer of octodecyltrichlorosilane (OTS) on air/water interface of a Langmuir trough and obtaining a surface pressure isotherm. Next the monolayer was transferred onto Si IRE by lifting the IRE vertically through the interface. The monolayer transfer was conducted at 5 different areas per molecule of OTS. The FTIR spectra of Si IREs were then taken and integrated absorbance in the region (~2945-2902 cm^{-1}) obtained. This region corresponds to the asymmetric stretch of the CH_2 molecules. The integrated absorbance was then plotted versus adsorbed number concentration of CH_2 groups (= 17/(area per molecule of OTS*Avogadro number)). The factor of 17 is included since 1 OTS molecule has 17 CH_2 groups. The slope of the plot is equal to $\epsilon_{bulk,CH2,a}/2$ (refer Equation 8.2, note that cb = concentration of CH_2

groups*2*length of OTS = 2*adsorbed amount of CH_2 groups). The factor 2 is included since when OTS is transferred on to IRE (see above), all the edges of the IRE get coated with OTS and thus when such an IRE is placed perpendicular to the IR beam (like was done to obtain spectra of IREs), the beam encounters 2 OTS monolayers. Thus the actual path length, b, (refer equation 8.2) is 2*the length of the OTS molecule.

The surface pressure isotherm of OTS at 18.6 C and subphase water pH of 5.7 is shown in Figure 9.3. The surface pressures at which the monolayer was transferred onto the Si IRE are shown with arrows. The integrated areas for the CH_2 asymmetric peak (2945-2902 cm^{-1}) were plotted versus the adsorbed molar concentration of OTS. The plot is shown in Figure 9.4. The plot is linear, as expected. $\epsilon_{bulk,CH2,a}$ as obtained from the slope of the plot is $1.7*10^6$ cm/mol (equation 8.2). This value of $\epsilon_{bulk,CH2,a}$ was used in equation 8.14 to obtain the adsorbed amount of CH_2 groups and thus the area per molecule of surfactant molecules (= 15/(adsorbed amount of CH_2 groups*Avogadro number)) for $C_{14}E_1$ and 25/(adsorbed amount of CH_2 groups*Avogadro number) for $C_{14}E_6$). The factors 15 and 25 are included above since $C_{14}E_1$ and $C_{14}E_6$ have 15 and 25 CH_2 groups in each molecule respectively.

The change in the adsorbed amount of $C_{14}E_1$ at the hydrophobic solid/solution interface, as a function of time is shown in Figure 9.5. The data are plotted assuming that the number of reflections in the IRE is 6. However, the

number of reflections can either be 6 or 7. The uncertainty in the calculation of N arises since the point of contact of the IR beam with the face of the IRE (refer Figure 8.3) is not known. In addition we expect the point of contact to be different for each flow run. From the known geometry of the IRE and assuming that the point of contact is at either of the two extremes of the face of the IRE, we determined the range of the value of N possible, viz. 6 or 7. Now by doing all calculations for N=6, we could be underestimating the area per molecule by 15 % (equation 8.14). The final area per molecule of $C_{14}E_1$ is 20 A^2/molecule (~60 hours). Thus it is possible to obtain a tightly packed monolayer of $C_{14}E_1$ at the hydrophobic solid/water interface, as was demonstrated earlier by fluorescence microscopy results.

The analogous plot for $C_{14}E_6$ is shown in Figure 9.6. The final area per molecule of $C_{14}E_6$ was much lower than that for $C_{14}E_1$ (~ 200 A^2/molecule in ~2.5 hours) (Figure 9.6). Note that adsorption experiment of $C_{14}E_6$ was conducted at various $C_{14}E_6$ concentrations to checked the reproducibility of our runs. We worked at different concentrations above the cmc of $C_{14}E_6$, to make sure that our results on adsorption kinetics of $C_{14}E_6$ were not an artifact due to surfactant depletion to the surface of the stock solution beaker. Note that for C_mE_n surfactants below the cmc, lower the surfactant concentration lower is the equilibrium surface concentration [13 - 15]. The effect of concentration on adsorption dynamics is shown in

Figure 9.6. Clearly for all three concentrations considered, viz. 5.19, 5.62 and 23.41 mg/L, all above the cmc of $C_{14}E_6$ (cmc of $C_{14}E_6$ is ~4.8 mg/L at 25 C [33]), the final area per molecule and the time taken to attain it are similar (~ 200 A^2/molecule and 2.5 hours respectively). We compared our $C_{14}E_6$ adsorption results with those obtained by Tiber [17]. Tiber has reported the final area per molecule and the time taken to attain it as 50 A^2/molecule and 3 minutes respectively. However, Tiber did not use a self-assembled OTS layer as the hydrophobic surface, rather he used a dimethyloctyltrichlorosilane monolayer as the surface. The dimethyloctyltrichlorosilane has 2 terminal methyl groups as compared to OTS (which has 1), but the former has only 7 methylenes as compared to 17 for OTS. It is not clear which of the two surfaces will be more hydrophobic and also whether the difference in the adsorption process of $C_{14}E_6$ over the two surfaces is due to differences in the properties of the surface. Having ascertained the validity of our data, we postulate that the discrepancy between our and Tiber results may be due to the difference in the structure of the self-assembled layer. A more detailed study of the two monolayers is needed at this point. Such a study has been initiated in our laboratory and involves studying the surface morphologies of the two monolayers using Atomic Force Microscope (AFM).

We compared the adsorption kinetics of $C_{14}E_1$ and $C_{14}E_6$ (Figures 9.5 and 9.6). Based on the cmc (solubility of $C_{14}E_1$

<.1 mg/L and it does not exhibit a cmc and cmc of $C_{14}E_6$ is ~4.8 mg/L [33] at 25 C) $C_{14}E_1$ has a lower monomeric concentration than $C_{14}E_6$. Thus we expect $C_{14}E_1$ to adsorb more slowly than $C_{14}E_6$. However, based on the headgroup size of the two surfactants (E_1 as opposed to E_6) we expect $C_{14}E_1$ to pack more densely than $C_{14}E_6$. Indeed the two expectations are true - $C_{14}E_1$ adsorbs much slower (60 hours as compared to 2.5 hours) and packs more densely (areas per molecule of ~20 as compared to ~200 A^2/molecule) than $C_{14}E_6$ (Figures 9.5 and 9.6).

Figure 9.1: Surface pressure isotherms of $C_{14}E_1$ and $C_{14}E_6$ at 22.5 C. (reference # 19).

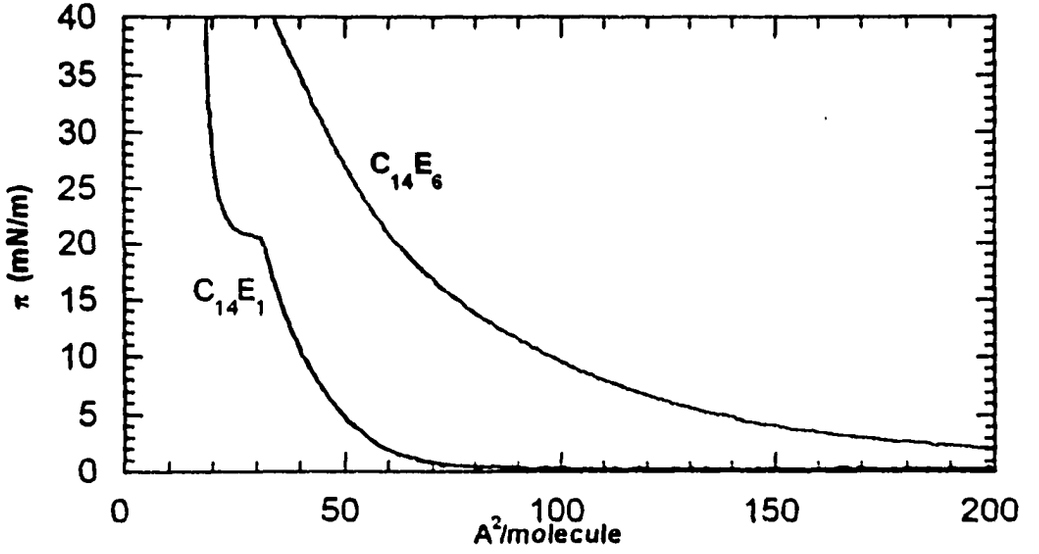

Figure 9.2: Fluorescence images of $C_{14}E_1$ at the LE/LC phase transition at the (a) air/water interface and (b) hydrophobic surface/water interface.

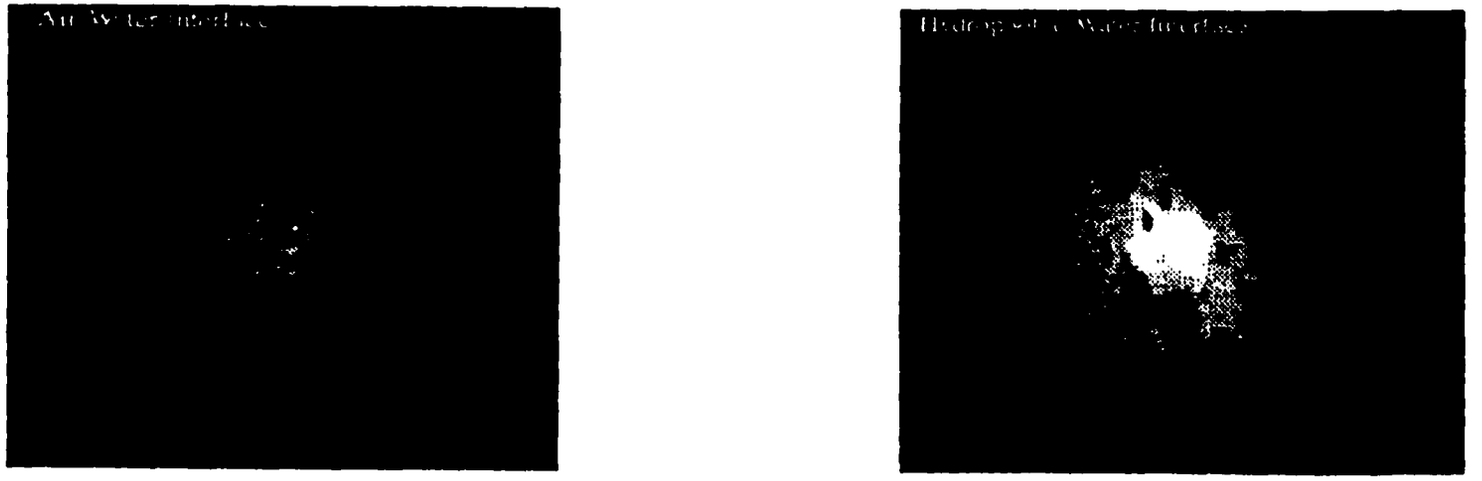

Figure 9.3: Surface pressure isotherm of OTS at 18.6. The arrows denote the points at which the transfer of OTS monolayer onto Si was conducted.

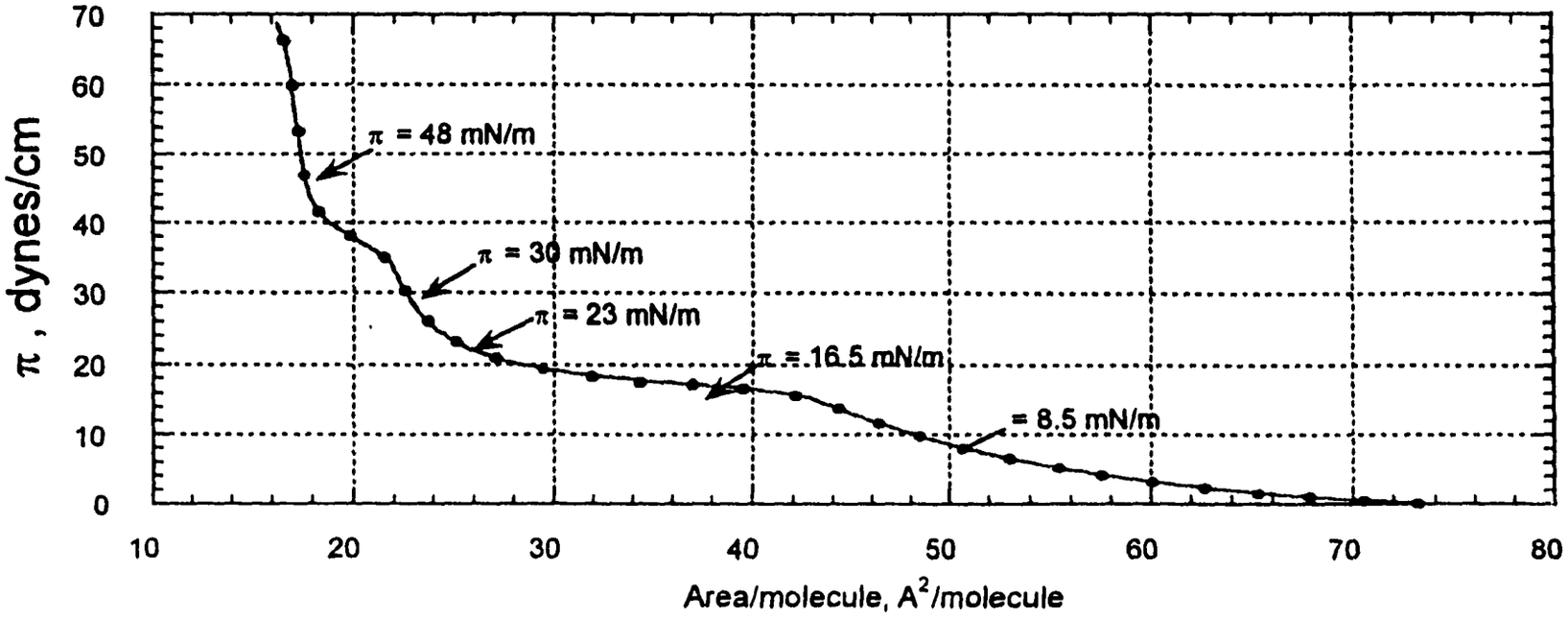

Figure 9.4: Calibration plot for the FTIR adsorption experiments.

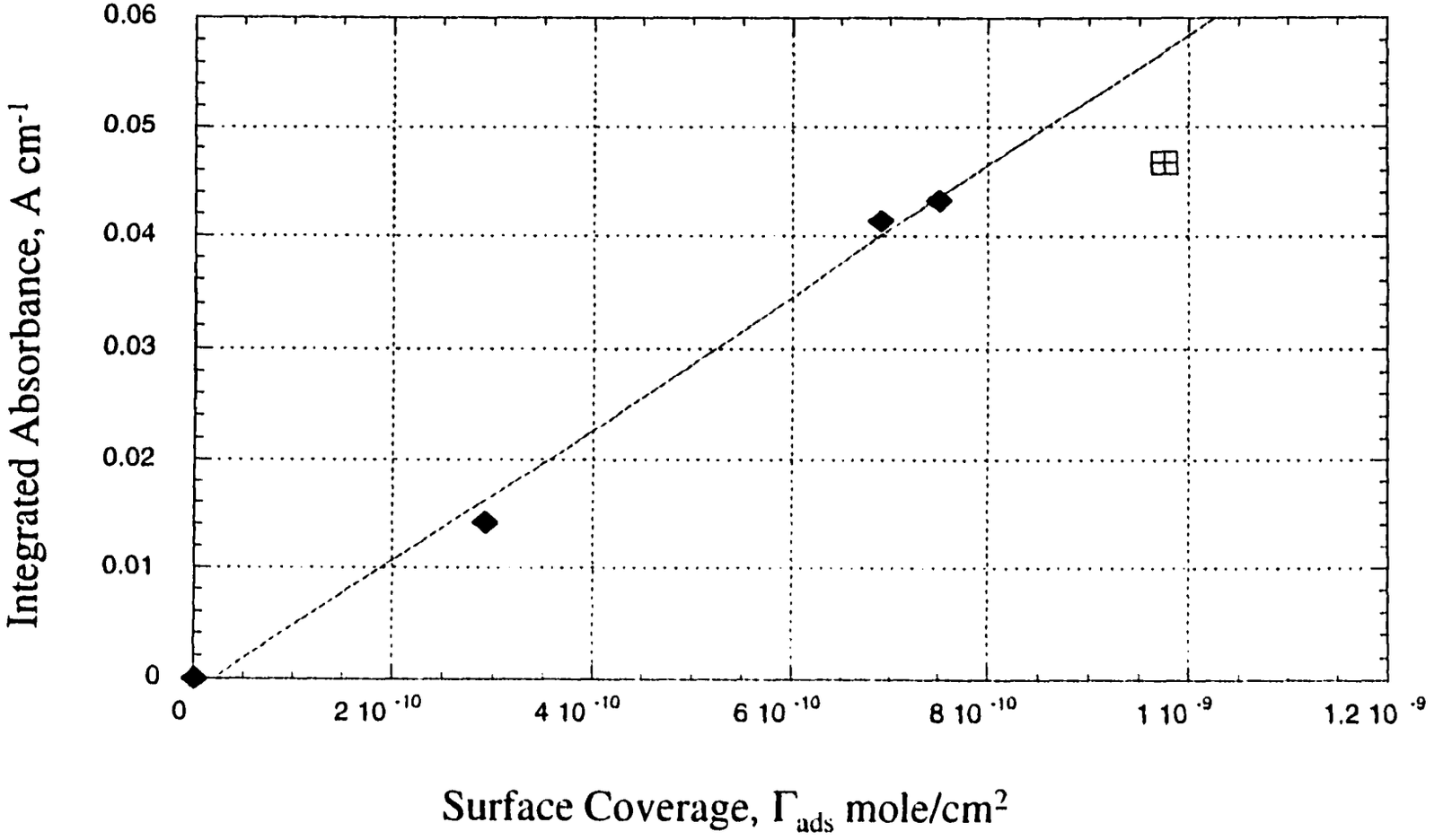

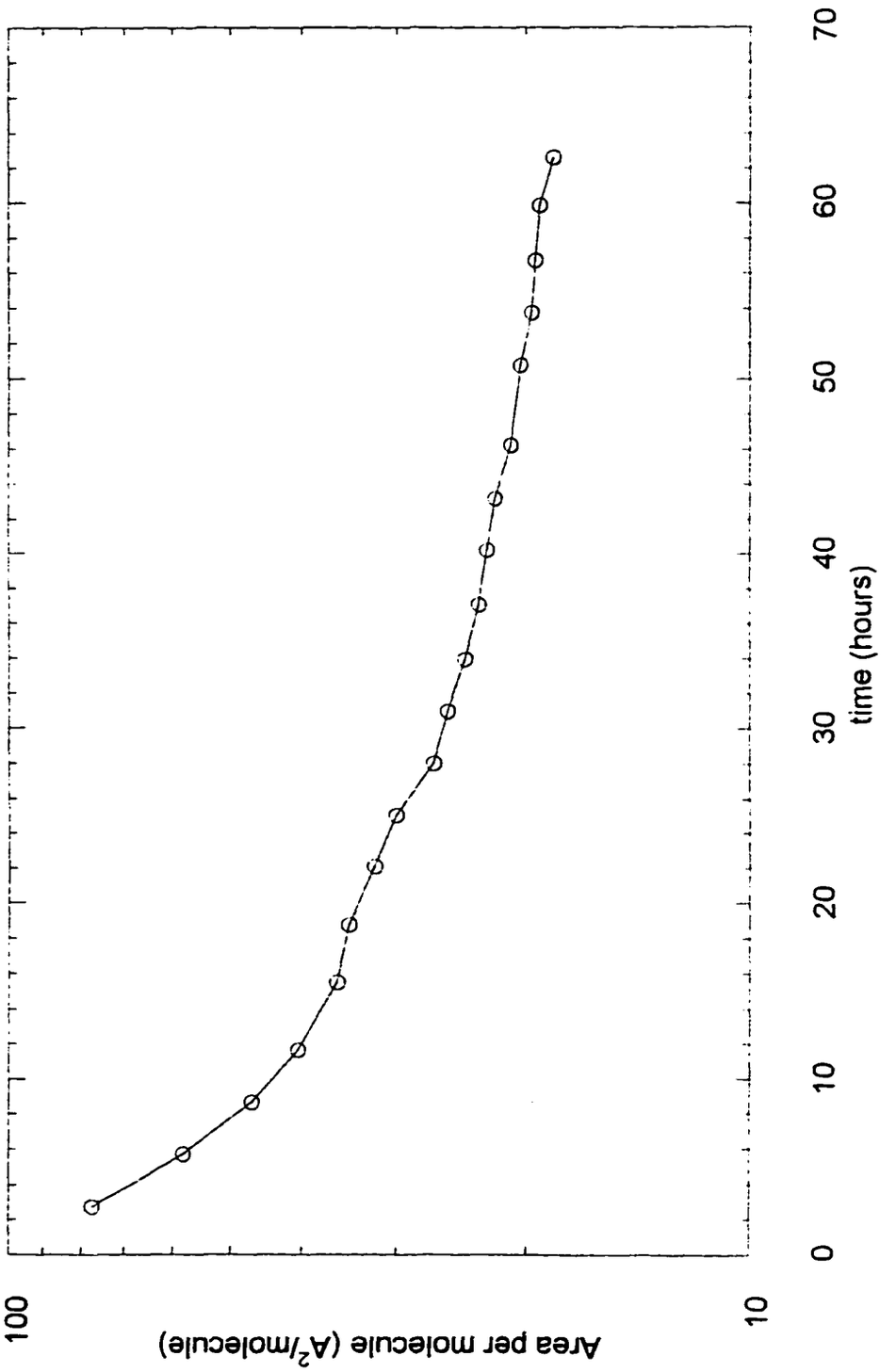

Figure 9.5: Adsorption dynamics of $C_{14}E_1$.

Figure 9.6: Adsorption dynamics of $C_{14}E_6$, showing the effect of $C_{14}E_6$ bulk concentration.

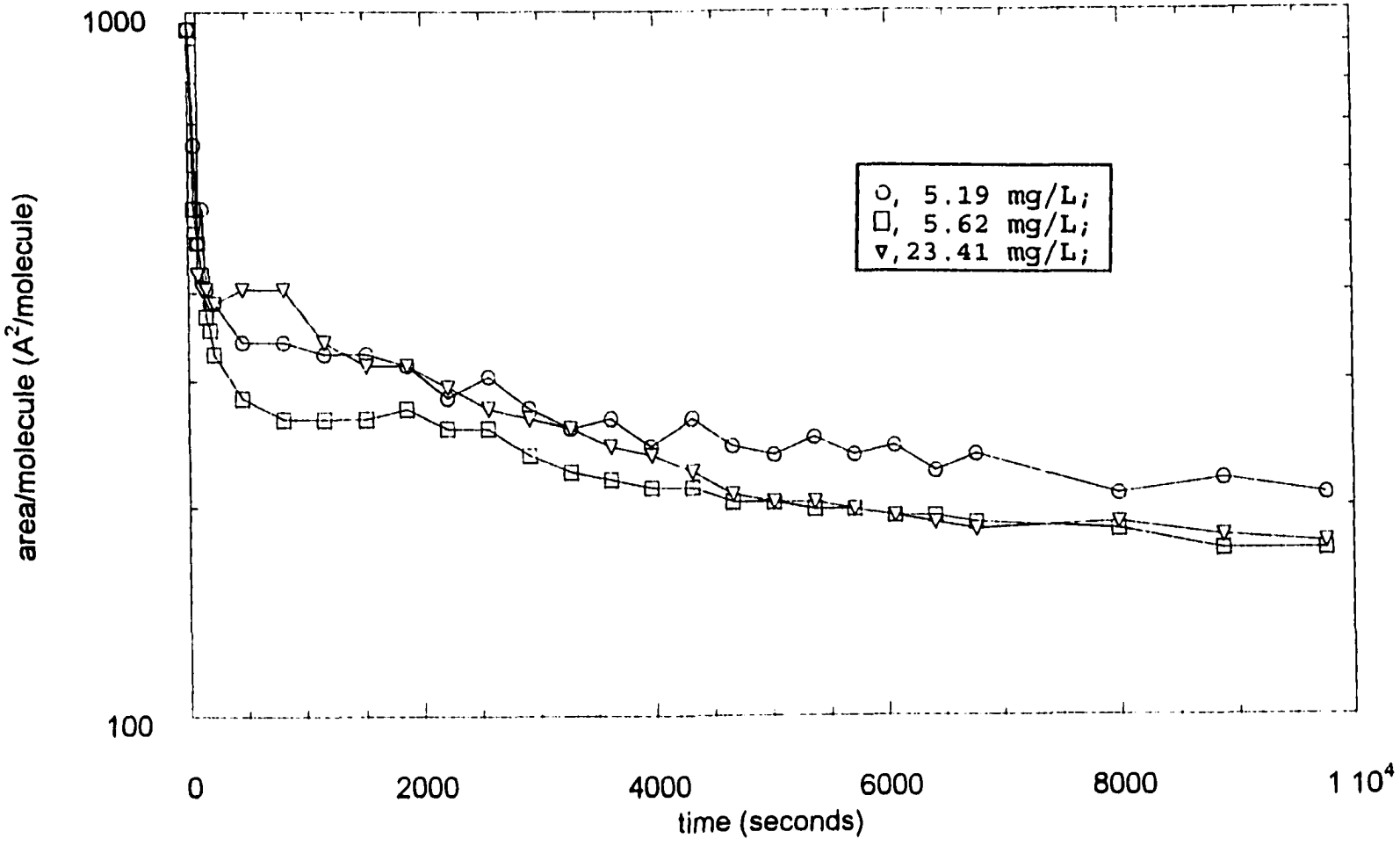

CHAPTER 10

Summary, conclusions and recommendations for future work

Having shown that $C_{14}E_1$ packs very densely at the solid/water interface, the next step should be be identify other C_mE_n surfactants which exhibit dense packing. Other studies in our lab have shown that $C_{12}E_6$ and $C_{16}E_2$ pack very densely at the air/water interface. It is reasonable to expect these two surfactants to pack densely at the hydrophobic solid/water interface as well.

The proposed work can be divided into 3 parts. The first part will be to design an experimental set-up which will allow us to study the spreading ability of a drop of surfactant solution onto hydrophobic surfaces. The second part should address the issue of increasing the rate of adsorption of $C_{14}E_1$. The third part should involve decreasing $\gamma_{v/L}$. Recall that as pointed out in the Literature Review, we expect that for a given adsorbed amount of surfactant, the lower the $\gamma_{v/L}$ the better is the spreading.

An experimental set-up for measuring the equilibrium spread areas and the spreading rate of a drop of surfactant solution is shown in Figure 10.1. The set-up consists of a chamber in which the hydrophobic surface can be placed. The chamber will be humidity and temperature controlled since we expect the hydrophobicity of the solid surfaces to be sensitive to these parameters. The chamber will have a small

hole on top (with a cover) for inserting the tip of a syringe containing the surfactant solution. After the drop is placed on the hydrophobic solid, the entire spreading process can be recorded on a video camera. This will enable us to obtain the spreading area of the drop as a function of time which will provide us with the dynamics of the spreading precess.

To increase the rate of adsorption of $C_{14}E_1$ and also to be able to decrease $\gamma_{v/L}$ as much as possible I propose adopting the 'synergistic' approach. It has been shown that some mixtures of surfactants exhibit interfacial properties which are more pronounced than those of the individual surfactants [18].

Figure 10.1: Experimental set-up for measuring spreading area and rate of surfactant solutions over hydrophobic solutions.

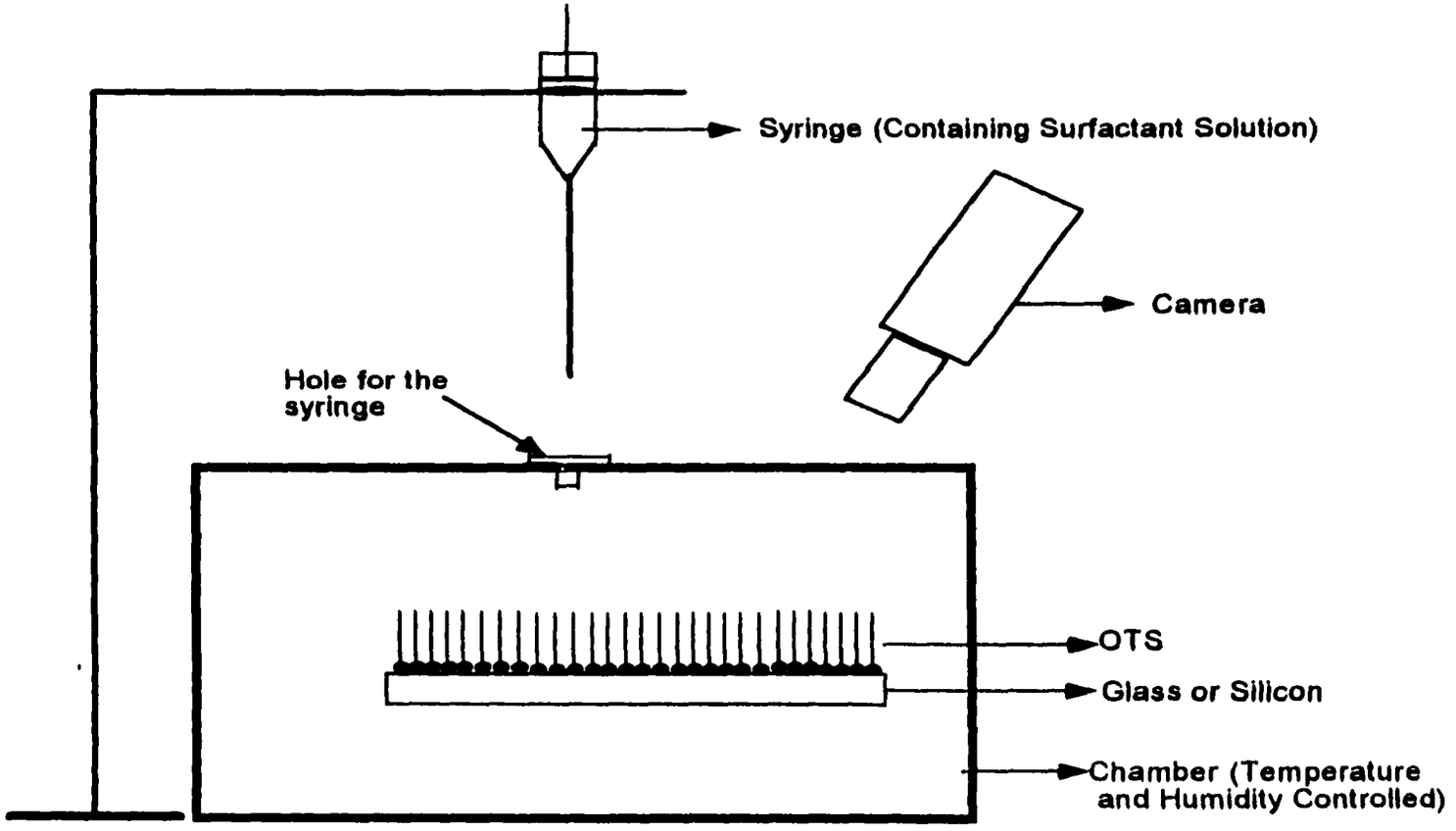

PART 1

References

1. Goddard, E.D. *Colloids Surf.* **1986** 19 255.

2. Goddard, E.D.; Hannan,R.B. In *Micellization, Solubilization, and Microemulsions*; Mittal, K.L.,Ed.; Plenum Press: New York,**1977**;Vol. 2.

3. Sabbadin, J.; LeMoigne, J.; Francois, J. In *Surfactants in Solution*;Mittal,K.L.,Lindman,B.,Eds.,Plenum Publishing: New York,**1984**;Vol.2.

4. Cabane, B.; Duplessix, R. *J. Phys.* **1982** 43 1529.

5. Cabane, B.; Duplessix, R. *J. Phys.* **1987** 48 6511.

6. Arai, H.; Murata, M.; Shinoda, K. *J. Colloid Interface Sci.* **1971** 37 223.

7. Tadros, Th.F. *J. Colloid Interface Sci.* **1974** 46 528.

8. Jones, M.N. *J. Colloid Interface Sci.* **1967** 23 36.

9. Sivadasan, K.; Somasundaran, P., *Colloids and Surfaces*, **1990** 49 229.

10. Dualeh, A.J.; Steiner, C.A. *Macromolecules* **1990** 23 251.

11. Dualeh, A.J.; Steiner, C.A. *Macromolecules* **1991** 24 112.

12. Tanaka, R.; Meadows, J.; Williams, P. A.; and Philips, G. O.; *Macromolecules* **1992** 25 1304.

13. Wu, S.Y; Varadaraj, R.; Steiner,C.A. *J. Phys. Chem.* **1996** 100 17316.

14. Iliopoulos, I.; Wang, K.T.; Audebert, R. *Langmuir* **1991**,7,617.

15. Sau, A.C. ; Landoll, L.M.; In *Polymers in Aqueous Media* Adv. Chem. Ser. 223,American Chemical Society, Washington,DC,1989, pp 343.

16. Biggs, S.; Selb, J.; Candau, F. *Langmuir* **1992** 8 838.

17. Steiner, C.A.; Gelman R.A., In *Cellulosics Utilization:Research and Rewards in Cellulosics*; Inagaki, H.; Phillips, G.O., Eds., Elsevier, London, 1989.

18. Varelas, C.G.; Steiner, C.A. "A microstructural analysis of polymer networks formed from graft copolymers in mixed aqueous solvents" *Absorbent polymer technology - studies in polymer science 8*, Brannon-Peppas, L.; Harland, R.S., Eds., Elsevier, 1990.

19. Winnik, F.M.; Ringsdorf, H.; Venzmer, J. "Interactions of surfactants with hydrophobically modified poly(N-iospropylacrylamides)- 1. Fluorescence probe studies". *Langmuir* **1991** 7 905.

20. Winnik, F.M.; Ringsdorf, H.; Venzmer, J. "Interactions of surfactants with hydrophobically modified poly(N-iospropylacrylamides)- 2. Fluorescence label studies". *Langmuir* **1991** 7 912.

21. Yang, Y. *Synthesis and chracterization of hydrophobically modified polyacrylamide-based polymers and their hydrogels* Ph.D. Thesis, City College of City University of New York (CUNY) 1996.

22. Magny, B.; Iliopoulos, I.; Audebert, R.; Piculell, L.; Lindman, B. *Progress in Colloid and Polymer Science* **1992** 89 118.

23. Piculell, L.; Guillemet, F.; Thuresson, K. ; Shubin, V. ;Ericson, O. *Advances in Colloid and Interfacial Science* **1996** 63 1.

24. Iliopoulos, I.; Wang, T.K.; Audebert,R. *Langmuir* **1991** 7 617.

25. Varelas, C.G; Steiner,C.A. *J. Polym. Sci. B: Polm. Phys. Ed.* **1992** 30 1233.

26. Varelas, C.G; Dixon,D.G.; Steiner,C.A. *J. Controlled Release* **1995** 34 185.

27. Wu, S.Y; Yang, Y.; Varadaraj, R.; Couzis, A.; Steiner, C.A.; in preparation.

28. Carlsson, A.; Karlstrom, G.; Lindman, B. *Colloids and Surfaces* **1990** 47 147.

29. Nystrom, B.; Walderhaug, H.; Hansen, F.K.; Lindman, B. *Langmuir* **1995** 11 750.

30. Zana, R. In Surfactant Solutions: New Methods of Investigation;Zana,R.,ed.,Marcel Dekker(New York),1986.

31. Kalyansundaram, K.; Thomas, J.K; *J. Am. Chem. Soc.* **1977** 99 2039.

32. Hiemenz, P.C. In *Polymer Chemistry - The basic concepts* Ed., Marcel Dekker, Inc. (New York),1980, pp 156.

33. Annable, T.; Ettelaie, *J. Phys. Chem.* **1996** 93 899.

34. Goddard, E.D.; *J. Colloid. and Interfacial Science* **1992** 152 578.

35. The Merck Index, Merck and Co., Inc., New Jersey, 11th Edition, **1989**, pp 1056.

36. Mukerjee, P.; Mysels, K.J. *Critical Micelle Concentrations Of Aqueous Surfactant Systems* National Standard Reference Data Series, National Bureau of Standards (U.S.) Washington DC 1971. pp 51, 53, 115, 122.

37. Piculell, L.; Thuresson, K.; Ericsson, O., *Faraday Discussion* **1995** 101 307.

38. Paulaitis, M.; Garde, S.; Ashbaugh, H. "The hydrophobic effect" *Current opinion in Colloid and Interface Science* **1996** 1 376.

39. Thalberg, K.; Lindman, B. "Gel formation in aqueous systems of a polyanion and an oppositely charged surfactant" *Langmuir* **1991** 7 277.

PART 2
REFERNCES

1. Zabkiewicz, J.A; Gaskin, R.E, *Adjuvants and Agrochemicals, Vol. 1, Mode of Action and Physiological Activity*, ed. N.P. Chow, *et al.* 1989, Boca Raton, FL: CRC Press. 142.

2. Knoche, M.; Tamura, H.; Bukovac, M.J., *J. Agric. Food Chem.* **1991** 39 202.

3. Smid-Korbar, J.; Kristl, J.; Stare, M., *Int. J. Cosmet. Sci.* **1990** 12 135.

4. Karsa, D.R., *Industrial Applications of Surfactants*, ed. D.R. Karsa. 1987, London: The Royal Society of Chemistry.

5. Zhu, S.; Miller, W.G.; Scriven, L.E.; Davis, H.T., "Superspreading of Water-Silicone surfactant on hydrophobic surfaces". *Colloids and Surfaces A: Physicochemical and Engineering Aspects* **1994** 90 63.

6. Stoebe, T.; Lin, Z.; Hill, M.; Ward, M. D.; Davis, H.D., "Surfactant-Enhanced Spreading". *Langmuir* **1996** 12 377.

7. Rosen, M.J.; Song, L.D.; "Superspreading, Skien Wetting, and Dynamic Surface Tension". *Langmuir* **1996** 12 4945.

8. He, M.; Hill R.M.; Lin, Z.; Scriven, L.E.; Davis, H.T., "Phase Behavior and Microstructure of Polyoxyethylene Trisiloxane Surfactants in Aqueous Solution". *Journal of Physical Chemistry* **1993** 97 8820.

9. Ananthapadmanabhan, K.P.; Goddard, E.D.; Chandar, P., "A Study of the Solution, Interfacial and Wetting Properties of Silicone Surfactants". *Colloids and Surfaces* **1990** 44 281.

10. Gaskin, R.E.; Kirkwood, R.C, *Adjuvants and Agrochemicals, Vol. 1, Mode of Action and Physiological Activity*, ed. N.P. Chow, *et al.* 1989, Boca Raton, FL: CRC Press. 129.

11. Guggenheim, E.A.; Adam, N.K., *Proc. Roy. Soc. (London)* **1933** A139 218.

12. Gibbs, J. W., *The Collected Works of J.W. Gibbs*. Vol. 1. 1931, New York: Longmans. 219.

13. Corkill, J.M.; Goodman, J.F.; Tate, J.R., *Transactions of Faraday Society* **1966** 62 979.

14. Glazman, Y.; Blashchuk, Z., *Kolloid. Zh.* **1969** 31 809.

15. Glazman, Y.; Blashchuk, Z., "On the mechanism of Lyophilic Sols Formation". *Journal of Colloid and Interfacial Sciences* **1977** 62(1) 158.

16. Fragneto, G.; Lu, J. R.; McDermott, D.C.; Thomas, R. K.; Rennie A. R.; Gallagher, P. D.; Satija, S. K., "Structure of Monolayers of Tetraethylene Glycol Monododecyl Ether Adsorbed on Self-Assembled monolayers on Silicon: A Neutron Reflectivity Study". *Langmuir* **1996** 12 477.

17. Tiberg, F., "Physical characterization of non-ionic surfactant layers at the hydrophilic and hydrophobic solid surfaces by time-resolved ellipsometry". *Journal of Chemical Society, Faraday Transactions* **1996** 92(4) 531.

18. Rosen, M.J.; Zhu, Z.H., "Enhancement of Wetting Properties of Water-Insoluble Surfactants via Solubilization". *Journal of American Oil Chemists' Society* **1993** 70(1) 65.

19. Pollard, M. L.; Pan, R.; Steiner, C. A.; Maldarelli, C., "Polymorphism in the Phase Behavior of Slightly Soluble Polyethoxylate Monolayers at the Air/Water Surface: Phase Coexistence, Transitions Driven by Bulk Exchange, and their Effect on Dynamic Tension". *submitted to Langmuir* **1997**.

20. Krishnan, S.; Couzis, A., "to be published". **1997**.

21. Gun, J.; Iscovici, R.; Sagiv, J., "On the Formation and Structure of Self-Assembling Monolayers II. A comparative Study of Langmuir-Blodgett and Adsorbed Films Using Ellipsometry and IR Reflection-Adsorption Spectroscopy". *Journal of Colloids and Interfacial Sciences* **1984** 101(1).

22. Gun, J.; Sagiv, J., "On the Formation and Structure of Self-Assembling Monolayers". *Journal of Colloids and Interfacial Sciences* **1986** 112(2) 457.

23. Maoz, R.; Sagiv, J., "On the Formation and Structure of Self-Assembling Monolayers 1. A Comparative ATR-Wettability Study of Langmuir-Blodgett and Adsorbed Films on Flat Substrates and Glass Microbeads". *Journal of Colloids and Interfacial Sciences* **1984** 100(2) 465.

24. Sagiv, J., "Organized Monolayers by Adsorption. 1. Formation and Structure of Oleophobic Mixed Monolayers on Solid Surfaces". *Journal of American Chemical Society* **1980** 102 92.

25. Losche, M.; Mohwald, H., *Rev. Sci. Instrum.* **1984** 55 1968.

26. Meller, P., "Computer-assisted videa microscopy for the investigation of monolayers on liquid and solid substrates". *Rev. Sci. Instrum.* **1988** 59 2225.

27. Harrick, N.J., *Internal Reflection Spectroscopy.* 1967, New York: Interscience, pp 27.

28. Tompkins, H.G., "The physical Basis for analysis of the Depth of Absorbing Species Using Internal Reflection Spectroscopy". *Applied Spectroscopy* **1974** 28 335.

29. Sperline, R.P.; Muralidharan, S.; Freiser, H., "In Situ Determination of Species Adsorbed at a Solid-Liquid Interface by Quantitative Infrared Attenuated Total Reflectance Spectrophotometry". *Langmuir* **1987** 3 198.

30. DePalma, V.; Tillman, N., *Langmuir* **1989** 5 868.

31. Wasserman, S.R.; Tao, Y. T.; Whitesides, G. M., *Langmuir* **1989** 5 1074.

32. Kumar, V.; Krishnan, S.; Steiner, C. A.; Maldarelli, C.; Couzis, A., "Measurement Of Infrared Molar Absorptivity Of a Surfactant Adsorbed Onto a Solid Substrate Over a wide range of Surface COncentrations Using Octadecyltrichlorosilane Langmuir-Blodgett Transferred Films". *submitted to Journal of Physical Chemistry B* **1997**.

33. Mukerjee, P.; Mysels, K.J., *Critical Micelle Concentrations of Aqueous Surfactant Systems.* National Standard Reference Data Series; National Bureau of Standards. 1971, Washington DC. 142, pp 142.